1-1-2008

Nano and microscale silica chemistry in block copolymer templates using supercritical carbon dioxide as a reaction medium.

Sivakumar Nagarajan
University of Massachusetts Amherst

NANO AND MICROSCALE SILICA CHEMISTRY IN BLOCK COPOLYMER TEMPLATES USING SUPERCRITICAL CARBON DIOXIDE AS A REACTION MEDIUM

A Dissertation Presented

by

SIVAKUMAR NAGARAJAN

Submitted to the Graduate School of the
University of Massachusetts Amherst in partial fulfillment
of the requirements for the degree of

DOCTOR OF PHILOSOPHY

September 2008

Polymer Science and Engineering

NANO AND MICROSCALE SILICA CHEMISTRY IN BLOCK COPOLYMER TEMPLATES USING SUPERCRITICAL CARBON DIOXIDE AS A REACTION MEDIUM

A Dissertation Presented

by

SIVAKUMAR NAGARAJAN

Approved as to style and content by:

_____

Thomas P. Russell, (Co-Chair)

_____

James J. Watkins, (Co-Chair)

_____

T. J. Mountziaris, Member

_____

Shaw Ling Hsu, Department Head
Polymer Science and Engineering

NANO AND MICROSCALE SILICA CHEMISTRY IN BLOCK COPOLYMER TEMPLATES USING SUPERCRITICAL CARBON DIOXIDE AS A REACTION MEDIUM

A Dissertation Presented

By

SIVAKUMAR NAGARAJAN

Approved as to style and content by:

Thomas P. Russell, Co-Chair

James J. Watkins, Co-Chair

T. J. Mountziaris, Member

Shaw Ling Hsu, Department Head
Polymer Science and Engineering

DEDICATION

To my late grandfather, Mr. D. Chockalingam

and

To my mother, Mrs. N. Hemalatha, father, Mr. V. Nagarajan,
and brother, Mr. N. Mohankumar.

ACKNOWLEDGMENTS

This dissertation is complete only if I acknowledge everyone who contributed, helped and supported me to get to this stage. First, I thank my dear advisors, Prof. Thomas P. Russell and Prof. James J. Watkins, from my heart, for their valuable guidance, support, training and help. I have been trained to look at a problem with two different and important perspectives; this has happened to me only because of Prof. Russell and Prof. Watkins. I wish to thank them separately for providing me with ample freedom in performing my projects and helping me when I am stuck in my projects. This is one of the important things that I enjoyed during my Ph D. I also have a special note of thanks to my advisors for their valuable questions and discussions during my original research proposal defense.

Next, I thank my committee member, Prof. T. J. Mountziaris for his valuable suggestions, support and especially for understanding the practical difficulties involved in scheduling meetings and making sure that they are held without delay.

I would like to thank my collaborators, Prof. Christopher K. Ober (Cornell U), Dr. Mingqi Li(Cornell U), Ms. Joan K. Bosworth(Cornell U), Dr. Detlef Smilgies (Cornell U), Dr. Uzo Oko(AMD) and Dr. Tom Wallow(AMD) for their valuable contributions and help.

I would like to express my gratitude to Dr. Dorothea Buechel, who supervised my summer internship at Seagate Technology and made my research experience, in a non-academic environment, enjoyable and valuable. I would also like to thank Dr. Ben Ocko(BNL), Dr. David Cookson(APS) and Dr. Peter Busch(Cornell U) for their valuable discussions.

I am very grateful to Lou, Sekar, Jack, John Nicholson and Evgenia for their help whenever needed in acquiring the data. I am thankful to all of the professors in PSE department for teaching the first year courses and more importantly, for laying a strong foundation for my career. I would like to convey my sincere thanks to Prof. Muthukumar and Prof. Bryan Coughlin for their support, guidance, suggestions and valuable discussions. I would like to thank Prof. R. Dhamodharan at IIT Madras for teaching my very first course on polymers during my masters program and for motivating me to pursue doctoral studies in polymer science. I would also like to express my gratitude to Prof. A.K. Mishra and Prof. Khader Ibrahim for their guidance and motivation.

I extend my gratitude to all PSE staff at the front office and group secretaries. I have bothered almost each of them with my questions, paperwork, course enrollments, signatures etc., during my stay here and they were all very patient and helpful to me.

Being a joint student for two advisors, I am fortunate enough to have wonderful lab members from two groups. I thank all of the past and present members of both the groups, professionally and personally, for their help, support and suggestions.

I convey my thanks to all of my friends, especially, Anand, Britto, Elam, Eshwar, Gunjun, Kanchan, Kate, KK, Malvika, Manoj, Matt at Golds, Naresh, Nivas, Priyanka, Raja, Ranga, Sarah, Sarvesh, Suresh, Velu, Venkatesan, Vikram and Vijay, who made my stay at Amherst very pleasant, enjoyable and memorable.

Last but definitely not least, my parents and my brother, without their support and encouragement, I would not have come this far. I simply do not have words to thank them and I dedicate this dissertation to them.

ABSTRACT

NANO AND MICROSCALE SILICA CHEMISTRY IN BLOCK COPOLYMER TEMPLATES USING SUPERCRITICAL CARBON DIOXIDE AS A REACTION MEDIUM

SEPTEMBER 2008

SIVAKUMAR NAGARAJAN, B.Sc., BHARATHIDASAN UNIVERSITY TIRUCHIRAPPALLI

M.Sc., INDIAN INSTITUTE OF TECHNOLOGY MADRAS

M.S., UNIVERSITY OF MASSACHUSETTS AMHERST

Ph.D., UNIVERSITY OF MASSACHUSETTS AMHERST

Directed by: Professor Thomas P. Russell and Professor James J. Watkins

The ability of block copolymers (BCPs) to self-assemble into well-defined arrays of nanoscopic structures has enabled them to be used as templates and scaffolds for the fabrication of nanostructured materials. Such materials find applications in several fields including microelectronics, photonics and sensors. In this dissertation nanostructured silicate films were fabricated by performing phase selective silica chemistry within self-assembled BCP templates using a discrete two step replication process: (i) template formation and (ii) supercritical fluid assisted silica deposition. The use of supercritical CO_2 as a reaction medium enabled facile transfer and diffusion of silicate precursor within the BCP film without disturbing its order. The sensitivity of the chosen precursor to acid, helped to control the silica condensation at nanoscopic and at microscopic length scales. Removal of templates yielded mesoporous silicate films in which the porous geometry can be completely controlled over multiple length scales.

The use of BCP films with cylindrical domains oriented normal to the substrate as templates for phase selective silica deposition yielded arrays of perpendicular nanochannels in silica films. Obtaining such morphology in mesoporous materials has proven to be challenging, although they are promising candidates for applications ranging from catalysis to sensors and the separations.

To fabricate directly patterned mesoporous silicate films, a photo acid generator was added in the BCP templates. Before performing phase selective precursor condensation, the templates were exposed to UV radiation through a photomask that has microscopic features. Photo-lithographic exposure triggered area selective generation of acid, which in turn led to patterned formation of silicate network. Because the acid generated in UV exposed field segregate further into hydrophilic domains of the BCP, precursor condensation is controlled in micro and nano-scopic length scales. De-templating via calcination yielded patterned mesoporous silicate films. These mesoporous silicate films inherited two levels of porosity. Microscopic features were inherited from the photomask and the nanoscopic features were inherited from the phase separated block copolymer template. Direct definition of the former followed by replication of pattern obviated the need for additional etching-cleaning steps and offers a cost-effective and compressed process routine for device level structures as small as 90 nm.

TABLE OF CONTENTS

LIST OF TABLES

LIST OF FIGURES

CHAPTER 1

INTRODUCTION

1.1 Block Copolymers

Linear block copolymers (BCPs) consist of two or more polymer chains covalently linked at one of their ends. Due to the connectivity, BCPs undergo microphase separation unlike polymer blends that macroscopically phase separate. BCP's have received enormous attention for applications, owing to their ability to microphase separate into a rich variety of well-defined morphologies. These morphologies are governed by total molecular weight of the copolymer, volume fraction of each block and the strength of interaction between the segments comprising each block, represented by the Flory-Huggins interaction parameter, χ[1-3]. The interaction between the segments can further be described by the Flory-Huggins equation (Equation 1), where f_i is the volume fraction of component 'i' and N is the degree of polymerization.

$$\Delta G/kT = N_1 \ln f_1 + N_2 \ln f_2 + N_0 f_1 f_2 \chi \qquad (1)$$

For the simplest case of a diblock copolymer (AB), the influence of χ and f_i on the microphase separated morphologies can be observed from the morphology diagram shown in the Figure 1.1, where the degree of segregation, χN, is plotted against the volume fraction, f. For any f, χN dictates whether the BCP is microphase separated or phase mixed. The boundary between the microphase separated and phase mixed structures is referred to as the order-disorder transition (ODT) and the boundary between one morphology to another is called the order-order transition (OOT). Depending upon f,

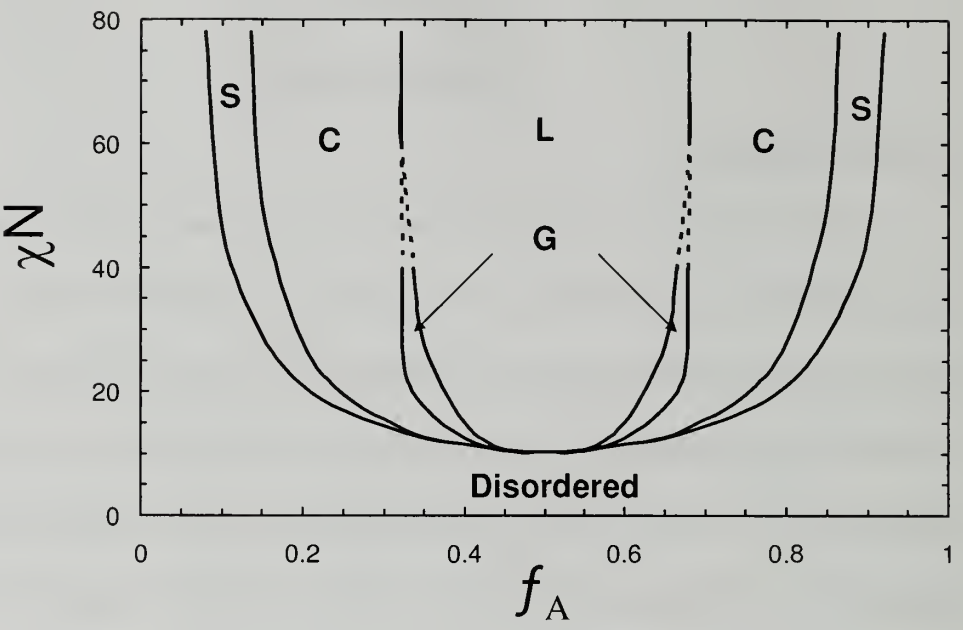

Figure 1.1: Representative phase diagram of diblock copolymer (AB)
(Adapted from Reference 3)

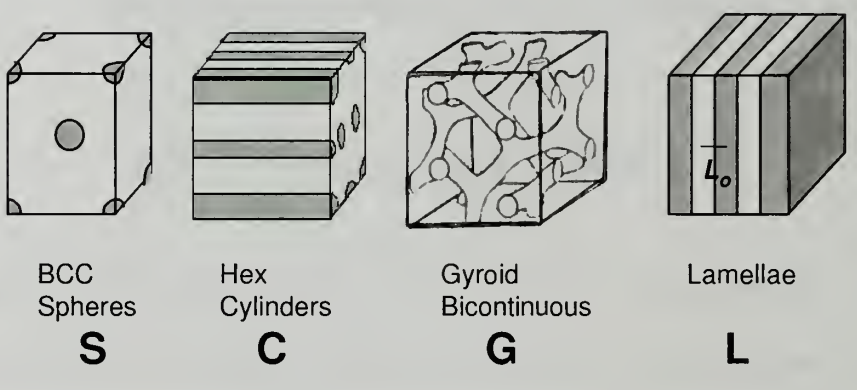

Figure 1.2: Pictorial Representation of diblock copolymer morphologies
(Adapted from Reference 3)

BCPs microphase separated into morphologies, including spherical (S), cylindrical (C), bicontinuous or gyroid (G) and lamellar (L). These morphologies are schematically shown in Figure 1.2.

1.1.1 Block Copolymer Films as Templates

Although bulk BCPs do find applications (for example, photonic crystals[4]), many of the applications realized or proposed to date rely on the microphase separated structure in thin BCP films coated on any suitable substrate[5, 6]. In thin films, the characteristics of the microphase separated morphologies also depend on the surface energy of the blocks, their interactions with substrate and the film thickness (relative to the equilibrium period (L_o) of the BCP in the bulk)[7-9]. Consequently, to control the orientation and ordering of the morphology in thin films, each of the above mentioned parameters have been controlled[8-15]. In addition, external fields like electric fields[6, 16-19], shear[20], eutectic solidification[21], crystallization[22], graphoepitaxy[23], temperature gradients[24], solvent evaporation[25-28] and solvent annealing[29-31] have also been used to control the orientation and ordering of the microphase separated morphologies.

The level of control that has been achieved in BCP films has enabled them to be used as templates and scaffolds for the fabrication of nanostructured materials with applications in data storage[32-34], microelectronics[35], and molecular separations. To generate functional nanostructures from BCP (nanopatterned) templates, various routes have been adopted that can be broadly categorized under two approaches. They are:

(1) the physical approach:[5, 6, 36-40] Block copolymer films are used as etch masks to transfer 'nanoholes' or 'nanodots' patterns into the substrate[41].

(2) the chemical approach:[42-65] Block copolymer films are used as scaffolds or nanoreactors to synthesize inorganic nanostructures[59, 60, 66].

This dissertation will focus on the chemical approach, using block copolymer films as scaffolds. To synthesize inorganic nanostructures using BCP films as scaffolds, various routes that have been adopted to date can further be grouped into two categories:

(i) phase-selective segregation of reactants into pre-formed BCP films[45, 46, 55] or into nanoporous replicas[49, 50, 64, 67] to generate templated nanostructures and

(ii) incorporation of functional precursors into block copolymer structures by incorporating a precursor into one of the blocks or by mixing a precursor with the block copolymer[59, 62, 68]. The subsequent self-assembly yields functional precursors within one of the microdomains, producing patterned materials to generate mesostructured materials[69, 70], nanoparticles[44, 53, 61, 65, 71, 72] or nanoclusters[48, 62, 73] after removing the template.

Both categories, though, have serious drawbacks. In first category, efficient delivery and transportation of reactants into BCP films are limited[74]. Moreover, the use of liquid solvents to deliver the reactants into the BCP template may also swell the microdomains leading to distortion or disruption of the existing morphology in the template. In the second, the requirement of a mutual solvent to dissolve the BCP, desired reactants and other additives limits the available choices of templates. Moreover the size, orientation, and long range order of microdomains cannot be completely controlled[70]. To realize the full potential of BCP templates and to overcome all of the above mentioned drawbacks, supercritical carbon dioxide (sc CO_2) was used as a reaction medium in this work.

1.2 Supercritical Carbon Dioxide

A fluid or any substance can be in a supercritical state above its critical temperature (T_c) and critical pressure (P_c). T_c and P_c denotes the highest temperature and pressure at which the fluid co-exists as a liquid and a vapor at equilibrium. Among many supercritical fluids (SCF), the most commonly used SCF as a solvent is carbon dioxide, since it is nonflammable, nontoxic, and has easily accessible critical properties (T_c = 31° C; P_c = 73.8 bar). The phase diagram[75] of CO_2 is shown in Figure 1.3. As the temperature and pressure is increased along the liquid-gas line, the distinction (meniscus) between these two states diminishes and, eventually, disappears as the two phases emerge as a surface tension-less supercritical phase. One of the important characteristics of SCF is the tunable solvent quality, which is related to its density. By changing the pressure and temperature, the density of SCF can be changed anywhere from less than 0.1 g/cm^3 to more than 1 g/cm^3 (Figure 1.4). Similar to density, other physicochemical properties, including the viscosity are also pressure dependent with values intermediate between those of the liquid and gaseous states, as shown in table 1.1. Liquid-like densities and gas-like diffusivity enable facile dissolution and transportation of many organic and organometallic compounds in SCFs[74]. These organic and organometallic compounds may also be precursors and reactants for subsequent reactions in the BCP templates.

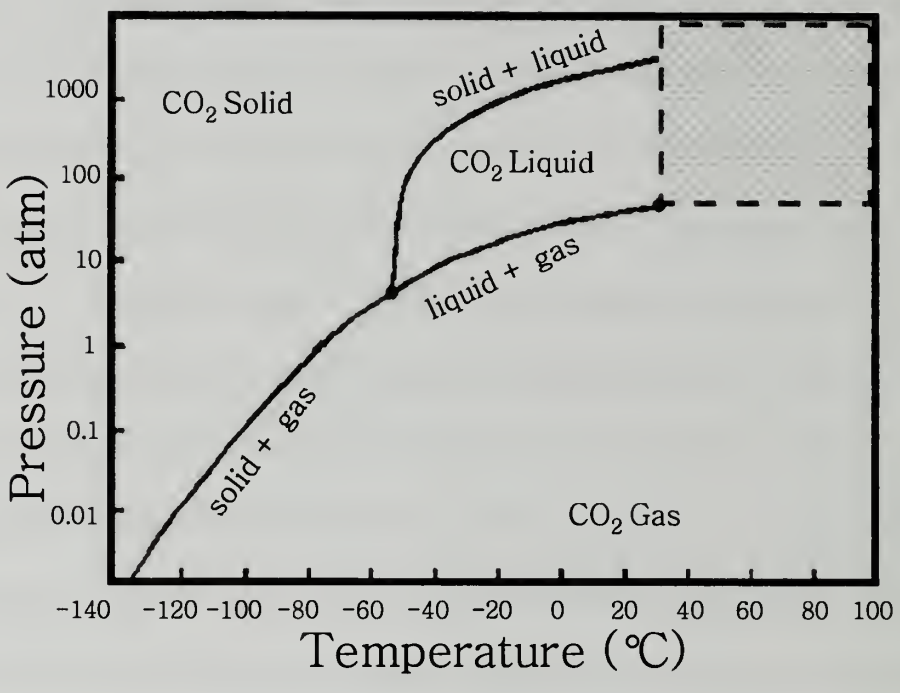

Figure 1.3: Phase Diagram of Carbon dioxide
(Adapted from Reference 75)

Table 1.1: Comparison of selected physicochemical properties of supercritical fluids to those of liquids and gases[76]

Physicochemical Properties	Liquid	Supercritical Fluid	Gas
Density (g/cm^3)	1	0.1- 1	10^{-3}
Viscosity (Pa-S)	10^{-3}	10^{-4} - 10^{-5}	10^{-5}
Diffusivity (cm^2/sec)	10^{-5}	10^{-3}	10^{-1}
Surface Tension (Dynes/cm)	20-50	0	0

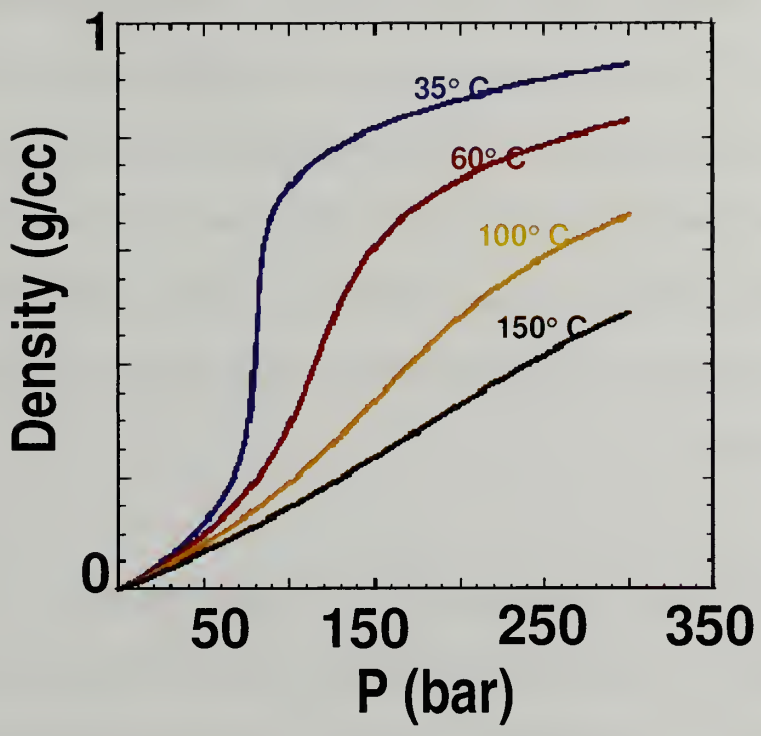

Figure 1.4: Density of CO_2 as a function of pressure for isotherms at 35 °C, 60 °C, 100 °C and 150 °C[76]

With the exceptions of silicones and fluorocarbons, most of polymers are insoluble in supercritical CO_2 (sc CO_2). However, sc CO_2, owing to its tunable density, can be used to swell the polymers with precise control over the degree of dilation[77]. The dilation of the polymers causes a depression in the glass transition temperature[78], which increase the diffusivity of small molecules within BCP[79, 80]. The combination of precursor/reactants solubility, swellability of polymers, favorable transport properties and the absence of surface tension enables solution based chemistry and processing in a supercritical medium that behaves much like a gas. Being a gas at ambient conditions, sc CO_2 can be easily removed at the end of a reaction by simply decreasing the pressure and temperature. Because of all of these favorable attributes, sc CO_2 has been used as a

reaction medium for variety of purposes[74, 81-83] including the preparation of polymer blends[84-86], conformal deposition of metal films[87-89], synthesis of metal nanoparticles[90, 91] and nanowires[92]. While performing reactions within block copolymer templates in sc CO_2 medium, SCF induced swelling can be adjusted in such a way that it is high enough to overcome transport limitations and it is still low enough to preserve order in the microdomains. Hence sc CO_2 is an ideal reaction medium to perform chemistry in BCPs. One such chemistry in sc CO_2, introduced in the following section, will be the focus of this dissertation.

1.3 Silica Chemistry in Supercritical CO_2 – Swollen Polymers

Recently, Watkins and co-workers developed a new approach to mesoporous metal oxide films by performing phase selective silica deposition in pre-organized BCP templates using sc CO_2 as a reaction medium[93, 94]. The schematic of the process is shown in Figure 1.5. The templates are prepared via spin-coating amphiphilic block copolymers from solutions that contain a trace amount of organic acid. Upon drying and annealing, the acid catalyst segregates into the hydrophilic domain of the block copolymer template. The template is then exposed to a solution of metal alkoxides, whereupon the precursor is infused into the template and undergoes hydrolysis and condensation polymerization selectively within the acid-doped hydrophilic domains to yield a silica network. Transport and diffusion of precursor into the template is enhanced due to the modest dilation of the template in sc CO_2. The template is then removed by calcination at 400 °C or by reactive plasma etching to produce mesoporous metal oxide films having the morphology of templates.

The concept was demonstrated using PEO-b-PPO-PEO (Pluronics) triblock copolymers as the templates and para-toluene sulfonic acid as the catalyst to condense the silicate network from the silica precursor, tetra ethyl orthosilicate (TEOS) to produce mesoporous silicate films[93]. Mesoporous organosilicate films[95] have also been prepared using appropriate organosilicate precursor and these films have been shown to be a promising candidate for semiconductor applications. The following paragraph summarizes some of the important features of this process.

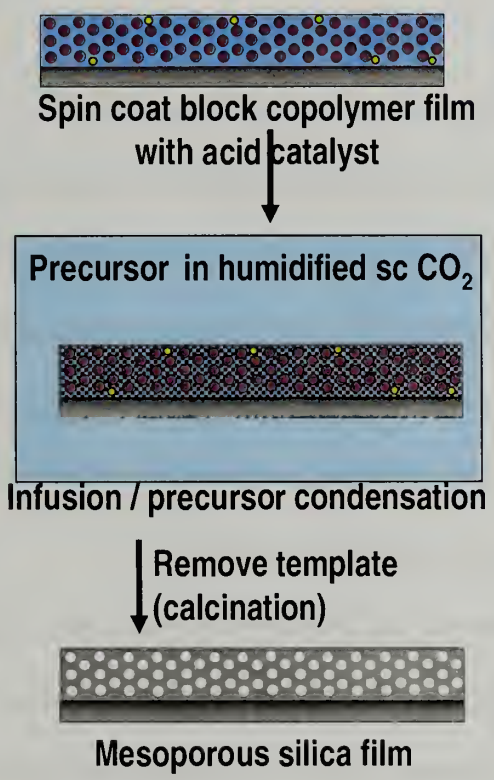

Figure 1.5: Schematic drawing of the synthesis of mesoporous metal oxides in sc CO_2 (Adapted from Reference 92)

First and foremost is the ability to separate template formation and precursor condensation, while the delivery and transport of precursor is not transport limited and, in fact, accelerated because of the usage of sc CO_2. (ii) Segregation of acid into one domain

is essential to restrict the condensation of precursor within one domain, and the generation of mesoporous materials. (iii) During alkoxide condensation, alcohol is formed as a by-product, which is miscible with sc CO_2 and can be extracted rapidly from the template during depressurization. Such rapid removal of alcohol drives the condensation towards completion and yields robust mesoporous silicate films having high threshold for cracking. (iv) As it is a heterogeneous approach, a mutual solvent that dissolves the block copolymer, precursor and other additives is not necessary.

1.4. Objective and Overview of this Dissertation

The central theme for this dissertation is derived from the fact that the above mentioned 3-D replication process is a two step approach, which enables a tuning of a specific morphology before the metal oxide network replication. Hence, the objective of this dissertation is to combine the recent advances in controlling the BCP morphology in thin films with the two-step method for silicate films so as to develop new routes toward fabrication of novel mesoporous materials.

While the rest of this chapter briefly discusses various characterization techniques used in this dissertation, Chapter 2 describes a novel route to mesoporous silicate films with perpendicular nanochannels[96]. Obtaining such a morphology in mesoporous materials has proven to be challenging, though they are promising candidates for applications ranging from catalysis to sensors and the separations. Chapters 3, 4 and 5 describe an extensive study that involves a simple, cost-effective route to preparation of patterned mesoporous silicate films[97]. In particular, Chapter 3 discusses the possibility of using Pluronics and poly (hydroxy styrene) block copolymers as templates. Chapter 4 and

5 report the results obtained from chemically amplifiable block copolymer templates, poly(tert-butyoxy carbonyloxy styrene) copolymers and poly(tert-butyl methacrylate) copolymers, respectively. Finally Chapter 6 concludes with overall summary and future directions for this work.

1.5. Characterization Techniques

Various imaging, scattering and spectroscopic techniques have been used in this dissertation to characterize block copolymer, silica infused nanocomposite and calcined silica films. A brief introduction to each of them is given in this section.

1.5.1 Imaging Techniques – Optical and Electron Microscopy

Optical microscopes are the simplest and oldest of the microscopes and they are often referred as 'light microscope'. A typical microscope consists of a source (of radiation), a condenser system, a specimen stage, an objective lens and a projector system. Optical microscopes (OMs) use visible light (0.4 – 0.7 μm) as a probing radiation to generate magnified images of small samples. Images can be generated in two common modes: (i) transmission and (ii) reflection. In transmission mode, visible radiation is allowed to transmit through the sample and such transmitted light is collected, magnified and projected on an imaging screen. The contrast in the image is originated from the differences in optical density (causing intensity variations) and/or differences in selected absorption of different wavelengths (giving rise to color variations). In reflection mode, sample is exposed to visible radiation and the radiation reflected off the sample is

collected. Surface topography is obtained using the constructive and destructive interferences of the incident and reflected light[98].

As the resolution of imaging technique is dependent on the wavelength of the radiation used, OM is used to image microscopic features and to image nanoscopic structures electron microscopes are used.

Transmission electron microscope (TEM) is comparable to OM except that the probing radiation in the former is a beam of electrons, which are generated by thermionic emission from a tungsten filament. The electrons are then accelerated by an electrical potential and focused by electrostatic and electromagnetic lenses onto an ultra-thin specimen[107]. The beam interacts with the matter depending on the differences in electron density. The beam that is transmitted through the specimen is collected, magnified and focused by an objective lens and further projected on an imaging screen or on a photographic plate. The path of the beam from source to detector in the TEM column is evacuated so that the transmitted radiation contains information only about the specimen and not about the surrounding medium. Under favorable conditions the most capable instruments can resolve detail at the 0.1 nm level[98], but such high resolution examination is seldom possible with polymers. However, it is possible to obtain information within the range of 1-100 nm with varying degrees of difficulty. A further advantage of TEM is that it can be rapidly adjusted to provide an electron diffraction pattern from a selected area, facilitating investigations of crystal structures, long range ordered morphologies and their orientations. The main disadvantage of the TEM is that it can be used only on thin samples, preferably less than 100 nm thick.

Scanning electron microscope (SEM), on the other hand, images the sample surface by scanning it with a high energy beam of electrons in a raster scan pattern. The electrons interact with the atomic species that comprise the sample and these interactions[98] can be described as follows:

(i) Some electrons are backscattered as a consequence of the electrostatic attraction between the negatively charged free electron in the incident primary beam and the positively charged nucleus within the specimen (Rutherford scattering)

(ii) Some primary beam electrons interact directly with electrons within the atoms of the specimen, knocking them free ('secondary electrons')

(iii) After a secondary electron has been removed from an inner shell, an electron from a less tightly bound state falls into the inner shell, with the emission of a photon which is often in the X-ray range of the electromagnetic spectrum.

Various detectors are arranged in the specimen chamber for the measurement of the several signals which are characteristic of the region of the specimen under bombardment. The electron beam can be moved over the surface of the specimen using a variable magnetic field provided by the current-carrying 'scan coils'. When the beam moves to a different site the characteristic signal measured by any of the detectors may change, and this is exploited to form 'image contrast'. One of the important limitations of SEM is the specimen damage caused by the specimen charging that occurs when the sample is non-conductive and by the bombardment of the high energy electron beam.

1.5.2 Imaging Techniques – Scanning Force Microscopy

Scanning force microscopy (SFM) is a high resolution surface imaging technique, in which variations in height (topology) and composition (material properties) can be measured[99]. The typical SFM instrument consists of a fine tip formed at the end of a cantilever spring. The tip, used to scan the sample surface, is usually fabricated from either silicon or silicon nitride. When the tip approaches the sample surface it experiences a combination of attractive and repulsive forces which are a function of the interatomic interactions between tip and surface[98]. The cantilever deflects in response to the atomic force vibrations between the sample and the tip and is monitored using a laser beam focused onto the end of the cantilever, at the tip. The back surface of the cantilever reflects the laser beam onto a split photo-diode detector and the output signal is compared with a reference to generate a topographic image or a map of any other physical properties of the sample surface.

SFM can be performed in different operational modes and the basic operational mode is called as contact mode. In this mode, the tip is dragged over the sample surface with a constant velocity and under a constant normal load while the tip is in intimate contact with the surface. The contact mode allows tracking of surface topography with a high precision and also provides the highest lateral resolution of 0.2 – 0.3 nm[98], but imposes a high local pressure and shear stresses on the surface. Such high local stresses can easily damage soft polymeric surfaces. To overcome the surface damage problems, an intermittent contact mode has been introduced. The basic idea of this dynamic mode (otherwise called as "tapping mode") is replacing the tip-surface contacts with brief approachings of the oscillating tip[100]. The stiff tip oscillates with a high frequency close

to its resonant frequency (usually, 200 – 400 kHz). In the vicinity of the surface, weak interactions can significantly change the amplitude of tip oscillations and lead to a phase shift. By measuring the changes in amplitude and in phase, variations in topology and in viscoelastic properties of the surfaces can be obtained respectively. Lateral resolution of the tapping mode is substantially lower than that for the contact mode and is about 1 nm for topography and 10 nm for other properties.

1.5.3 Scattering Techniques – Small Angle X-ray Scattering (SAXS)

Small angle X-ray scattering (SAXS) is an analytical X-ray application technique for the structural characterization of solid and fluid materials in the nanometer range. In order for the X-rays to be scattered, an electron density difference is required in the sample[101]. In a typical SAXS experiment, monochromatic X-ray beam is sent through a polymer sample and the scattered radiation is collected in the detector as a function of scattering wavevector 'q'. A general scattering diagram is shown in the Figure 1.6 and the mathematical expression for q is given in equation 2.

$$q = k_i - k_f = (4\pi/\lambda)\sin\theta \qquad (2)$$

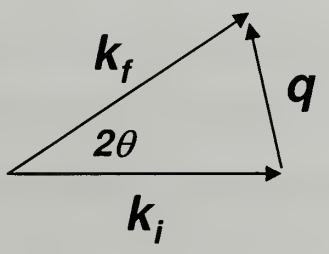

Figure 1.6: Vectorial representation of a scattering geometry

The relationship between the scattering angle and the distance, d, between periodic planes containing the scatterers is given by Bragg's Law (equation 3). Combining equations 2 and 3, one can get a direct relation between d and scattering wavevector q, as it is given in equation 4

$$2d\sin\theta = n\,\lambda \qquad (3)$$

$$d = 2\,\pi/q \qquad (4)$$

$$I(q) = KF(q)S(q) \qquad (5)$$

The inverse relationship between the scattering angle and d-spacing is evident in equation 4 and, hence, the larger the lattice in the sample, the smaller the scattering angle and vice versa.

Irrespective of the radiation used for scattering, the intensity of scattering is given by equation 5. In general, there are two contributions to the scattering, one is the shape of the scatterer, which is referred as form factor, F(q). The form factor is the Fourier transform of the shape of the scatterers. The second contribution is the spatial organization of the scatterers, which is referred as structure factor S(q). In the case of block copolymers, microdomains are the scatterers. The constructive and destructive interference of these scattering contributions give rise to the angular dependence(q) of the small angle scattering. Optical constant, K, is proportional to the square of the appropriate property difference between the scatterers and their environment.

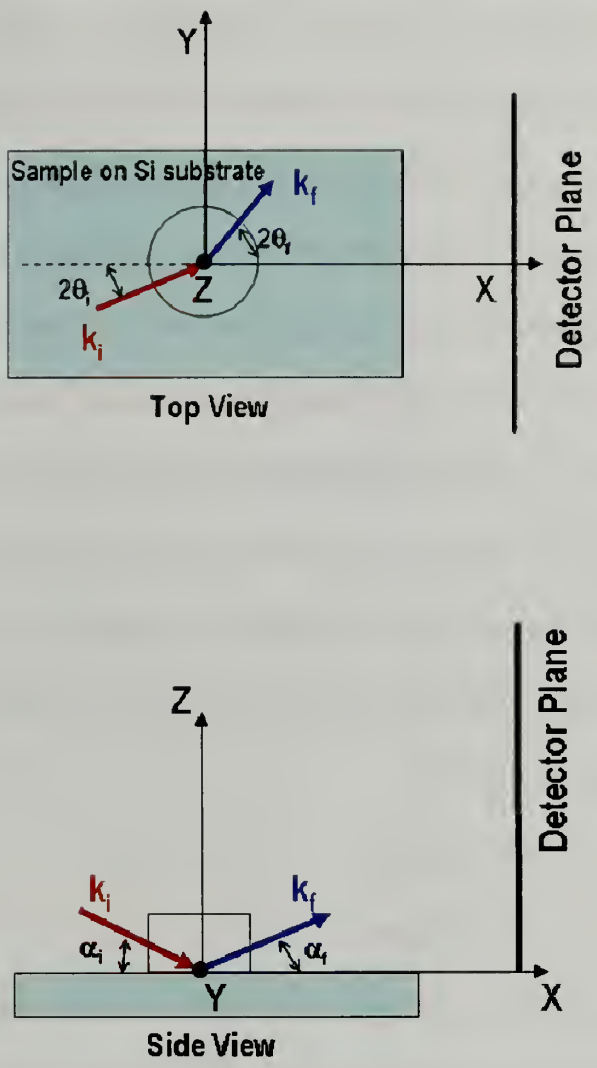

Figure 1.7: Scattering geometry in GISAXS set-up
(Adapted from Reference 101)

Grazing-incidence small angle X-ray scattering is used for characterizing density correlations at surfaces, at buried interfaces or in thin films. The scattering geometry[102] (top view and side view) is shown in Figure 1.7. A monochromatic X-ray beam impinges onto a surface at an angle near the critical angle of the film and the scattered radiation is collected in a 2-dimensional detector plate. The area detector records the scattered rays

over a range of exit angles α_f and in-plane scattering angles $2\theta_f$. GISAXS intensity distribution in the vertical direction corresponds to a detector scan in reflectivity and the intensity distribution parallel to the surface corresponds to SAXS. Hence both the lateral organization of scatterers and their orientation/distribution through the sample can be derived from the GISAXS patterns. Moreover, by changing the incident angle of the impinging radiation, the depth of penetration in the sample can also be controlled. To obtain GISAXS patterns corresponding to the scatterers at the surface, the incident angle must be less than or equal to critical angle, whereas to get information about the buried scatterers or to get a representative data of entire film, incident angle must be higher than critical angle. Critical angle (θ_c), defined as an angle below which the incident radiation is totally externally reflected, can be mathematically represented, using Snell's law, as shown in equations 6 and 7

$$n_1\cos\theta_1 = n_2\cos\theta_2 \qquad (6)$$

$$\theta_c = \arccos(n_2/n_1) \qquad (7)$$

where n_1 and n_2 refer to the refractive index of the medium and that of the thin film and θ_1 and θ_2 denote the angles of incidence and the refraction.

1.5.4 Spectroscopic Techniques – FT-IR Spectroscopy

Infra-red spectroscopy is one of the common techniques used to identify the chemical composition in the polymeric systems[103, 104]. Energy required for molecular vibrations are in the same range as the energy corresponding to the infra red radiation (Planck's equation). In simple terms, the infrared spectrum of a sample is collected by passing a beam of infrared light through the sample. Examination of the transmitted light

reveals how much energy was absorbed at each wavelength. This can be done with a monochromatic beam, which changes in wavelength over time, or by using a Fourier transform instrument to measure all wavelengths at once. From this, a transmittance or absorbance spectrum can be produced, showing at which IR wavelengths the sample absorbs. Analysis of these absorption characteristics reveals details about the molecular structure of the sample.

In this work, FT-IR spectroscopy is used to follow the changes in the chemical functionalities, present in the polymer templates, after various processing conditions.

1.5.5 Spectroscopic Techniques – Spectroscopic Ellipsometry

Ellipsometry is a non-destructive optical technique to determine the properties of thin films, such as thickness, refractive index, surface roughness, absorption coefficient and number of layers[105, 106]. In this technique, a radiation of known polarization is allowed to reflect off the thin film under study and the change in polarization of the reflected radiation with respect to that of incident radiation is measured. The instrument measures only two parameters, ψ and Δ, where ψ denotes relative amplitude change and Δ denotes relative phase change and they are related by the following equations 8 and 9, where ρ is the complex ratio of Fresnel reflection coefficients (R_p and R_s) of *p* and *s* polarized waves (*s* refers to the oscillations perpendicular to the plane of incidence and parallel to the sample surface, and *p* refers to the oscillations parallel to the plane of incidence). Thickness and other above mentioned properties are extracted using a model based analysis of the obtained data.

$$R_p/R_s = \rho = \tan\psi . e^{i\Delta} \qquad (8)$$

$$R_p = /R_p/e^{i\Delta p} \quad \& \; R_s = /R_s/e^{i\Delta s} \qquad (9)$$

Standard ellipsometry uses radiation of one wavelength at one angle of incidence for analysis, whereas spectroscopic ellipsometry (SE) uses a spectrum of wavelength at one angle of incidence. Further, variable angle spectroscopic ellipsometry (VASE) uses spectrum of radiation with many angles of incidence. In this dissertation, SE with one angle of incidence (75) and radiation in visible spectrum (400 – 800 nm) was used to determine thickness and refractive index of thin films.

1.6. References

1. Leibler, L., *Macromolecules* **1980,** 13, 1602.

2. Bates, F. S.; Fredrickson, G. H., *Annu. Rev. Phys. Chem.* **1990,** 41, 525.

3. Bates, F. S.; Fredrickson, G. H., *Physics Today* **1999,** 52, 32.

4. Fink, Y.; Urbas, A. M.; Bawendi, M. G.; Joannopoulos, J. D.; Thomas, E. L., *J. Lightwave Technol.* **1999,** 17, 1963.

5. Hamley, I. W., *Nanotechnology* **2003,** 14, R39.

6. Hawker, C. J.; Russell, T. P., *Mrs Bulletin* **2005,** 30, 952.

7. Fasolka, M. J.; Mayes, A. M., *Annu. Rev. Mater. Res.* **2001,** 31, 323.

8. Fasolka, M. J.; Banerjee, P.; Mayes, A. M.; Pickett, G.; Balazs, A. C., *Macromolecules* **2000,** 33, 5702.

9. Russell, T. P.; Coulon, G.; Deline, V. R.; Miller, D. C., *Macromolecules* **1989,** 22, 4600.

10. Elhadj, S.; Woody, J. W.; Niu, V. S.; Saraf, R. F., *Appl. Phys. Lett.* **2003,** 82, 871.

11. Fasolka, M. J.; Harris, D. J.; Mayes, A. M.; Yoon, M.; Mochrie, S. G. J., *Phys. Rev. Lett.* **1997,** 79, 3018.

12. Kimura, M.; Misner, M. J.; Xu, T.; Kim, S. H.; Russell, T. P., *Langmuir* **2003,** 19, 9910.

13. Lin, Y.; Boker, A.; He, J. B.; Sill, K.; Xiang, H. Q.; Abetz, C.; Li, X. F.; Wang, J.; Emrick, T.; Long, S.; Wang, Q.; Balazs, A.; Russell, T. P., *Nature* **2005,** 434, 55.

14. Mansky, P.; Liu, Y.; Huang, E.; Russell, T. P.; Hawker, C., *Science* **1997,** 275, 1458.

15. Park, S. M.; Craig, G. S. W.; La, Y. H.; Solak, H. H.; Nealey, P. F., *Macromolecules* **2007,** 40, 5084.

16. Boker, A.; Knoll, A.; Elbs, H.; Abetz, V.; Muller, A. H. E.; Krausch, G., *Macromolecules* **2002,** 35, 1319.

17. Mansky, P.; DeRouchey, J.; Russell, T. P.; Mays, J.; Pitsikalis, M.; Morkved, T.; Jaeger, H., *Macromolecules* **1998,** 31, 4399.

18. Morkved, T. L.; Lu, M.; Urbas, A. M.; Ehrichs, E. E.; Jaeger, H. M.; Mansky, P.; Russell, T. P., *Science* **1996,** 273, 931.

19. Olayo-Valles, R.; Guo, S. W.; Lund, M. S.; Leighton, C.; Hillmyer, M. A., *Macromolecules* **2005,** 38, 10101.

20. Register, R. A.; Angelescu, D. E.; Pelletier, V.; Asakawa, K.; Wu, M. W.; Adamson, D. H.; Chaikin, P. M., *J. Photopolym. Sci. Technol.* **2007,** 20, 493.

21. De Rosa, C.; Park, C.; Thomas, E. L.; Lotz, B., *Nature* **2000,** 405, 433.

22. Park, C.; De Rosa, C.; Thomas, E. L., *Macromolecules* **2001,** 34, 2602.

23. Segalman, R. A.; Yokoyama, H.; Kramer, E. J., *Adv.Mater.* **2001,** 13, 1152.

24. Bodycomb, J.; Funaki, Y.; Kimishima, K.; Hashimoto, T., *Macromolecules* **1999,** 32, 2075.

25. Kim, G.; Libera, M., *Macromolecules* **1998,** 31, 2569.

26. Kim, G.; Libera, M., *Macromolecules* **1998,** 31, 2670.

27. Lin, Z. Q.; Kim, D. H.; Wu, X. D.; Boosahda, L.; Stone, D.; LaRose, L.; Russell, T. P., *Adv. Mater.* **2002,** 14, 1373.

28. Li, M. Q.; Douki, K.; Goto, K.; Li, X. F.; Coenjarts, C.; Smilgies, D. M.; Ober, C. K., *Chem. Mater.* **2004,** 16, 3800.

29. Kim, S. H.; Misner, M. J.; Xu, T.; Kimura, M.; Russell, T. P., *Adv.Mater.* **2004,** 16, 226.

30. Kim, S. H.; Misner, M. J.; Russell, T. P., *Adv. Mater.* **2004,** 16, 2119.

31. Park, S.; Wang, J. Y.; Kim, B.; Chen, W.; Russell, T. P., *Macromolecules* **2007,** 40, 9059.

32. Cheng, J. Y.; Ross, C. A.; Chan, V. Z. H.; Thomas, E. L.; Lammertink, R. G. H.; Vancso, G. J., *Adv. Mater.* **2001,** 13, 1174.

33. Asakawa, K.; Hiraoka, T.; Hieda, H.; Sakurai, M.; Kamata, Y., *J. Photopolym. Sci. Technol.* **2002,** 15, 465.

34. Hieda, H.; Yanagita, Y.; Kikitsu, A.; Maeda, T.; Naito, K., *J. Photopolym. Sci. Technol.* **2006,** 19, 425.

35. Black, C. T.; Ruiz, R.; Breyta, G.; Cheng, J. Y.; Colburn, M. E.; Guarini, K. W.; Kim, H. C.; Zhang, Y., *Ibm Journal of Research and Development* **2007,** 51, 605.

36. Cheng, J. Y.; Ross, C. A.; Thomas, E. L.; Smith, H. I.; Vancso, G. J., *Appl. Phys. Lett.* **2002,** 81, 3657.

37. Guarini, K. W.; Black, C. T.; Zhang, Y.; Kim, H.; Sikorski, E. M.; Babich, I. V., *Journal of Vacuum Science & Technology B* **2002,** 20, 2788.

38. Harrison, C.; Park, M.; Chaikin, P. M.; Register, R. A.; Adamson, D. H., *Journal of Vacuum Science & Technology B* **1998,** 16, 544.

39. Park, C.; Yoon, J.; Thomas, E. L., *Polymer* **2003,** 44, 6725.

40. Shin, K.; Leach, K. A.; Goldbach, J. T.; Kim, D. H.; Jho, J. Y.; Tuominen, M.; Hawker, C. J.; Russell, T. P., *Nano Lett.* **2002,** 2, 933.

41. Park, M.; Harrison, C.; Chaikin, P. M.; Register, R. A.; Adamson, D. H., *Science* **1997,** 276, 1401.

42. Aizawa, M.; Buriak, J. M., *Chem. Mater.* **2007,** 19, 5090.

43. Antonietti, M.; Wenz, E.; Bronstein, L.; Seregina, M., *Adv. Mater.* **1995,** 7, 1000.

44. Cheng, K. W.; Chan, W. K., *Langmuir* **2005,** 21, 5247.

45. Cornelissen, J.; van Heerbeek, R.; Kamer, P. C. J.; Reek, J. N. H.; Sommerdijk, N.; Nolte, R. J. M., *Adv. Mater.* **2002,** 14, 489.

46. Cummins, C. C.; Schrock, R. R.; Cohen, R. E., *Chem. Mater.* **1992,** 4, 27.

47. Du, P.; Li, M. Q.; Douki, K.; Li, X. F.; Garcia, C. R. W.; Jain, A.; Smilgies, D. M.; Fetters, L. J.; Gruner, S. M.; Wiesner, U.; Ober, C. K., *Adv. Mater.* **2004,** 16, 953.

48. Kane, R. S.; Cohen, R. E.; Silbey, R., *Chem. Mater.* **1996,** 8, 1919.

49. Kim, H. C.; Jia, X. Q.; Stafford, C. M.; Kim, D. H.; McCarthy, T. J.; Tuominen, M.; Hawker, C. J.; Russell, T. P., *Adv. Mater.* **2001,** 13, 795.

50. Kim, D. H.; Lin, Z. Q.; Kim, H. C.; Jeong, U.; Russell, T. P., *Adv. Mater.* **2003,** 15, 811.

51. Kim, D. H.; Lau, K. H. A.; Robertson, J. W. F.; Lee, O. J.; Jeong, U.; Lee, J. I.; Hawker, C. J.; Russell, T. P.; Kim, J. K.; Knoll, W., *Adv. Mater.* **2005,** 17, 2442.

52. Li, R. R.; Dapkus, P. D.; Thompson, M. E.; Jeong, W. G.; Harrison, C.; Chaikin, P. M.; Register, R. A.; Adamson, D. H., *Appl. Phys. Lett.* **2000,** 76, 1689.

53. Misner, M. J.; Skaff, H.; Emrick, T.; Russell, T. P., *Adv. Mater.* **2003,** 15, 221.

54. Nardin, C.; Widmer, J.; Winterhalter, M.; Meier, W., *European Physical Journal E* **2001,** 4, 403.

55. Cohen, R. E., *Current Opinion in Solid State & Materials Science* **1999,** 4, 587.

56. Olayo-Valles, R.; Lund, M. S.; Leighton, C.; Hillmyer, M. A., *J. Mater. Chem.* **2004,** 14, 2729.

57. Park, S.; Kim, B.; Wang, J. Y.; Russell, T. P., *Adv. Mater.* **2008,** 20, 681.

58. Sankaran, V.; Yue, J.; Cohen, R. E.; Schrock, R. R.; Silbey, R. J., *Chem. Mater.* **1993,** 5, 1133.

59. Spatz, J. P.; Herzog, T.; Mossmer, S.; Ziemann, P.; Moller, M., *Adv. Mater.* **1999,** 11, 149.

60. Spatz, J. P.; Mossmer, S.; Hartmann, C.; Moller, M.; Herzog, T.; Krieger, M.; Boyen, H. G.; Ziemann, P.; Kabius, B., *Langmuir* **2000,** 16, 407.

61. Sun, Z. C.; Gutmann, J. S., *Physica a-Statistical Mechanics and Its Applications* **2004,** 339, 80.

62. Tadd, E. H.; Bradley, J.; Tannenbaum, R., *Langmuir* **2002,** 18, 2378.

63. Temple, K.; Kulbaba, K.; Power-Billard, K. N.; Manners, I.; Leach, K. A.; Xu, T.; Russell, T. P.; Hawker, C. J., *Adv. Mater.* **2003,** 15, 297.

64. Thurn-Albrecht, T.; Schotter, J.; Kastle, C. A.; Emley, N.; Shibauchi, T.; Krusin-Elbaum, L.; Guarini, K.; Black, C. T.; Tuominen, M. T.; Russell, T. P., *Science* **2000,** 290, 2126.

65. Yin, D.; Horiuchi, S.; Masuoka, T., *Chem. Mater.* **2005,** 17, 463.

66. Spatz, J. P.; Chan, V. Z. H.; Mossmer, S.; Kamm, F. M.; Plettl, A.; Ziemann, P.; Moller, M., *Adv. Mater.* **2002,** 14, 1827.

67. Jeoung, E.; Galow, T. H.; Schotter, J.; Bal, M.; Ursache, A.; Tuominen, M. T.; Stafford, C. M.; Russell, T. P.; Rotello, V. M., *Langmuir* **2001,** 17, 6396.

68. Haupt, M.; Miller, S.; Glass, R.; Arnold, M.; Sauer, R.; Thonke, K.; Moller, M.; Spatz, J. P., *Adv. Mater.* **2003,** 15, 829.

69. Kresge, C. T.; Leonowicz, M. E.; Roth, W. J.; Vartuli, J. C.; Beck, J. S., *Nature* **1992,** 359, 710.

70. Yang, P. D.; Zhao, D. Y.; Margolese, D. I.; Chmelka, B. F.; Stucky, G. D., *Nature* **1998,** 396, 152.

71. Horiuchi, S.; Fujita, T.; Hayakawa, T.; Nakao, Y., *Langmuir* **2003,** 19, 2963.

72. Minelli, C.; Geissbuehler, I.; Hinderling, C.; Heinzelmann, H.; Vogel, H.; Pugin, R.; Liley, M., *J. Nanosci. Nanotechnol.* **2006,** 6, 1611.

73. Chan, Y. N. C.; Craig, G. S. W.; Schrock, R. R.; Cohen, R. E., *Chem. Mater.* **1992,** 4, 885.

74. O'Neil, A.; Watkins, J. J., *Mrs Bulletin* **2005,** 30, 967.

75. Shakhashiri Carbon Dioxide. http://scifun.chem.wisc.edu/chemweek/PDF/CarbonDioxide.pdf (May 2008),

76. Linstrom, P. J.; Mallard, M. G. NIST Standard Reference Database Number 69. http://webbook.nist.gov (June 2005),

77. Wissinger, R. G.; Paulaitis, M. E., *Journal of Polymer Science Part B-Polymer Physics* **1987,** 25, 2497.

78. Sirard, S. M.; Ziegler, K. J.; Sanchez, I. C.; Green, P. F.; Johnston, K. P., *Macromolecules* **2002,** 35, 1928.

79. Gupta, R. R.; RamachandraRao, V. S.; Watkins, J. J., *Macromolecules* **2003,** 36, 1295.

80. Gupta, R. R.; Lavery, K. A.; Francis, T. J.; Webster, J. R. P.; Smith, G. S.; Russell, T. P.; Watkins, J. J., *Macromolecules* **2003,** 36, 346.

81. Jones, C. A.; Zweber, A.; DeYoung, J. P.; McClain, J. B.; Carbonell, R.; DeSimone, J. M., *Critical Reviews in Solid State and Materials Sciences* **2004,** 29, 97.

82. Namatsu, H., *Journal of Photopolymer Science and Technology* **2002,** 15, 381.

83. Xie, B.; Muscat, A. J., *Microelectronic Engineering* **2004,** 76, 52.

84. Watkins, J. J.; McCarthy, T. J., *Macromolecules* **1994,** 27, 4845.

85. Watkins, J. J.; McCarthy, T. J., *Chem. Mater.* **1995,** 7, 1991.

86. Watkins, J. J.; McCarthy, T. J., *Macromolecules* **1995,** 28, 4067.

87. Blackburn, J. M.; Long, D. P.; Watkins, J. J., *Chemistry of Materials* **2000,** 12, 2625.

88. Blackburn, J. M.; Long, D. P.; Cabanas, A.; Watkins, J. J., *Science* **2001,** 294, 141.

89. Cabanas, A.; Long, D. P.; Watkins, J. J., *Chem. Mater.* **2004,** 16, 2028.

90. Cason, J. P.; Khambaswadkar, K.; Roberts, C. B., *Industrial & Engineering Chemistry Research* **2000,** 39, 4749.

91. Kitchens, C. L.; Roberts, C. B., *Industrial & Engineering Chemistry Research* **2004,** 43, 6070.

92. Davidson, F. M.; Schricker, A. D.; Wiacek, R. J.; Korgel, B. A., *Advanced Materials* **2004,** 16, 646.

93. Pai, R. A.; Humayun, R.; Schulberg, M. T.; Sengupta, A.; Sun, J. N.; Watkins, J. J., *Science* **2004,** 303, 507.

94. Vogt, B. D.; Pai, R. A.; Lee, H. J.; Hedden, R. C.; Soles, C. L.; Wu, W. L.; Lin, E. K.; Bauer, B. J.; Watkins, J. J., *Chemistry of Materials* **2005,** 17, 1398.

95. Pai, R. A.; Watkins, J. J., *Adv.Mater.* **2006,** 18, 241.

96. Nagarajan, S.; Li, M. Q.; Pai, R. A.; Bosworth, J. K.; Busch, P.; Smilgies, D. M.; Ober, C. K.; Russell, T. P.; Watkins, J. J., *Adv. Mater.* **2008,** 20, 246.

97. Nagarajan, S.; Bosworth, J. K.; Ober, C. K.; Russell, T. P.; Watkins, J. J., *Chem. Mater.* **2008,** 20, 604.

98. Campbell, D.; Pethrick, R. A.; White, J. R., *Polymer Characterization*. second ed.; Stanley Thornes Ltd: Glos, 2000; p 481.

99. Lapshin, R. V., *Nanotechnology* **2004,** 15, 1135.

100. Ratner, D. B.; Tsukruk, V. V., *Scanning Probe Microscopy of Polymers*. American Chemical Society: Washington, DC, 1996; p 367.

101. Guinier, A.; Fournet, G., *Small Angle Scattering of X-Rays*. Wiley: New York, 1955; p 264.

102. Lazzari, R., *Journal of Applied Crystallography* **2002,** 35, 406.

103. Socrates, G., *Infrared Characteristic Group Frequencies*. Second ed.; John Wiley & Sons: West Sussex, 1994; p 249.

104. Young, R. J.; Lovell, P. A., *Introduction to Polymers*. second ed.; Chapman & Hall: New York, 1991; p 443.

105. Tompkins, H. G.; McGahan, W. A., *Spectroscopic Ellipsometry and Reflectometry*. Second ed.; John Wiley & Sons: West Sussex, 1999; p 353.

106. Richards, R. W.; Peace, S. K., *Polymer Surfaces and Interfaces III*. John Wiley & Sons: West Sussex, 1999; p 304.

107. http://www.wikipedia.com.

CHAPTER 2

AN EFFICIENT ROUTE TO MESOPOROUS SILICA FILMS WITH PERPENDICULAR NANOCHANNELS

2.1 Introduction

The fabrication of mesoporous silica films with well-defined morphologies[1] offers tremendous opportunity for device structures. In particular the generation of a mesoporous silica film with cylindrical nanochannels of prescribed diameters oriented normal to the substrate holds great promise for applications in catalysis,[2] bio-molecular separations, sensors,[3] photonics,[4] synthesis of aligned metallic nanowires[5-7] and carbon nanotubes[8-10] and for guest-host applications with electrically[11, 12] and/or optically[13] active species. However fabricating well-defined, robust films by conventional evaporation-induced cooperative self-assembly approaches has proven to be extremely challenging.

The general approach to mesoporous materials is based on the discovery[14] that metal oxide precursors and structure-directing surfactants or amphiphilic block copolymers can self-assemble cooperatively to yield ordered composites from aqueous alcohol solutions via controlled solvent evaporation.[15, 16] The organic surfactant can be removed to produce an inorganic mesoporous network. The size and shape of the pore are governed by the molecular mass and composition of the block copolymer, the nature of the precursor, solution acidity, temperature and concentration.[17] The ability to control pore size, morphology and orientation in these materials has been the subject of significant research[1, 18, 19] since their initial discovery.[14, 20] While evaporation-induced cooperative self-assembly is a remarkably powerful approach, it has a number of

limitations. One is poor control over orientational alignment of the cylindrical pores. Simultaneous structural evolution from cooperative block copolymer self-assembly and precursor condensation coupled with preferential affinity of one of the components of the sol solution for the interfaces (substrate/film or film/air) leads to a parallel orientation of the cylindrical pores with respect to the substrate. Magnetic fields[21] have been used as an external agent to align the cylindrical channels along the field direction. However, the direct preparation of mesoporous silica film with perpendicularly oriented cylindrical channels on conductive or non-conductive substrates without using any external agents has remained elusive. Recently it has been reported that porous anodic aluminum oxide membranes can be used as orientation inducing scaffolds to generate vertically aligned mesoporous silica channels within the pores of the membranes.[22, 23] However, the preparation of the aluminum oxide scaffold is tedious and its use as a support produces a composite film containing only a small fraction of mesoporous silica channels.

While it is challenging to control the orientation of nanochannels in inorganic materials, it is relatively easier to control them in soft materials like block copolymer films. In this chapter, we demonstrate an efficient route to robust mesoporous silica films with nanochannels oriented normal to the substrate surface by a direct block copolymer template replication process. We used a block copolymer, where the cylindrical domains can be oriented normal to the substrate surface. Further, phase-selective silica chemistry, controlled at the nanoscale, is performed in supercritical CO_2 medium to get mesoporous silicate films.

Among various strategies discussed in the previous chapter, solvent evaporation[24-26] is one of the non-invasive routes to influence the orientation and lateral long range

order of the cylindrical domains. Ober and coworkers, recently reported the synthesis of an amphiphilic block copolymer, poly(α-methyl styrene-*b*-hydroxy styrene) (PMS-PHOST).[27] It was found that the spin-coated films of PMS-PHOST exhibited a perpendicular orientation of the cylindrical microdomains of PMS over the entire thickness of the films. This block copolymer is used as a template to generate mesoporous inorganic networks with vertical nanochannels by our direct replication, two step approach.[28]

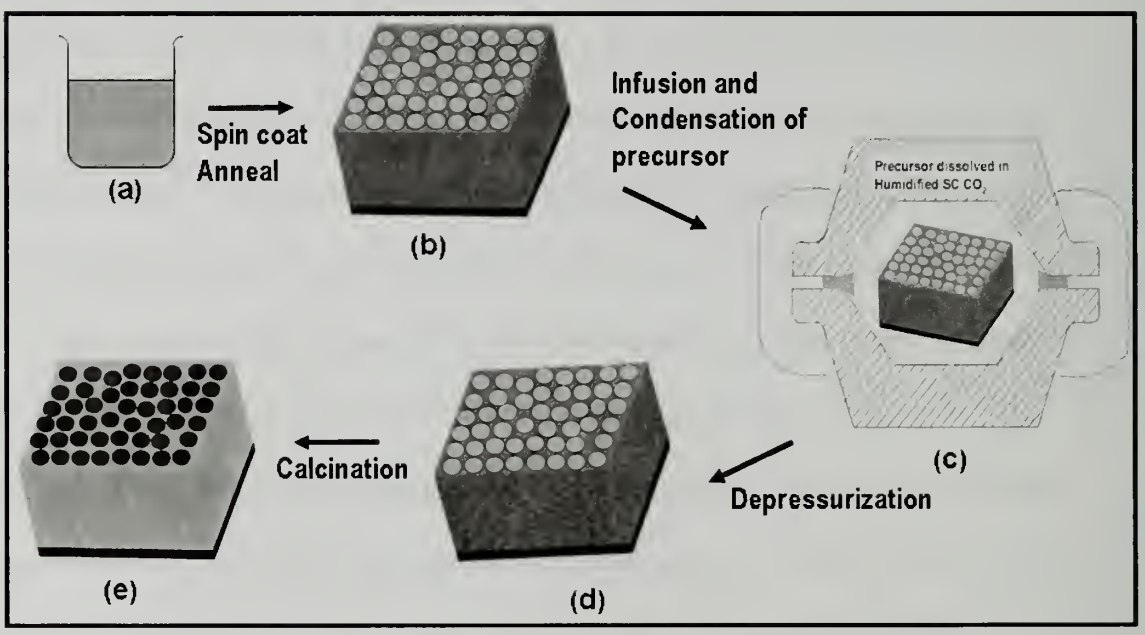

Figure 2.1: Schematic representation[29] of synthesis of mesoporous silicate films with perpendicular nanochannels. Self assembled block copolymer film (b) with cylindrical domains oriented normal to the substrate is obtained by spin coating from the solution of block copolymer and acid catalyst (a). The film is dilated in humidified $scCO_2$ in the presence of TEOS, to form silica selectively in the hydrophilic domain (matrix) of the block copolymer template yielding the organic-inorganic nanocomposite film (d). The organic template is then removed to yield mesoporous silicate film with vertical nanochannels (e)

Figure 2.1 depicts the overall scheme of this work.[30] The organic template with the desired oriented morphology is prepared by spin-coating from a solution of

amphiphilic block copolymer, comprised of ~ 70:30 ratios of hydrophilic and hydrophobic domains, and the acid catalyst. During solvent evaporation, the acid catalyst segregates selectively into the hydrophilic domains of the template. The template is then exposed to the silica precursor, TEOS, dissolved in humidified supercritical CO_2 (sc CO_2). Partitioning of acid catalyst ensures that hydrolysis and further condensation of precursor to metal oxide network occur only within the hydrophilic matrix and not in the hydrophobic cylinders or in the bulk fluid phase.[28] After depressurization the organic component of the nano-composite is removed by calcination to produce a mesoporous silica film with cylindrical pores oriented normal to the substrate surface.

2.2 Experimental Section

Template Preparation: Asymmetric diblock copolymers of poly(hydroxy styrene) (PHOST) and poly(alpha-methyl styrene) (PMS), having molecular weights of 62,200 gm/mol (62.2K), 27,700 gm/mol (27.7K) and 22,900 gm/mol (22.9K) with PHOST volume fractions of 0.73, 0.72 and 0.65, respectively, were used as templates for synthesis of mesoporous silicate films. These diblock copolymers were synthesized by sequential anionic polymerization as described elsewhere.[27] The molecular weights and compositions were determined using SEC and NMR. Approximately 100 nm thick template films were prepared by spin coating solutions of block copolymer with catalytic amounts of p-toluenesulfonic acid (pTSA) in propylene glycol monomethyl ether acetate (PGMEA) onto undoped silicon substrates. The amount of pTSA was maintained at 3 wt. % with respect to the mass of block copolymer in the solution. The spinning speed and time were maintained at 1500 rpm and 60 seconds, respectively. Solvent, PGMEA,

pTSA, and the silicate precursor, tetraethylorthosilicate (TEOS), used in this study were purchased from Aldrich Inc.,

Phase-selective Silica Infusion: Dilation of the block copolymer and condensation of TEOS within one phase of the template were performed in humidified supercritical carbon dioxide ($scCO_2$) at 60°C and 125 bar in a high pressure reactor. The high-pressure reactor was built from two stainless steel blind hubs with a graphite-coated stainless steel seal ring. This reaction vessel has ~160 ml of internal volume and machined ports for charging and discharging of CO_2 and for the measurements of temperature and pressure. A template film spun on ~ 1.25"×1.25" Si wafer piece was placed inside the reactor along with small amount of water (~0.5g) and TEOS (1.0 – 5.0 μL). After sealing, the reactor was heated to 60°C using external band heaters. CO_2 was then slowly injected into the reactor using a high-pressure syringe pump (ISCO, Inc. Model 500HP) until the desired pressure of ~125 bar was reached. Coleman-grade carbon dioxide (CO_2) was obtained from Merriam-Graves and used as received. The total pressurization and reaction time was maintained at 2 hours and then CO_2 was slowly released at the rate of ~0.3 bar/minute. The organic template was removed from the nano-composite film by calcination at 400°C for 6 hours in air using a heating rate of 1.67 °C/min.

Characterization of Organic Templates and Mesoporous Silicate Films: The infusion of the silica and further removal of the organic template were qualitatively assessed by Fourier transform infrared spectrometer (Bio-Rad Excalibur Series FTS 3000). The surface morphologies of the films were imaged using a scanning force microscope (SFM, Digital Instruments Dimension 3000) and a scanning electron

microscope (FESEM, JEOL 6320F instrument). Transmission electron microscopy was performed on calcined films using a JEOL 2000 CX microscope operating at 200 kV. The samples were prepared by scraping ~ 40 nm films off the substrate using a razor blade to make slurry of pieces of film in ethanol. A few drops of this slurry were dropped on the formvar resin-coated copper grid (Electron Microscopy Sciences) and dried prior to examination under microscope. Grazing incidence small angle x-ray scattering experiments were performed at D1 station of the Cornell High Energy Synchrotron Source (CHESS). The wavelength of x-rays used was 1.55 Å and the angle of incidence was chosen to be above the critical angle of the film under study, to make sure that the collected scattered radiation is the representation of the entire film thickness. The scattered radiation was collected with a two-dimensional charge-coupled device (CCD) camera with image sizes of 1024 pixels by 1024 pixels. The thicknesses of the films were measured using a spectroscopic ellipsometer (Sopra Inc., GES5) and a profilometer (Dektak).

2.3 Results and Discussions

2.3.1. Imaging Characterizations

The typical phase scanning force microscopy images, collected in the phase mode, of 62.2K PMS-PHOST asymmetric block copolymer film obtained after spin coating onto a Si substrate and of the silica-infused nano-composite film obtained after phase-selective precursor condensation in supercritical CO_2 are shown in Figure 2.2 and 2.3 respectively. The phase signal in the SFM images is sensitive to differences in the material properties of the two blocks, such as adhesion, hardness and viscoelasticity.[31]

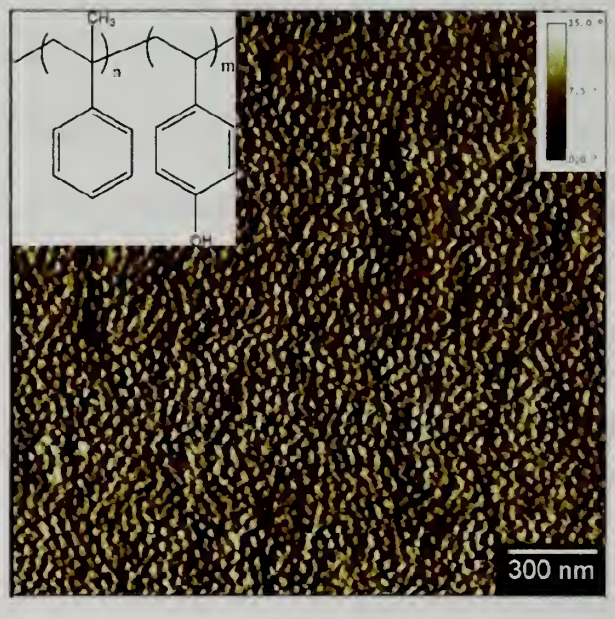

Figure 2.2: Phase scanning force micrograph of as-spun 62.2K PMS-PHOST film. Insets on the left show the chemical structure of PMS-PHOST and on the right show the SFM color scale

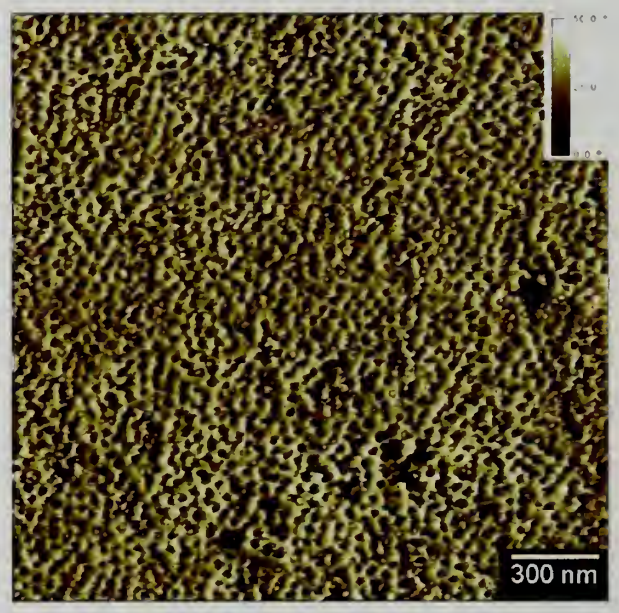

Figure 2.3: Phase scanning force micrograph of silica-infused 62.2K PMS-PHOST film Inset on the right show the SFM color scale

The stronger the difference in the material properties of the two blocks, the higher the phase contrast in the image. In Figure 2.2, the harder cylinders of hydrophobic PMS are oriented normal to the substrate in the relatively softer matrix of PHOST. The average center- to-center distance of the cylindrical domains is ~37 nm with an average cylinder diameter of ~25 nm. It is worth mentioning that this particular template exhibits a modest lateral organization of cylindrical domains in the matrix (template lateral order) rather than a perfect hexagonal close packing. The weak lateral order could be attributed to the nonequilibrium fast evaporation of the solvent in the spin coating process and the high T_g of both the blocks. The inset in the figure shows the chemical structure of the block copolymer. Comparison of figures 2.2 and 2.3 indicates that the template lateral order, domain dimensions and orientation remain essentially the same, while the phase contrast has become much stronger between the matrix and the nanoscopic cylindrical microdomains. This is the result of the selective infusion of inorganic network in the polar matrix (and not in the nonpolar cylindrical micro domains).

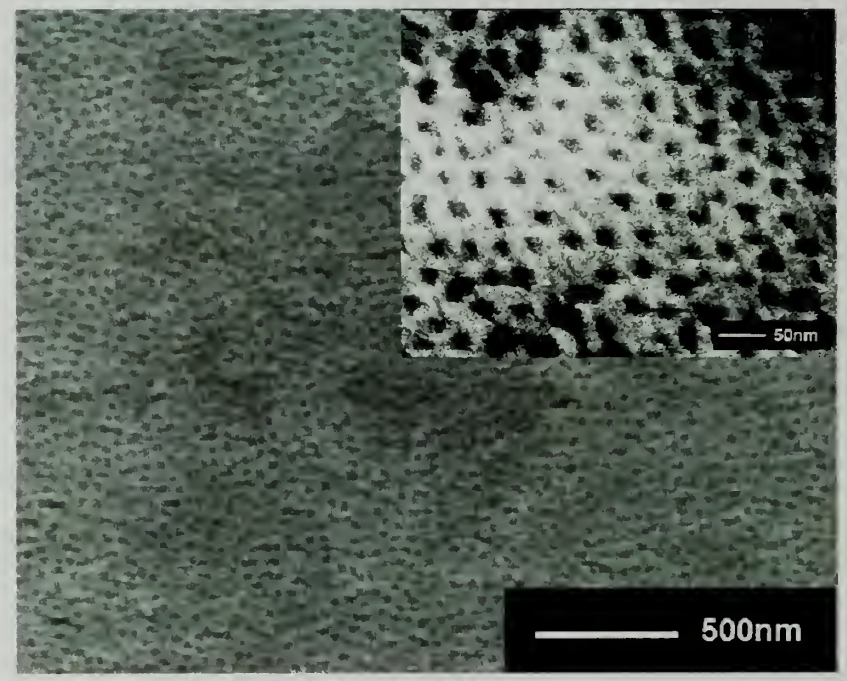

Figure 2.4: Field emission scanning electron micrograph of a calcined mesoporous silica film showing accessible pores oriented normal to the substrate. The inset displays a high magnification image of the same film

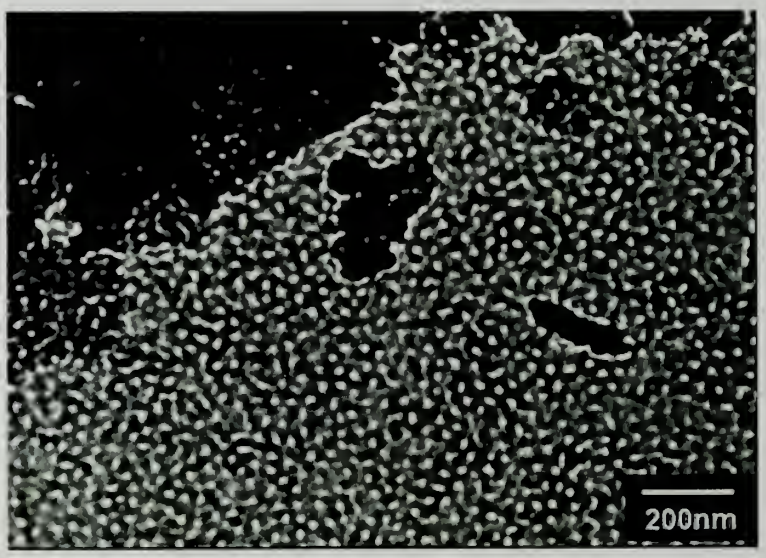

Figure 2.5: Transmission electron micrograph of a thin section of the mesoporous silica film. The pores traverse the entire thickness of the film

The silica-infused nano-composite film was then calcined at 400°C for ~6 hours in air to remove the organic template and yield a complete inorganic network with perpendicular nanochannels. Top-down field emission scanning electron micrograph (FESEM) of the calcined mesoporous silica film (Figure 2.4) reveals the accessible porous channels oriented normal to the substrate in the matrix of silica. The diameter of the pores is essentially the same as that of the nanoscopic cylindrical domains of PMS in the block copolymer template. There is also a comparable degree of lateral order of domains/pores in the block copolymer template and in the mesoporous silica film. In order to probe the depth of the pores into the film, a very thin section of the film was imaged using transmission electron microscope (TEM). The electron density contrast between silica and air is sufficient to easily determine the extent of penetration of the pores through the film. The TEM image in Figure 2.5 demonstrates the porous structures of the film which corresponds to the FESEM image (Figure 2.4), indicating that the pores probably span the entire thickness of the film. Dark areas in the image result from multiple layers of film where the electrons are attenuated.

2.3.2. Scattering Characterizations

In order to obtain statistically averaged information on the internal structure of these films, grazing-incidence small angle x-ray scattering (GISAXS) was used. In GISAXS a highly collimated monochromatic X-ray beam impinges on the surface of the film at grazing angles.[32] The in-plane scattering provides information on the lateral correlation of the scatterers at the surface of the film or within the film.[33] By varying the incident angle below the critical angle of the film, depth-sensitive information can also be

obtained.[34] The 2D-scattering profile of a 76 nm thick mesoporous silica film templated from the 62.2K PMS-PHOST is shown in Figure 2.6 (a). The scattering profile contains two prominent vertical streaks, indicative of porous channels oriented normal to the film surface.[24, 25, 27] The position of the scattering maxima with respect to the q_y axis, the wave vector parallel to the surface of the film, corresponds to the lateral packing of the cylindrical pores. The q_y value of 0.01684 $Å^{-1}$, at scattering maxima, corresponds to the average cylindrical pore-to-pore spacing of 37.3 nm ($d_{spacing} = 2\pi/q_y$) in the XY plane of the film surface. The streaking of the scattering along q_z, the wave vector normal to the surface of the film, corresponds to the truncation of the cylindrical channels at the surface of the film and at the substrate. It is worth mentioning that no other scattering intensity is seen in the profile, which strongly suggests that the film consists only of porous channels oriented normal to the surface. The absence of off-specular scattering (aside from the vertical streaks) essentially rules out the possibility of having 3-D or disordered structures within the film. The 1-D intensity profiles, plotted against q_y of the GISAXS data, collected for the same time in each case, of the as-spun 62.2K PMS-PHOST template (Figure 2.7), the silica-infused nanocomposite (Figure 2.8), and the calcined mesoporous silica film are plotted in the Figure 2.6 (d). The peak position in the as-spun film case corresponds to the cylinder-to-cylinder spacing of 37.2 nm. The scattering profiles reveal that the as-infused and calcined films exhibit the same interdomain spacing as the "as-spun" template, indicating that the phase-selective silica infusion does not induce any change in the lateral dimensions of the structure. However, there is a significant intensity enhancement in the calcined film compared to the "as- infused" film and a slight increase in the scattering intensity in the "as-infused" film compared to the

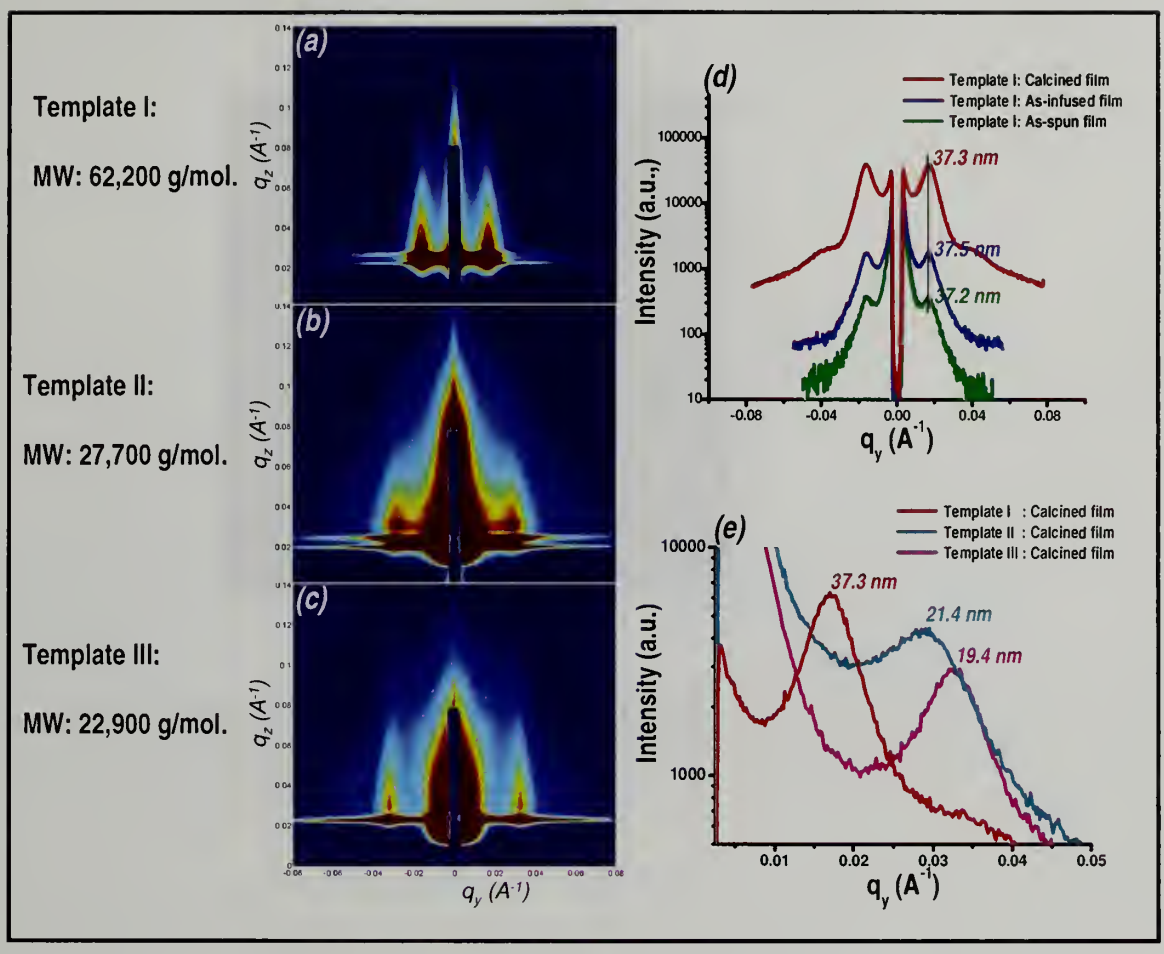

Figure 2.6 (a-e): 2-D GISAXS scattering profiles of the calcined mesoporous silica film templated from 62.2K, 27.7K and 22.9K PMS-PHOST respectively. (d): Intensity profiles plotted against lateral momentum transfer vector qy of as-spun, silica-infused and calcined mesoporous silica film templated from 62.2K PMS-PHOST. (e): Intensity profiles plotted against q_y for three different GISAXS patterns shown in figure 2.6(a-c)

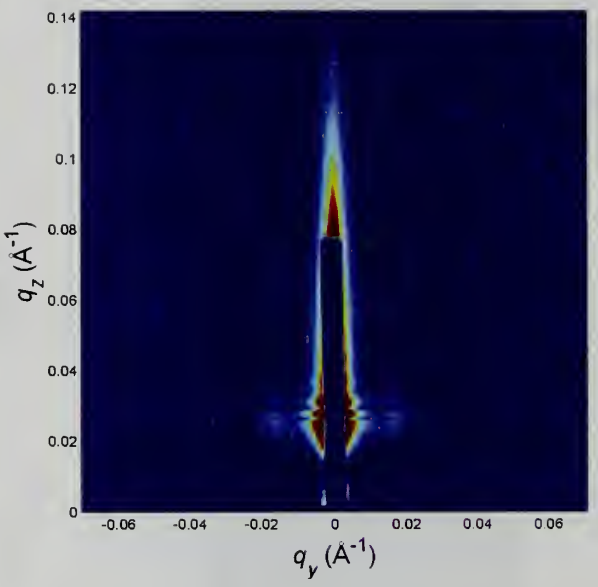

Figure 2.7: GISAXS patterns of as-spun 62.2K PMS-PHOST template film

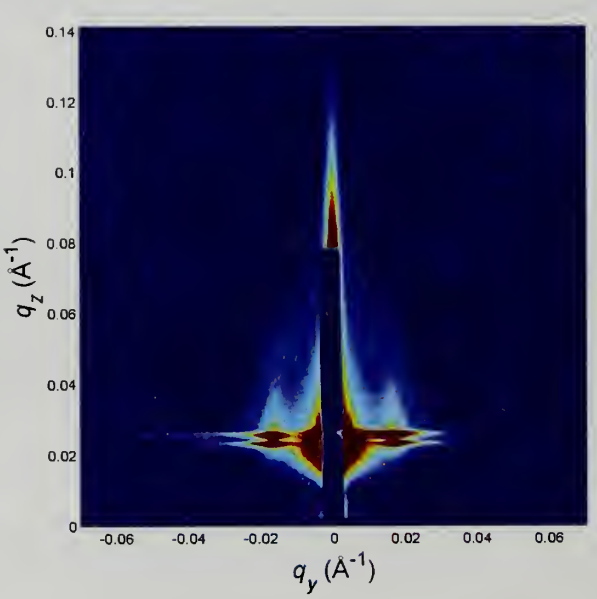

Figure 2.8: GISAXS patterns of silica infused film of 62.2K PMS-PHOST template

"as-spun" film. The intensity differences are expected, since the electron density contrast in the "as-spun" film is very low in comparison to that in the "as-infused" film. The electron density contrast is dramatically enhanced when the polymer is removed leaving only the silica matrix and cylindrical pores.

Silica infusion was carried out using three different molecular weight PMS-PHOST templates to demonstrate control over the pore size. Figure 2.6 (a, b and c) shows the GISAXS patterns of the calcined mesoporous silica films, templated from 62.2K, 27.7K and 22.9K PMS-PHOST, respectively. As the molecular weights of the templates decrease, the center-to-center (C-C) distance of nearest neighbor cylinders and the pore size decreases, i.e., the vertical streaks in GISAXS patterns move to higher q_y, which is also shown in the intensity profiles plotted in Figure 2.6 (e).

2.3.2.1 Simulation of GISAXS Patterns

While, it was possible to determine the interference function i.e., structure factor and the qualitative information about the shape of the scatterers from the GISAXS patterns, it was not possible to directly determine information about the size of the scatterers (form factor). To extract more information from obtained GISAXS results, theoretical GISAXS patterns were simulated, as described below, so that the simulated and experimental results can be compared. GISAXS patterns corresponding to the vertically oriented cylindrical morphology were simulated using the IsGISAXS software package[35] written by Lazzari. The simulations involved choosing a cylindrical scatterer with radius and height similar to those found in 62.2K as form factor. Hexagonal symmetric lattice with average lattice period of 37 nm, found in 62.2 K, was chosen for

structure factor. It is noted that our films actually correspond to cylindrical holes in a matrix, however, applying Babinet's theorem the scattering intensity can be described by the inverse system of cylinders on a substrate as well[36]. Since the system of interest does not display high degree of lateral order, smaller domain sizes have been selected as the grain size to

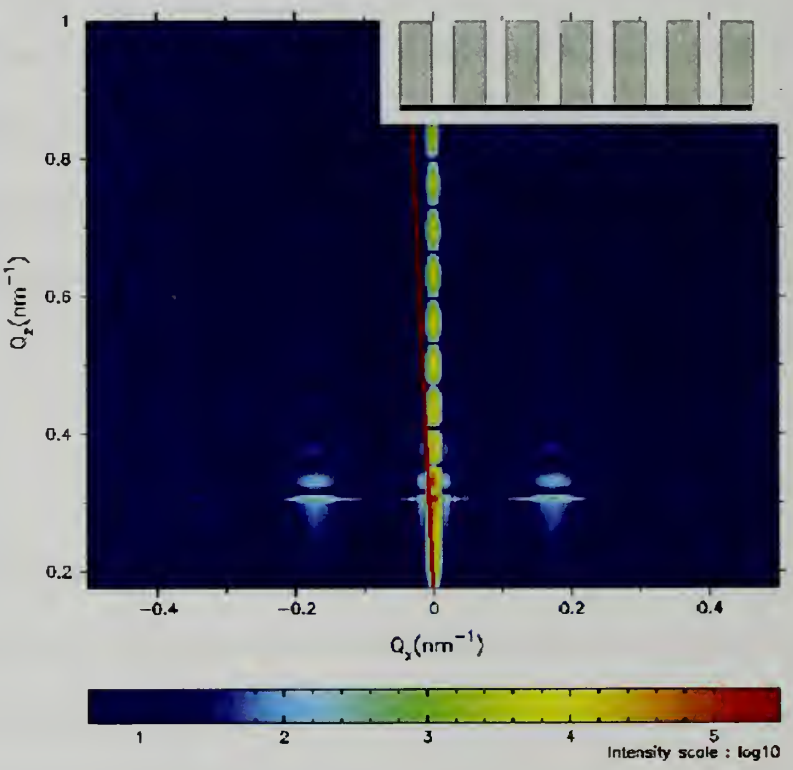

Figure 2.9: Simulated GISAXS pattern for perfectly defined cylindrical domains oriented normal to the substrate with zero roughness in the sample (depicted in the inset)

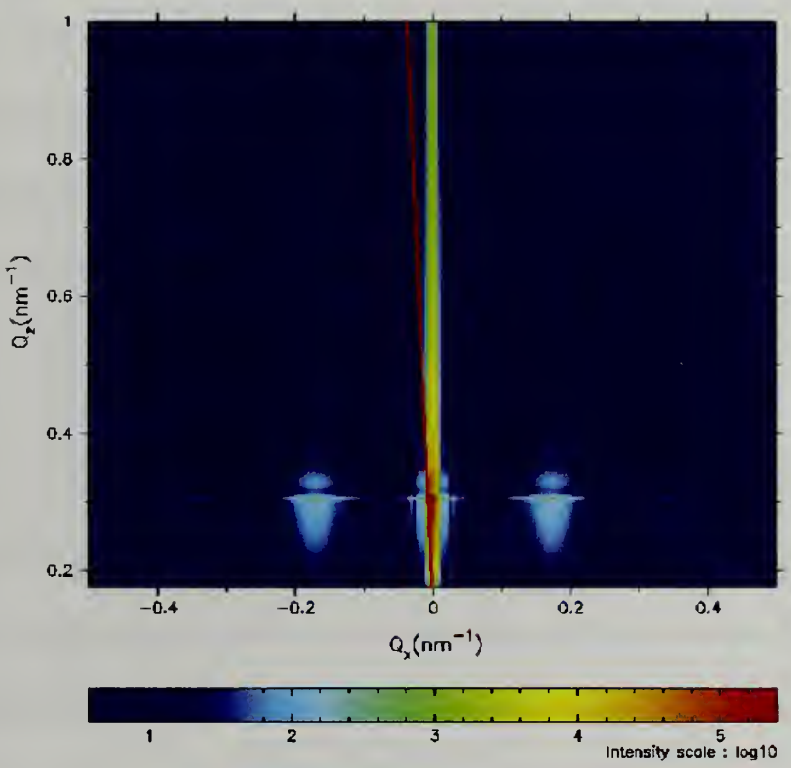

Figure 2.10: Simulated GISAXS pattern for the case of a Gaussian distribution in cylinder heights with σH/R = 0.10

represent short range order among the cylindrical scatterers. The simulated GISAXS pattern for the case of uniformly defined cylindrical scatterers with zero roughness is shown in Figure 2.9. The scattered intensity along the plane of the film, q_x has a maximum at ~0.17 nm^{-1}, corresponding to lattice period of 37 nm, and weak higher order peaks similar to what is observed in the actual GISAXS pattern of calcined mesoporous silica film templated from 62.2K template figure 2.6 (a and d). However, oscillations

along q_z in the primary peak seen in the simulated GISAXS pattern were not observed in the experimental GISAXS pattern. In principle, the observed rods (i.e. streaks in q_z) are determined by the mean cylinder height and the height distribution. By assuming a small distribution in cylinder heights, the oscillations are strongly attenuated at higher q_z (Figure 2.10) which matches well with the experimental GISAXS data (Figure 2.6 (a)). The simulation in Figure 2.10 was obtained by invoking a Gaussian distribution for cylinder heights with a ±5% deviation from the mean height. Such height distributions can be attributed to the roughness associated with thickness variations in thin films of porous inorganic networks, as observed in the FESEM data.

2.3.3 Elliposmetric Characterizations

Spectroscopic ellipsometry was used to track the changes in thickness and refractive indices of the films after each stage of the replication process. Table 2.1 summarizes a representative data set for 100 nm thick 62.2K PMS-PHOST templates. Moving from as-spun to silica infused films, the thickness has increased by ~ 20 % due to the condensation of silicate network in PHOST matrix. Such an anisotropic, unidirectional swelling with no change in lattice parameters (as suggested by TEM, GISAXS results), can give rise to a stretching of PMS chains in cylindrical domains. Such stretching is speculated, as these cylindrical domains do not contain silicate network unlike PHOST matrix. However, PMS domains may very well contain non-condensable TEOS molecules, which may partly provide a material balance when the PMS chains are stretched. TEOS molecules in PMS domains are non-condensable as these domains lack acid catalyst. One can also notice that the thickness and refractive index decrease after

calcination. A drop in refractive index is due to the removal of the template and introduction of porosity in the films. Shrinkage of films is due to densification or complete condensation of silicate network during calcination, which suggests the presence of uncondensed and partially condensed TEOS in silica infused films.

Table 2.1: Thickness and Refractive index of films at different stages of the replication process

Film	Thickness	Refractive Index
PMS-PHOST as-spun film	~ 100 nm	1.49
Silica Infused Film	~ 120 nm	1.55
Calcined Mesoporous Silica film	~ 75 nm	1.22

2.4 Conclusions

In conclusion, we have shown that with the advances in the orientation of block copolymer domains and a discrete two-step, template formation and supercritical fluid phase infusion, a straightforward preparation of mesoporous silica films with cylindrical pores oriented normal to the surface can be achieved. Such films are useful for the majority of applications that rely on vertical channels. Although PMS-PHOST block copolymer film serves as a suitable template to demonstrate an efficient route to mesoporous silica with perpendicular nanochannels, these templates lack long-range lateral order and therefore so does the final mesoporous silica films. Applications that rely on individually addressable arrays will require long range lateral order in both the template and the corresponding mesoporous silica film.

2.5 References

1. Wu, Y. Y.; Cheng, G. S.; Katsov, K.; Sides, S. W.; Wang, J. F.; Tang, J.; Fredrickson, G. H.; Moskovits, M.; Stucky, G. D., *Nature Materials* **2004,** 3, 816.

2. Sayari, A., *Chem.Mater.* **1996,** 8, 1840.

3. Wirnsberger, G.; Scott, B. J.; Stucky, G. D., *Chemical Communications* **2001**, 119.

4. Bockstaller, M.; Kolb, R.; Thomas, E. L., *Advanced Materials* **2001,** 13, 1783.

5. Zhang, Z. T.; Dai, S.; Blom, D. A.; Shen, J., *Chemistry of Materials* **2002,** 14, 965.

6. Thurn-Albrecht, T.; Schotter, J.; Kastle, C. A.; Emley, N.; Shibauchi, T.; Krusin-Elbaum, L.; Guarini, K.; Black, C. T.; Tuominen, M. T.; Russell, T. P., *Science* **2000,** 290, 2126.

7. Erts, D.; Polyakov, B.; Saks, E.; Olin, H.; Ryen, L.; Ziegler, K.; Holmes, J. D., Semiconducting nanowires: Properties and architectures. In *Functional Nanomaterials for Optoelectronics and Other Applications*, 2003; Vol. 99-100, pp 109.

8. Duesberg, G. S.; Graham, A. P.; Liebau, M.; Seidel, R.; Unger, E.; Kreupl, F.; Hoenlein, W., *Nano Letters* **2003,** 3, 257.

9. Huang, L.; Wind, S. J.; O'Brien, S. P., *Nano Letters* **2003,** 3, 299.

10. Murakami, Y.; Yamakita, S.; Okubo, T.; Maruyama, S., *Chemical Physics Letters* **2003,** 375, 393.

11. Nguyen, T. Q.; Wu, J. J.; Doan, V.; Schwartz, B. J.; Tolbert, S. H., *Science* **2000,** 288, 652.

12. Doherty, W. J.; Armstrong, N. R.; Saavedra, S. S., *Chemistry of Materials* **2005,** 17, 3652.

13. Okabe, A.; Fukushima, T.; Ariga, K.; Aida, T., *Angewandte Chemie-International Edition* **2002,** 41, 3414.

14. Kresge, C. T.; Leonowicz, M. E.; Roth, W. J.; Vartuli, J. C.; Beck, J. S., *Nature* **1992,** 359, 710.

15. Forster, S.; Antonietti, M., *Advanced Materials* **1998,** 10, 195.

16. Yang, P. D.; Deng, T.; Zhao, D. Y.; Feng, P. Y.; Pine, D.; Chmelka, B. F.; Whitesides, G. M.; Stucky, G. D., *Science* **1998,** 282, 2244.

17. Imperor-Clerc, M.; Davidson, P.; Davidson, A., *Journal of the American Chemical Society* **2000,** 122, 11925.

18. Gibaud, A.; Grosso, D.; Smarsly, B.; Baptiste, A.; Bardeau, J. F.; Babonneau, F.; Doshi, D. A.; Chen, Z.; Brinker, C. J.; Sanchez, C., *Journal of Physical Chemistry B* **2003,** 107, 6114.

19. Brinker, C. J.; Lu, Y. F.; Sellinger, A.; Fan, H. Y., *Advanced Materials* **1999,** 11, 579.

20. Beck, J. S.; Vartuli, J. C.; Roth, W. J.; Leonowicz, M. E.; Kresge, C. T.; Schmitt, K. D.; Chu, C. T. W.; Olson, D. H.; Sheppard, E. W.; McCullen, S. B.; Higgins, J. B.; Schlenker, J. L., *Journal of the American Chemical Society* **1992,** 114, 10834.

21. Tolbert, S. H.; Firouzi, A.; Stucky, G. D.; Chmelka, B. F., *Science* **1997,** 278, 264.

22. Lu, Q. Y.; Gao, F.; Komarneni, S.; Mallouk, T. E., *Journal of the American Chemical Society* **2004,** 126, 8650.

23. Yamaguchi, A.; Uejo, F.; Yoda, T.; Uchida, T.; Tanamura, Y.; Yamashita, T.; Teramae, N., *Nature Materials* **2004,** 3, 337.

24. Kim, S. H.; Misner, M. J.; Russell, T. P., *Advanced Materials* **2004,** 16, 2119.

25. Kim, S. H.; Misner, M. J.; Xu, T.; Kimura, M.; Russell, T. P., *Advanced Materials* **2004,** 16, 226.

26. Lin, Z. Q.; Kim, D. H.; Wu, X. D.; Boosahda, L.; Stone, D.; LaRose, L.; Russell, T. P., *Advanced Materials* **2002,** 14, 1373.

27. Li, M. Q.; Douki, K.; Goto, K.; Li, X. F.; Coenjarts, C.; Smilgies, D. M.; Ober, C. K., *Chemistry of Materials* **2004,** 16, 3800.

28. Pai, R. A.; Humayun, R.; Schulberg, M. T.; Sengupta, A.; Sun, J. N.; Watkins, J. J., *Science* **2004,** 303, 507.

29. Nagarajan, S.; Li, M. Q.; Pai, R. A.; Bosworth, J. K.; Busch, P.; Smilgies, D. M.; Ober, C. K.; Russell, T. P.; Watkins, J. J., *Adv. Mater.* **2008,** 20, 246.

30. Nagarajan, S.; Bosworth, J. K.; Ober, C. K.; Russell, T. P.; Watkins, J. J., *Chem. Mater.* **2008,** 20, 604.

31. Garcia, R.; San Paulo, A., *Physical Review B* **1999,** 60, 4961.

32. Levine, J. R.; Cohen, L. B.; Chung, Y. W.; Georgopoulos, P., *Journal of Applied Crystallography* **1989,** 22, 528.

33. Smilgies, D. M.; Busch, P.; Posselt, D.; Papadakis, C. M., *Synchrotron Radiation News* **2002,** 15, 35.

34. Factor, B. J.; Russell, T. P.; Toney, M. F., *Physical Review Letters* **1991,** 66, 1181.

35. Lazzari, R., *Journal of Applied Crystallography* **2002,** 35, 406.

36. Guinier A., a. F. G., *Small Angle Scattering of X-Rays*. Wiley: New York, 1955; p 264.

CHAPTER 3

FABRICATION OF MICRO-PATTERNED MESOPOROUS SILICATE FILMS FROM POLY (ETHYLENE OXIDE) AND POLY (HYDROXY STYRENE) COPOLYMERS

3.1 Introduction

Mesoporous metal oxide films have been the subject of extensive research, due to their potential use for sensors[1], microfluidics[2], microelectronics, optoelectronics, microelectromechanical systems[3, 4] and catalysis[5]. Many of these applications require the patterning of the mesoporous device layers to integrate other components necessary for intended applications. Moreover, these mesostructured films have several specific properties that make them a very challenging material for patterning. Patterning of mesoporous materials has been accomplished to date using a broad range of strategies including soft lithography[6-9], micropen lithography[10, 11], ink-jet printing[10, 12], dip-pen lithography[13], electron beam lithography[14], x-ray direct writing[15, 16], micro-patterned self-assembled monolayer templating[6, 17-19], photochemical variation in acid concentration and surfactant degradation[20, 21].

While each of the patterning strategies has its own advantages and disadvantages, mesoscopic structures in all these approaches are prepared through cooperative assembly of the hydrolyzed silica precursor species and organic surfactants or block copolymers in the presence of acid and excess amount of alcohol. The alcohol is required to slow the condensation of TEOS to permit adequate time for assembly to occur, which can result in long processing times and incomplete network condensation[22]. Because the structure evolution and precursor condensation occur simultaneously in this approach, the final film morphology cannot be completely prescribed before silica network formation.

Moreover, because assembly occurs in solution or in solvated films, rapid diffusion of reactants and catalysts can result in poor resolution of patterning techniques that rely on spatial discrimination. One potential solution is to decouple structure generation from precursor condensation. Such an approach provides the potential for complete definition of desired hierarchical structure in a suitable template followed by precursor condensation to translate the defined architecture into the inorganic network. The two step replication process in sc CO_2, discussed in the previous chapters, can be a wise choice if the desired pattern can be registered in the block copolymer template.

This chapter discusses the possibilities of using poly (ethylene oxide) copolymers (pluronics) and poly (hydroxy styrene) copolymers as templates to produce micro patterned mesoporous silicate films. Pluronics are chosen as templates, as these copolymers were previously shown to yield robust, blanket mesoporous silicate films that passed chemical mechanical planarization(CMP) tests[23], typically done during chip fabrication in microelectronics industry. Poly(hydroxy styrene) copolymers are chosen as templates, as their patternability using photolithography is well-studied and moreover they have been shown to be one of the suitable templates to perform phase selective silica chemistry[24] in sc CO_2 as well (Chapter 2).

Having mentioned that the 3-D replication process in sc CO_2 translates the structural details present in the template to a metal oxide network, the logical starting point to obtain patterned mesoporous silicate films would be patterned block copolymer templates. Recently, Ober and coworkers reported a method to prepare patterned poly (α- methyl styrene-b-hydroxy styrene) BCP films using photolithographic techniques[25]. This method is utilized in this chapter to generate patterned templates (figure 3.1), that

are then subjected to silica deposition. For simplicity, poly (hydroxy styrene) (PHOST) homopolymer is used initially, instead of a BCP, to prepare patterned templates, as shown in figure 3.1. PHOST films containing small amount of photo acid generator (PAG) and crosslinker (CL) are spun on to Si wafer. Such films are exposed to UV through a photomask. Upon exposure to UV radiation, PAG generates an acid that initiates a crosslinking reaction between the crosslinker and PHOST, when the exposed films are briefly baked at elevated temperature, e.g., 90 °C. The role of the added crosslinker is to introduce slight crosslinking into the PHOST matrix. A slightly crosslinked PHOST matrix has different developing (dissolving) properties than the uncrosslinked PHOST matrix. Uncrosslinked or unexposed portions of the film can be dissolved selectively by using an appropriate developer. Such developed and hence patterned PHOST films are used for silica deposition processes. After template removal by calcination, the films are examined using Optical microscopy (OM). The outcome of this study is used to design further experiments in BCP templates.

If the template patterning and the replication are successfully done, then the mesoporous silicate films would have porous structures at two different length scales as depicted in Figure 3.2. Porous structures on the nanoscopic length scale are derived from block copolymer template morphology and the other porosity, on microscopic length scale, is derived from registered micro-patterns in the template. Nanoscopic structures are named as 'domain level definitions' and microscopic structures are termed as 'device level definitions'.

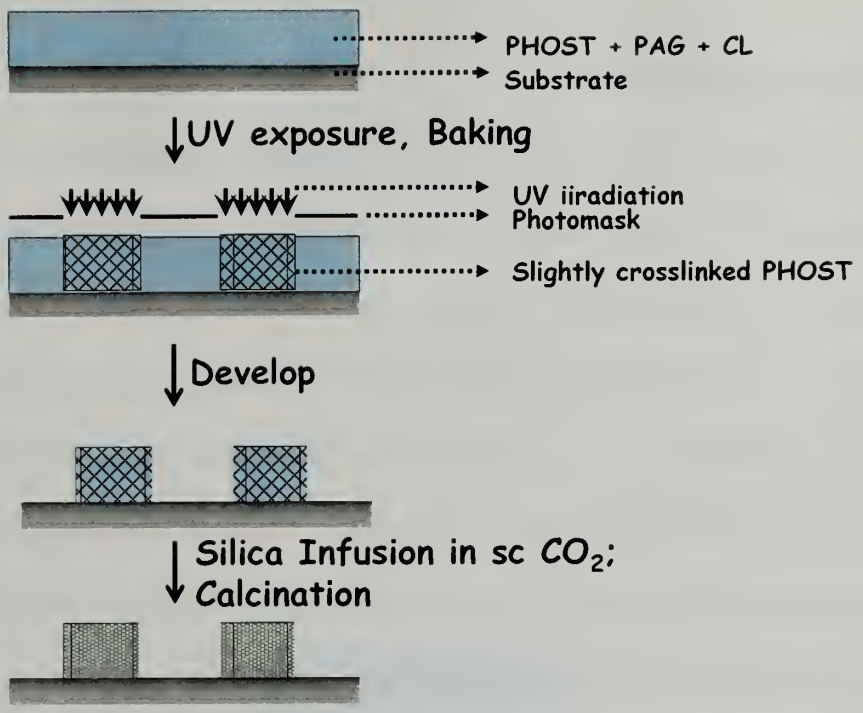

Figure 3.1: Schematic showing the steps involved in fabrication of patterned silicate structures from developed PHOST films

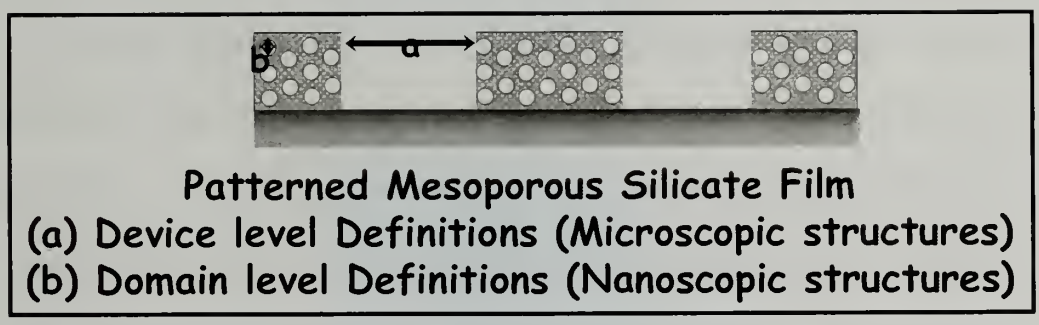

Figure 3.2: Pictorial representation of micro-patterned mesoporous silicate films

3.2 Experimental Section

Materials: PHOST (Sigma-aldrich), pluronic F108 (BASF Inc.,), triphenyl sulfonium triflate (Sigma-aldrich), tetramethyl methoxy glyocluril (Cytec Chemicals), tetraethyl orthosilicate (Sigma-aldrich), anhydrous methanol (Acros Chemicals) and propylene glycol monomethyl ether acetate (Sigma-aldrich) were used as received. PMS-PHOST used in this study is synthesized, as reported elsewhere, in Prof. Ober's laboratory at Cornell University. The molecular weight of PMS-PHOST is 100,000 gm/mol, in which the volume fraction of PHOST is ~ 70%. The molecular weight of PHOST used in this study is 20000 gm/mol.

Template Preparation: (1) PHOST Templates: Solutions of 3 wt% PHOST in propylene glycol monomethyl ether acetate (PGMEA) were prepared with 5 wt% (with respect to polymer weight) PAG, triphenyl sulfonium triflate (TPST) and 1 wt% (with respect to polymer weight) CL, tetramethyl methoxy glycoluril (TMMGU). Approximately ~300 nm thick template films were spun coat from this solution onto Si wafers by spinning the wafers at 2000 rpm for 60 seconds. After photolithographic UV exposure, the TPST generates triflic acid[26] as shown in figure 3.3. The films were baked at 90 °C for about 90 seconds to crosslink the exposed regions. Crosslinking reaction[25] between hydroxyl groups in PHOST and CL in the presence of photoacid and heat is shown in figure 3.4. To dissolve away the unexposed regions, the films were developed a in 1:1 mixture of isopropanol and cyclohexane developer.

(2) F108 templates: Pluronic F108 $[(PEO)_{135}(PPO)_{52}(PEO)_{135}]$ is a triblock copolymer of polyethylene oxide (PEO) and polypropylene oxide (PPO). A 6 wt % solution of F108 was prepared in anhydrous methanol containing 6 wt% photoacid

generator, triphenyl sulfonium triflate (TPST). Approximately ~200 nm thick template films were spun coat from this solution onto Si wafers by spinning the wafers at 1500 rpm for 60 seconds.

(3) PMS-PHOST templates: A 3 wt % solution of PMS-PHOST was prepared in PGMEA containing 5 wt% TPST. Approximately ~ 250 nm thick template films were spin coated from this solution onto Si wafer by spinning the wafer at 1500 rpm for 60 seconds.

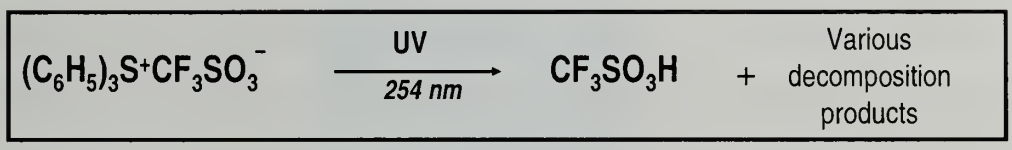

Figure 3.3: Photogeneration of triflic acid from triphenyl triflate upon exposure to 254 nm radiation

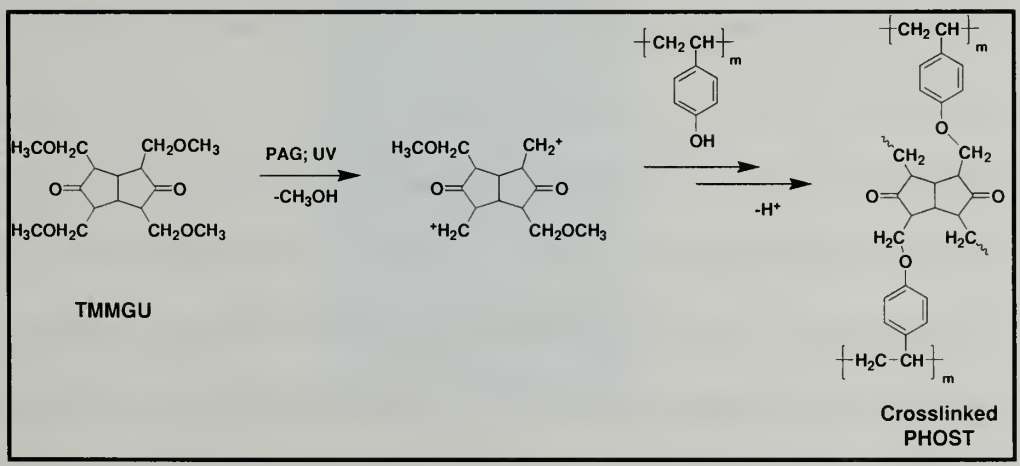

Figure 3.4: Crosslinking reaction between TMMGU and PHOST (Adapted from Reference 25)

Photolithographic UV Exposure: (1) Homopolymer Templates: A laboratory-scale bench top UV lamp (UV Products) was used to irradiate the PHOST films through a photomask. In this case, photomask is simply a piece of Aluminum foil with ~ 4 mm^2 square holes. UV radiation chosen for our exposure was in the range of 220 – 300 nm with maximum at 254 nm, as the TPST generates triflic acid upon exposure to 254 nm radiation. (2) Block copolymer templates: An HTG contact aligner at the Cornell Nanoscale Science and Technology Facility (CNF) was used to irradiate the F108 and PMS-PHOST templates through a photomask, which was present in soft contact with template during the UV exposure. The photomask used in this case is a quartz plate containing cubically packed metal dots. The diameter of each dot is ~ 13 microns. The optical micrograph of the photomask imaged in transmission mode is shown in figure 3.5. UV radiation chosen for our exposure was in the range of 220 – 300 nm with maximum at 254 nm. All of the template films were exposed in the range of 20 – 60 mJ/cm^2.

Domain Selective Silica Deposition: Silica deposition was performed by exposing the templates to silica precursor, tetraethyl orthosilicate (TEOS), dissolved in supercritical carbon dioxide ($scCO_2$) at 60 °C and 125 bar in a high pressure reactor. The high-pressure reactor was built from two stainless steel blind hubs with a graphite-coated stainless steel seal ring. This reaction vessel has ~160 ml of internal volume and machined ports for charging and discharging of CO_2 and for the measurements of temperature and pressure. Si wafer pieces having homopolymer or block copolymer templates, irradiated, baked and developed as detailed above, was placed inside the reactor along with TEOS (5.0 – 10.0 μL). After sealing, the reactor was heated to 60 °C using external band heaters. CO_2 was then slowly injected into the reactor using a high-

pressure syringe pump (ISCO, Inc. Model 500HP) until the desired pressure of ~125 bar was reached. Coleman-grade carbon dioxide (CO_2) was obtained from Merriam-Graves and used as received. The total pressurization and reaction time were maintained at 2 hours and then CO_2 was slowly released at the rate of ~0.3 bar/minute. The organic template was removed from the nanocomposite film by calcination at 400°C for 6 hours at the heating rate of 1.67 °C/min.

Characterization of Organic Template and Mesoporous Silicate Films: The surface morphologies (top view) of the films were imaged using a scanning force microscope (SFM, Digital Instruments Dimension 3000) and an optical microscope (Olympus BX60). To image the pore structure, transmission electron microscopy was performed on calcined films using a JEOL 2000 CX microscope operating at 200 kV. The samples were prepared by scraping the silica film off the substrate using a razor blade to make slurry of pieces of film in ethanol. A few drops of this slurry were dropped on the Formvar® resin-coated copper grid (Electron Microscopy Sciences) and dried prior to examination under the microscope.

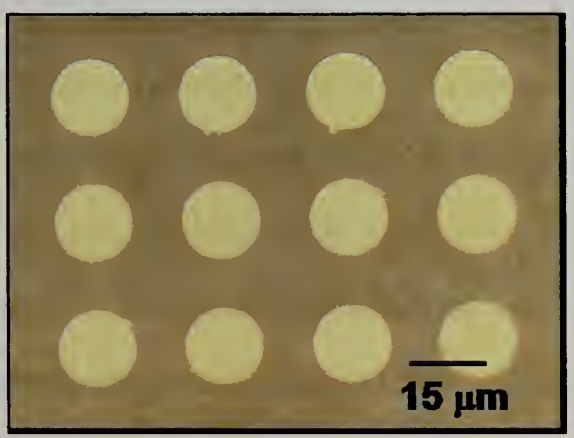

Figure 3.5: Optical micrograph of the photomask used in this study

3.3 Results and Discussions

3.3.1 Patterned Silicate Films from Developed PHOST Templates

The outcome of silica deposition in developed PHOST templates are shown in Figure 3.6. Snapshots of the sample at each stage namely, before silica deposition, after silica deposition and after calcination are shown from left to right respectively. If the silica deposition is successful, then calcination would remove the organic template and leave patches of silica on the wafer. As one can notice in Figure 3.6, there is no film left after calcination indicating that the silica deposition is unsuccessful. Failure of silica deposition process in developed PHOST films suggests the following:

(i) The acid necessary for precursor, TEOS, hydrolysis is not present in the developed template indicating that acid mat have leached out during development step.

(ii) Crosslinked portions of the film remaining after development can give rise to limited swellability[27] in sc CO_2, as compared to that of uncrosslinked templates. Such hindered swellability might have restricted the delivery of precursor inside the film.

3.3.2 Patterned Silicate Films from UV-Exposed PHOST Templates

To overcome the above mentioned problems, the schematic is modified as shown in Figure 3.7. In this case, the PHOST template does not have crosslinker and moreover the development step is omitted. Silica deposition is performed after UV exposure and Figure 3.8 shows the snapshots of the UV-exposed, silica deposited and calcined films respectively. It can be clearly observed that the silica deposition occurred selectively in the UV exposed regions or in the regions where acid is generated.

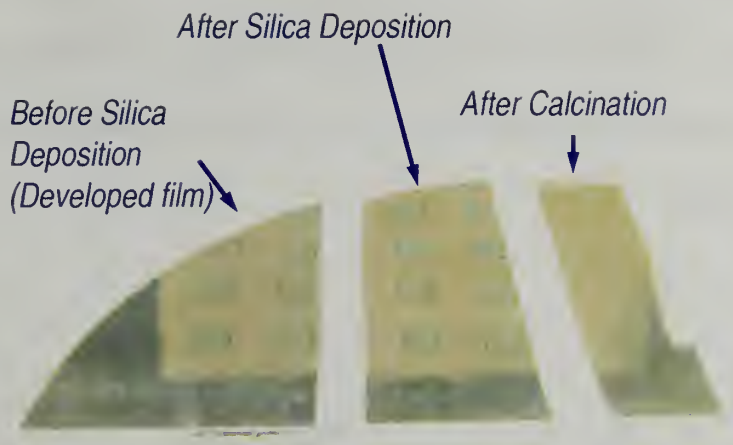

Figure 3.6: Photograph of developed PHOST film at various stages of silica deposition process

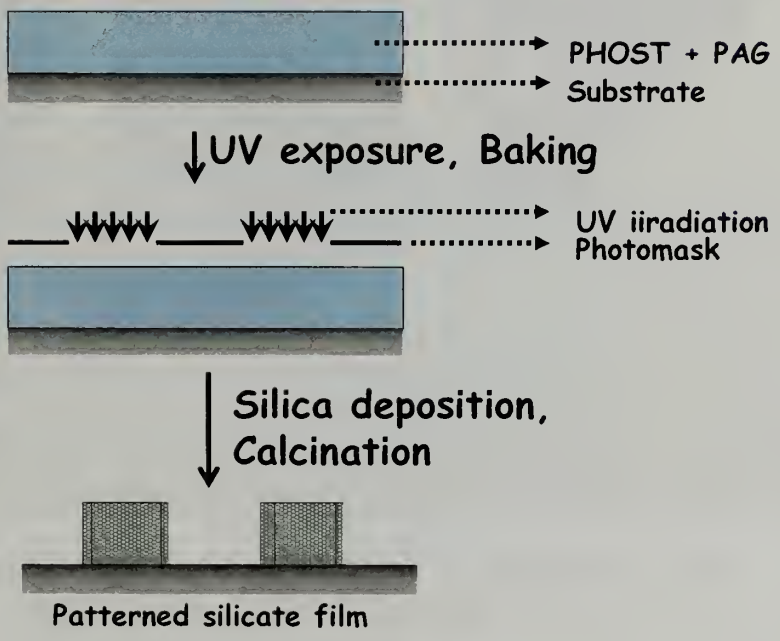

Figure 3.7: Schematic showing the steps involved in preparation of patterned silicate films from UV exposed PHOST templates

Calcination removed the organic template and left patches of silica on the wafer. All these observations indicate that patterned silicate films can be prepared by performing silica depositions in uncrosslinked/UV exposed films rather than in crosslinked or developed films.

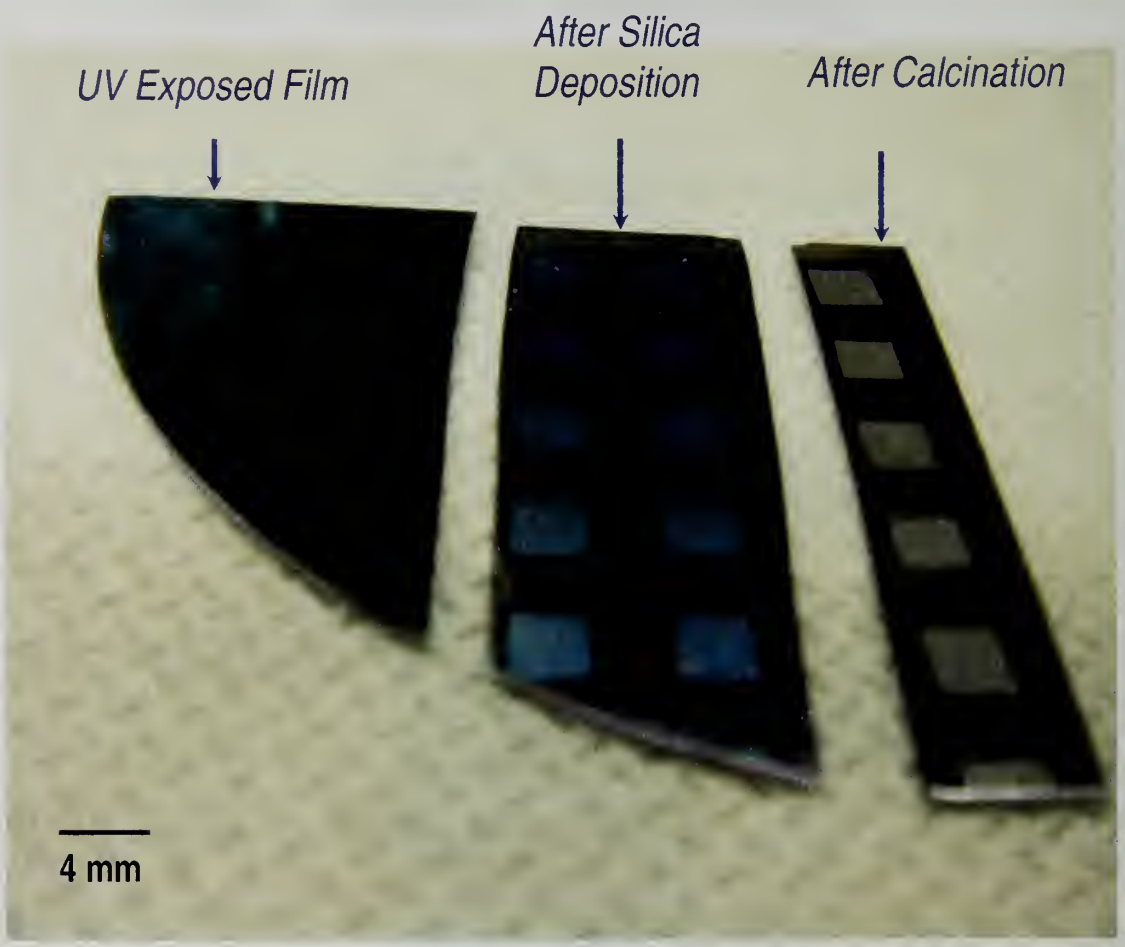

Figure 3.8: Photograph showing the UV-exposed PHOST film at different stages of silica deposition process

3.3.3 Patterned Silicate Films from UV-Exposed F108 Templates

Although silica deposition in homopolymer templates helped to understand the process, the patterned silicate films obtained from these homopolymer templates do not possess mesoporosity. To obtain micropatterned mesoporous silicate films with domain and device level definitions as shown in Figure 3.2, the information obtained from homopolymer experiments is implemented in block copolymers templates and then silica deposition is performed as shown in Figure 3.9.

Figure 3.10 and 3.12 show the TEM and optical micrograph of the patterned mesoporous silica film templated from F108 respectively. Domain level replication can be seen in Figure 3.10 where well-ordered nanoporous structures templated from self-assembled F108 films are evident. This is also supported by the presence of sharp peaks in the scattering data shown in Figure 3.11. This observation indicates that the triflic acid generated from TPST segregates to hydrophilic PEO domain where it serves as an effective silica condensation catalyst. Device level replication can be seen in Figure 3.12 where the micron-scale pattern transferred from the photomask is noticeable. Although domain level replication is excellent in F108 template films, device level replication is less effective. The features present in the optical micrograph lack sharp boundaries, as seen in image wise section analysis (Figure 3.13), suggesting that the acid generated readily diffused from the exposed portion to the unexposed portion of the film.[28]

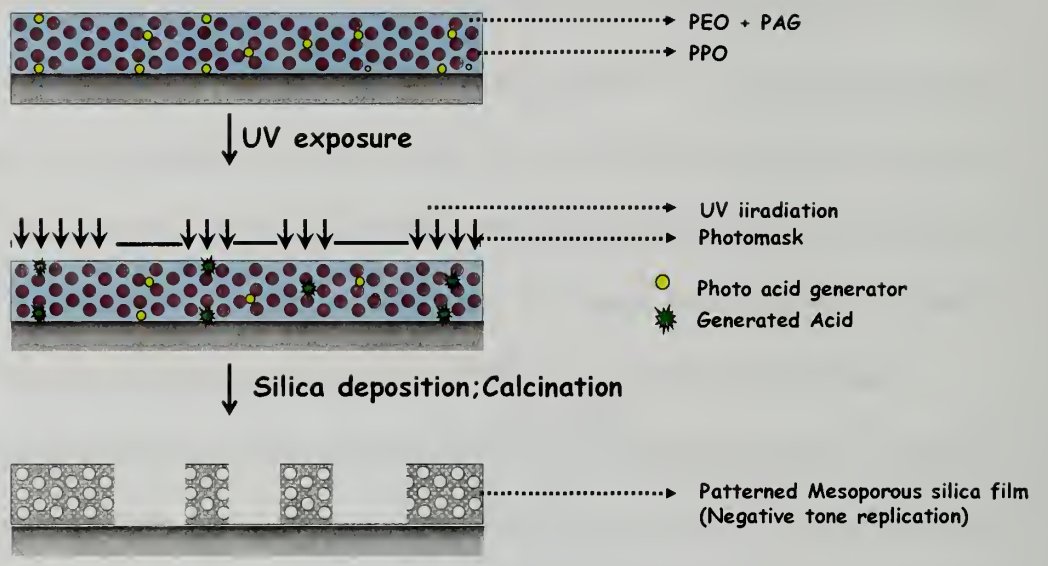

Figure 3.9: Schematic showing the steps involved in fabrication of micropatterned mesoporous silicate films from UV-exposed block copolymer templates

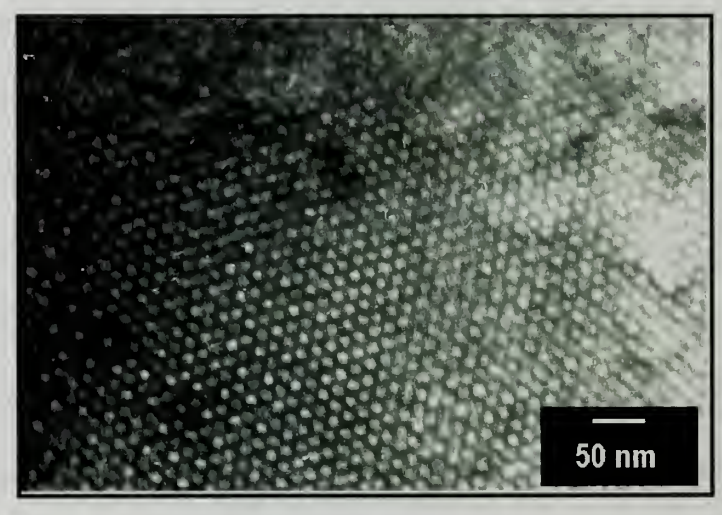

Figure 3.10: Transmission electron micrograph showing the domain level structures in mesoporous silica films templated from F108 film

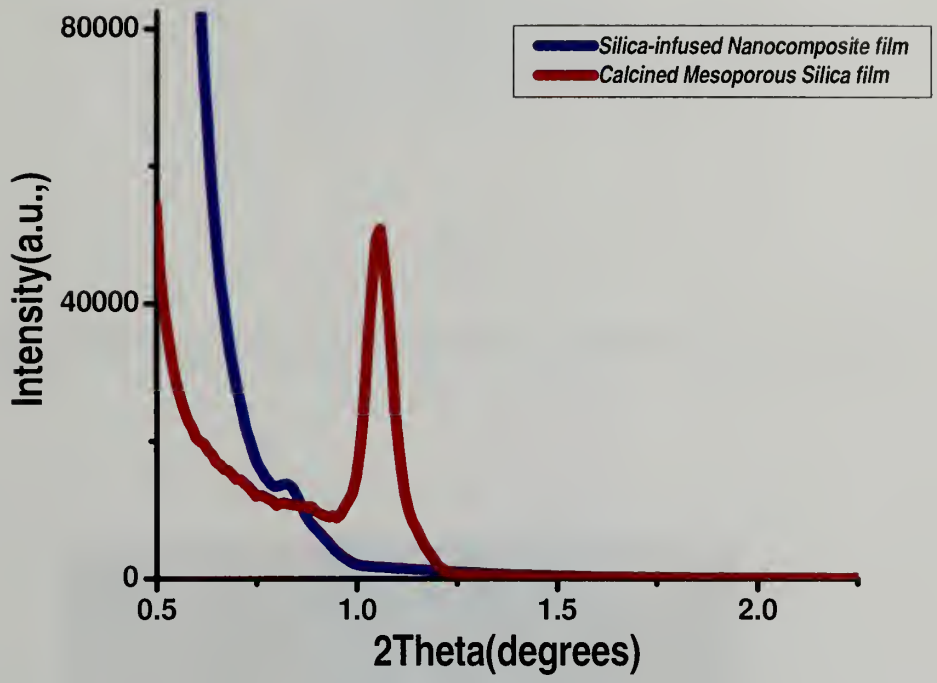

Figure 3.11: XRD patterns for silica infused and mesoporous silicate film templated from UV-exposed F108 films

Figure 3.12: Optical micrograph of mesoporous silica films templated from F108 film showing the device level structures

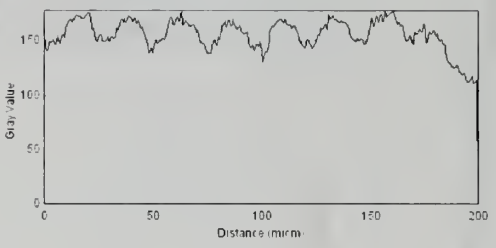

Figure 3.13: Section profile of the optical micrograph shown in Figure 3.12

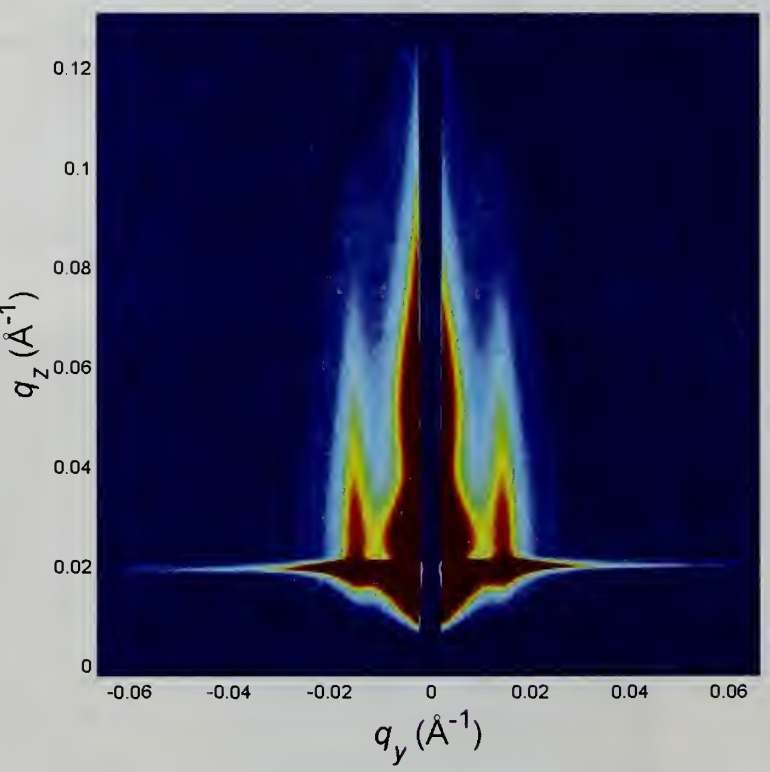

Figure 3.14: GISAXS data confirming the domain level replications in mesoporous silicate film templated from PMS-PHOST films

3.3.4 Patterned Silicate Films from UV-Exposed PMS-PHOST Templates

Domain and device level definitions in patterned mesoporous silicate films templated from PMS-PHOST templates are shown in figures 3.14 and 3.15 respectively. GISAXS data shown in figure 3.14 confirms the presence of perpendicular nanochannels[24] (see Chapter 2 for detailed analysis) in silicate films and indicates that the triflic acid generated segregates into hydrophilic PHOST matrix. Pattern replicated from the photomask can be seen in the scanning force micrograph and its section analysis in figures 3.15 and 3.16 respectively. As one can notice, the device level replications exhibit shallow boundaries, similar to the case of F108 templates, suggesting the diffusion of acid from UV exposed to unexposed regions.

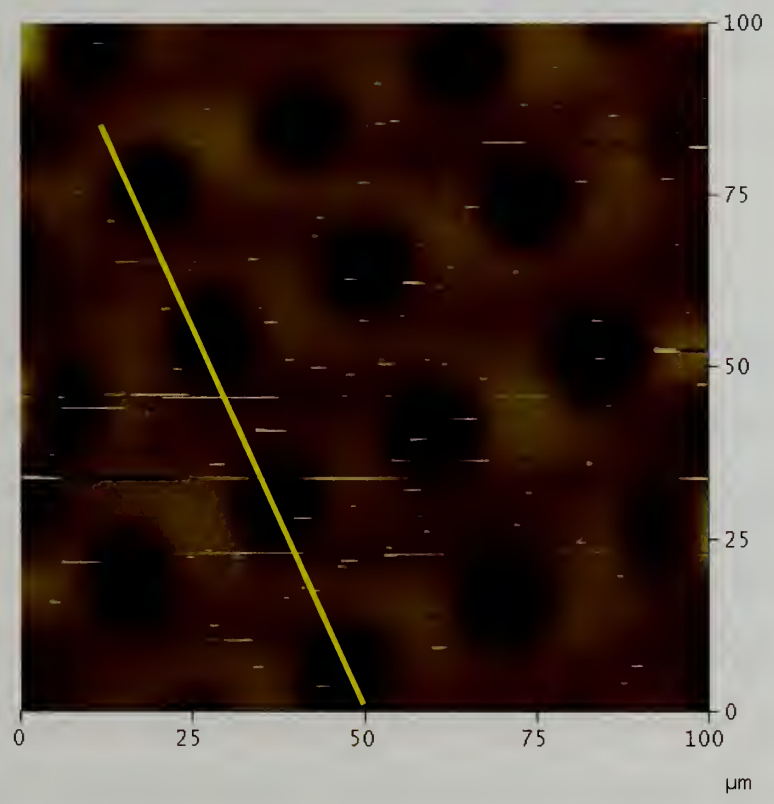

Figure 3.15: SFM image showing the device level replications in mesoporous silicate film templated from PMS-PHOST film

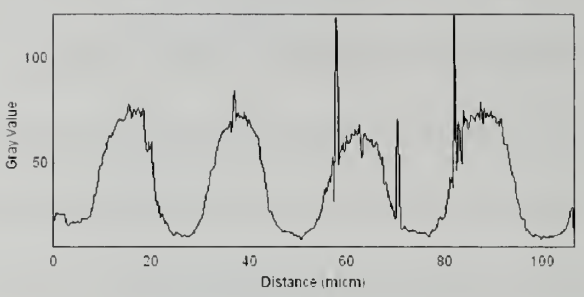

Figure 3.16: Section profile of the SFM image shown in Figure 3.15

In both block copolymers, partitioning of acid towards the hydrophilic domains enabled sharp domain level replications. However, inability of acid to differentiate hydrophilic domains in UV-exposed and unexposed regions led to diffusion of acid between these regions and hence device level replications are not promising.

3.4 Conclusions

In conclusion, use of PEO and PHOST based copolymers as templates to produce micropatterned mesoporous silicates films are explored in this chapter. From PHOST homopolymer templates, it is found that (i) silica deposition in crosslinked and developed films are unsuccessful due to acid loss problem and (ii) UV exposed and uncrosslinked films are suitable templates to produce patterned silicate films. In the case of block copolymer templates, segregation of photo acid into hydrophilic domain helped to obtain excellent domain level replications. However, diffusion of photoacid from UV exposed regions to unexposed regions resulted in less effective device level replications.

3.5 References

1. Wirnsberger, G.; Yang, P. D.; Huang, H. C.; Scott, B.; Deng, T.; Whitesides, G. M.; Chmelka, B. F.; Stucky, G. D., *J. Phys. Chem. B* **2001,** 105, 6307.

2. Schmuhl, R.; Nijdam, W.; Sekulic, J.; Chowdhury, S. R.; van Rijn, C. J. M.; van den Berg, A.; ten Elshof, J. E.; Blank, D. H. A., *Anal. Chem.* **2005,** 77, 178.

3. Schuth, F.; Schmidt, W., *Adv. Mater.* **2002,** 14, 629.

4. Jeong, H. K.; Chandrasekharan, R.; Chu, K. L.; Shannon, M. A.; Masel, R. I., *Ind. Eng. Chem. Res.* **2005,** 44, 8933.

5. Sayari, A., *Chem. Mater.* **1996,** 8, 1840.

6. Yang, H.; Coombs, N.; Ozin, G. A., *Adv. Mater.* **1997,** 9, 811.

7. Yang, P. D.; Rizvi, A. H.; Messer, B.; Chmelka, B. F.; Whitesides, G. M.; Stucky, G. D., *Adv. Mater.* **2001,** 13, 427.

8. Trau, M.; Yao, N.; Kim, E.; Xia, Y.; Whitesides, G. M.; Aksay, I. A., *Nature* **1997,** 390, 674.

9. Yang, P. D.; Wirnsberger, G.; Huang, H. C.; Cordero, S. R.; McGehee, M. D.; Scott, B.; Deng, T.; Whitesides, G. M.; Chmelka, B. F.; Buratto, S. K.; Stucky, G. D., *Science* **2000,** 287, 465.

10. Fan, H. Y.; Lu, Y. F.; Stump, A.; Reed, S. T.; Baer, T.; Schunk, R.; Perez-Luna, V.; Lopez, G. P.; Brinker, C. J., *Nature* **2000,** 405, 56.

11. Fan, H. Y.; Reed, S.; Baer, T.; Schunk, R.; Lopez, G. P.; Brinker, C. J., *Microporous Mesoporous Mater.* **2001,** 44, 625.

12. Mougenot, M.; Lejeune, M.; Baumard, J. F.; Boissiere, C.; Ribot, F.; Grosso, D.; Sanchez, C.; Noguera, R., *J. Am. Ceram. Soc.* **2006,** 89, 1876.

13. Su, M.; Liu, X. G.; Li, S. Y.; Dravid, V. P.; Mirkin, C. A., *J. Am. Chem. Soc.* **2002,** 124, 1560.

14. Wu, C. W.; Aoki, T.; Kuwabara, M., *Nanotechnology* **2004,** 15, 1886.

15. Malfatti, L.; Kidchob, T.; Costacurta, S.; Falcaro, P.; Schiavuta, P.; Amenitsch, H.; Innocenzi, P., *Chem. Mater.* **2006,** 18, 4553.

16. Cerrina, F., *Journal of Physics D-Applied Physics* **2000,** 33, R103.

17. Sugimura, H.; Hozumi, A.; Kameyama, T.; Takai, O., *Adv. Mater.* **2001,** 13, 667.

18. Hozumi, A.; Kojima, S.; Nagano, S.; Seki, T.; Shirahata, N.; Kameyama, T., *Langmuir* **2007,** 23, 3265.

19. Hozumi, A.; Kizuki, T.; Inagaki, M.; Shirahata, N., *Journal of Vacuum Science & Technology A* **2006,** 24, 1494.

20. Doshi, D. A.; Huesing, N. K.; Lu, M. C.; Fan, H. Y.; Lu, Y. F.; Simmons-Potter, K.; Potter, B. G.; Hurd, A. J.; Brinker, C. J., *Science* **2000,** 290, 107.

21. Lu, Y. F.; Yang, Y.; Sellinger, A.; Lu, M. C.; Huang, J. M.; Fan, H. Y.; Haddad, R.; Lopez, G.; Burns, A. R.; Sasaki, D. Y.; Shelnutt, J.; Brinker, C. J., *Nature* **2001,** 410, 913.

22. Yang, P. D.; Deng, T.; Zhao, D. Y.; Feng, P. Y.; Pine, D.; Chmelka, B. F.; Whitesides, G. M.; Stucky, G. D., *Science* **1998,** 282, 2244.

23. Pai, R. A.; Humayun, R.; Schulberg, M. T.; Sengupta, A.; Sun, J. N.; Watkins, J. J., *Science* **2004,** 303, 507.

24. Nagarajan, S.; Li, M. Q.; Pai, R. A.; Bosworth, J. K.; Busch, P.; Smilgies, D. M.; Ober, C. K.; Russell, T. P.; Watkins, J. J., *Adv. Mater.* **2008,** 20, 246.

25. Li, M. Q.; Douki, K.; Goto, K.; Li, X. F.; Coenjarts, C.; Smilgies, D. M.; Ober, C. K., *Chem. Mater.* **2004,** 16, 3800.

26. Dektar, J. L.; Hacker, N. P., *J. Am. Chem. Soc.* **1990,** 112, 6004.

27. Thurecht, K. J.; Hill, D. J. T.; Whittaker, A. K., *Macromolecules* **2005,** 38, 3731.

28. Nagarajan, S.; Bosworth, J. K.; Ober, C. K.; Russell, T. P.; Watkins, J. J., *Chem. Mater.* **2008,** 20, 604.

CHAPTER 4

FABRICATION OF MICRO-PATTERNED MESOPOROUS SILICATE FILMS FROM CHEMICALLY AMPLIFIED POLY (T-BUTOXY CARBONYLOXY STYRENE) (PTBOCST) COPOLYMERS

4.1 Introduction

The motivation for the work described in this chapter is derived from the conclusions drawn in previous chapter. Domain level replications from F108 and PMS-PHOST block copolymer templates have been obtained with high fidelity. However, device level replications lack sharp boundaries due to the diffusion of acid generated. Although the diffusion of acid is unfavorable, it is not completely unexpected. Enhanced diffusion of small molecules is well-known in SCF-dilated polymer matrices[1, 2]. In the case of inorganic precursors, for example, TEOS, accelerated diffusion is favorable to ensure homogeneous distribution of precursor throughout the film. It is desirable to use polymer templates, in which the diffusion of small molecules, for instance, precursor, is not disturbed while the diffusion of acid, from UV exposed regions to unexposed regions, is restricted. Such templates would lead to preparation of crack-free, robust mesoporous films with sharp domain and device level definition. This chapter discusses the possibilities of using chemically amplifiable, PtbocSt, copolymer templates to control acid diffusion and improve device scale resolution.

The concept of chemical amplification (CA) was first proposed and demonstrated by Ito, et al.[3, 4] Their approach is to generate a catalyst, photochemically, within the polymer or resist film. The role of the generated catalyst is to induce cascade of chemical transformations in the polymer matrix surrounding the catalytic species. Subsequently these chemical transformations translate into a large change in the solubility properties of

the polymer in the UV exposed areas of the film. Thus, the quantum efficiency of the photochemistry is amplified hundreds or even thousands times through the catalytic chain reactions. The solubility switch produced in the film by the chemical amplification process can be utilized to develop either positive or negative images by selective dissolution. The most popular chemical amplification process involved in PtbocSt system[5, 6] is shown in Figure 4.1.

Upon generation of the photoacid, via exposure and a post-exposure bake, the PtbocSt (hydrophobic) block is deprotected to yield poly(4-hydroxystyrene) (PHOST) domains which are hydrophilic. In a typical photoresist application[5, 7], this polarity switch would provide the basis for development by dissolution in a selective solvent. In this project, the template is not developed, but rather the exposed template is infused directly with TEOS in CO_2 solution.

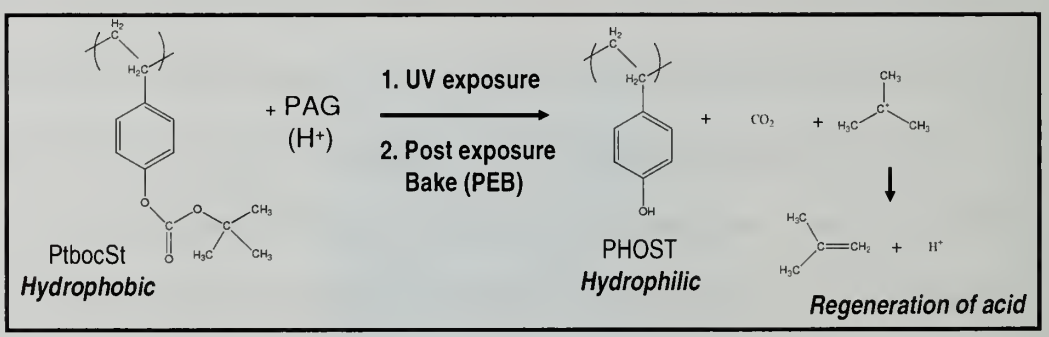

Figure 4.1: Chemical amplification process involved in PtbocSt

One of the key advantages of the CA systems is that the generated acid initiating the deprotection is regenerated along with other gaseous by-products (isobutene and carbon dioxide)[5, 8]. Such acid, regenerated or generated, is expected to hydrolyze the metal oxide precursor, besides deprotecting PtbocSt into PHOST. Due to the existence of

polarity difference between the UV-exposed (hydrophilic) and unexposed (hydrophobic) regions, the diffusion of acid from UV-exposed to unexposed regions in CA polymers is expected to be highly limited, compared to that found in F108 and PHOST copolymers.

To determine the feasibility of using PtbocSt copolymers as templates, PtbocSt homopolymer is initially used as templates to fabricate patterned silicate structures, as shown in Figure 4.2. PtbocSt films containing small amount of PAG are spun onto Si wafer. Films are UV irradiated through a photomask followed by post-exposure baked (PEB) at 80 °C for 90 seconds to convert PtbocSt to PHOST in the UV exposed regions. Such baked films are subjected to silica deposition. After template removal by calcination, the films are analyzed using OM. The outcome of this study is used to design further experiments in block copolymer templates, which will be discussed in the following sections of this chapter.

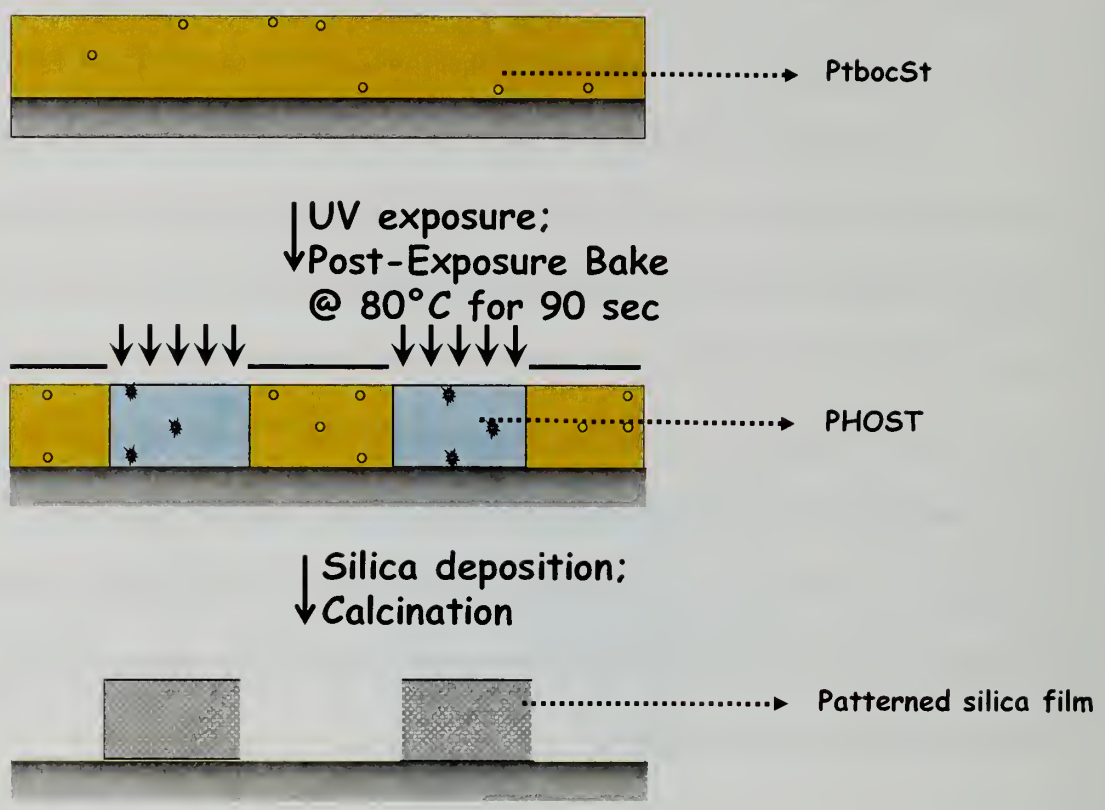

Figure 4.2: Schematic showing the steps involved in fabrication of patterned silicate films from PtbocSt homopolymer films

4.2 Experimental Section

Materials: Triphenyl sulfonium triflate (Sigma-Aldrich), tetraethyl orthosilicate (Sigma-Aldrich), and propylene glycol monomethyl ether acetate (Sigma-Aldrich) were used as received. PtbocSt of ~ 30000 gm/mol was synthesized, as reported elsewhere.

The diblock copolymer, poly (styrene-b-t-butoxycarbonyloxy styrene) (PS-b-PtbocSt) was synthesized in three steps, as described below in Prof. Ober's laboratory in Cornell University. In the first step, poly(styrene-block-t-butoxystyrene) (PS-b-PtboSt) was synthesized by sequential anionic polymerization and then deprotected to

poly(styrene-b-4-hydroxystyrene) (PS-b-PHOST), as described elsewhere[9]. In the third step, the hydroxyl groups were reprotected by adding di-*tert*-butyl dicarbonate (Sigma-Aldrich, excess) in acetone (Sigma-Aldrich) dropwise to a solution of the polymer with catalytic 4-(dimethylamino)pyridine (Sigma-Aldrich) in acetone using previously reported procedure[10]. The solution was precipitated with water. The polymer was then dissolved in tetrahydrofuran (Fisher) and precipitated with distilled water twice for purification. The molecular weight of initial block copolymer PS-PtboSt was measured by GPC to be 34,000g/mol-b-29,000g/mol with a distribution of 1.10. Complete deprotection of PS-b-PtboSt to PS-b-PHOST and subsequent reprotection to PS-b-PtbocSt was confirmed to be complete with FT-IR spectroscopy. Calculated molecular weight of PS-b-PtbocSt was 34,000 gm/mol-b-39,000 gm/mol.

Template Preparation: (1) PtbocSt templates: A 5 wt. % solution of PtbocSt was prepared in propylene glycol monomethyl ether acetate (PGMEA) containing 3 wt. % (with respect to polymer) triphenyl sulfonium triflate (TPST). Approximately ~ 200 nm thick template films were spin coated from this solution onto Si wafers at 2000 rpm for 60 seconds.

(2) PS-b-PtbocSt templates: A 3 wt. % solution of PS-b-PtbocSt was prepared in PGMEA containing 5 wt. % TPST. Approximately ~ 250 nm thick template films were spin coated from this solution onto Si wafer at 1500 rpm for 60 seconds.

Photolithographic UV Exposure: An HTG contact aligner at the Cornell Nanoscale Science and Technology Facility (CNF) was used to irradiate the templates through a photomask, which was present in soft contact with template during the UV

exposure. UV radiation chosen for our exposure was in the range of 220 – 300 nm with maximum at 254 nm. All of the templates were exposed in the range of 20 – 60 mJ/cm^2.

Domain Selective Silica Deposition: Silica deposition was performed by exposing the templates to silica precursor, tetraethyl orthosilicate (TEOS), dissolved in supercritical carbon dioxide ($scCO_2$) at 60 °C and 125 bar in a high pressure reactor. However to reach the desired temperature and pressure, two different routes have been followed, as described below.

Post-Exposure Bake (PEB) Followed by Silica Deposition: In this case, templates (PtbocSt) were spin coated, irradiated and baked at ambient conditions and then placed inside the reactor along with TEOS (5.0 – 10.0 μL). After sealing, the reactor was heated to 60 °C using external band heaters. CO_2 was then slowly injected into the reactor using a high-pressure syringe pump (ISCO, Inc. Model 500HP) until the desired pressure of ~125 bar was reached. Coleman-grade carbon dioxide (CO_2) was obtained from Merriam-Graves and used as received. The total pressurization and reaction time were maintained at 2 hours and then CO_2 was slowly released at the rate of ~0.3 bar/minute.

Simultaneous Post-Exposure Bake and Silica Deposition: In this case, templates (PtbocSt and PS-b-PtbocSt) were spun and irradiated at ambient conditions and then placed inside the reactor along with TEOS (5.0 – 10.0 μL). After sealing, the reactor was filled with CO_2 up to 70 bar at room temperature (21 °C – 24 °C). Then, the reactor was heated to 60 °C using external band heaters to reach the desired pressure of 125 bar. At this stage, post-exposure bake and TEOS infusion occur simultaneously. The reaction time was maintained at 2 hours and then CO_2 was slowly released at the rate of ~0.3 bar/minute.

The organic template was removed from the nanocomposite film by reactive ion etching under oxygen plasma followed by calcination at 400 °C for 6 hours under nitrogen atmosphere at the heating rate of 1.67 °C /min.

Characterization of organic template and mesoporous silicate films: The surface morphologies (top view) of the films were imaged using a scanning force microscope (SFM, Digital Instruments Dimension 3000) and optical microscope (Olympus BX60). To image the pore structure, transmission electron microscopy was performed on calcined films using a JEOL 2000 CX microscope operating at 200 kV. The samples were prepared by scraping the silica film off the substrate using a razor blade to make slurry of pieces of film in ethanol. A few drops of this slurry were dropped on the Formvar® resin-coated copper grid (Electron Microscopy Sciences) and dried prior to examination under microscope.

4.3 Results and Discussions

4.3.1 Patterned Silicate Films from Post-Exposure Baked PtbocSt Templates

Figure 4.3 shows the optical micrograph of the film after silica deposition in sc CO_2. As depicted in Figure 4.2, the template is exposed and baked (PEB) at ambient conditions before performing silica deposition. Although the OM in Figure 4.3 is encouraging, as it exhibits sharp boundaries, no film remained on the wafer after calcination indicating that silica deposition is unsuccessful.

Figure 4.3: Optical Micrograph of PtbocSt film after silica deposition and before calcination

The absence or inactivity of the acid catalyst is one possible reason for not depositing silica. Successful formation of pattern after PEB (figure 4.3) and unsuccessful deposition of silica suggest that the generated acid is active enough to deprotect PtbocSt to PHOST but the regenerated acid, as depicted in figure 4.1, may not be effective enough to hydrolyze TEOS. Interestingly, previous reports[11-15] about PtbocSt polymers support the abovementioned speculation by showing that the acid, regenerated upon deprotection of PtbocSt, is short lived and becomes unreactive by getting trapped in decomposition products generated from PAG and/or polymer. Moreover, regenerated acid can also be neutralized or poisoned by amines present in ambient conditions.

4.3.1.1 Process Modification

To overcome the acid deactivation problem, process conditions are modified in such a way that the generated photo acid hydrolyses TEOS while deprotecting PtbocSt. Modified process conditions are shown in Figure 4.4. UV exposed templates are pressurized first and heated next. By doing so, precursor will be infused into the template well before the onset of thermally induced deprotection. Hence, deprotection and TEOS hydrolysis happen simultaneously when the template is heated and there is no need to depend on regenerated acid. For comparison, the original process conditions are shown in Figure 4.5. One can observe that heating the template first and pressurizing later led to acid deactivation and, hence, silica deposition was unsuccessful.

Figure 4.6 shows the SFM image of the calcined film obtained from PtbocSt templates by following the modified process conditions (Figure 4.4). The presence of well-defined silicate structures with sharp boundaries suggest simultaneous hydrolysis of TEOS and deprotection of PtbocSt and significantly restricted diffusion of acid. The simultaneous PEB-Silica deposition is performed at 60 °C and to determine the completeness of deprotection at this temperature, FT-IR spectroscopy is used to analyze the templates baked at 60 °C for various times. As it is shown in Figure 4.7, disappearance of carbonyl group's absorption peak even after 90 seconds bake indicates complete deprotection at 60 °C.

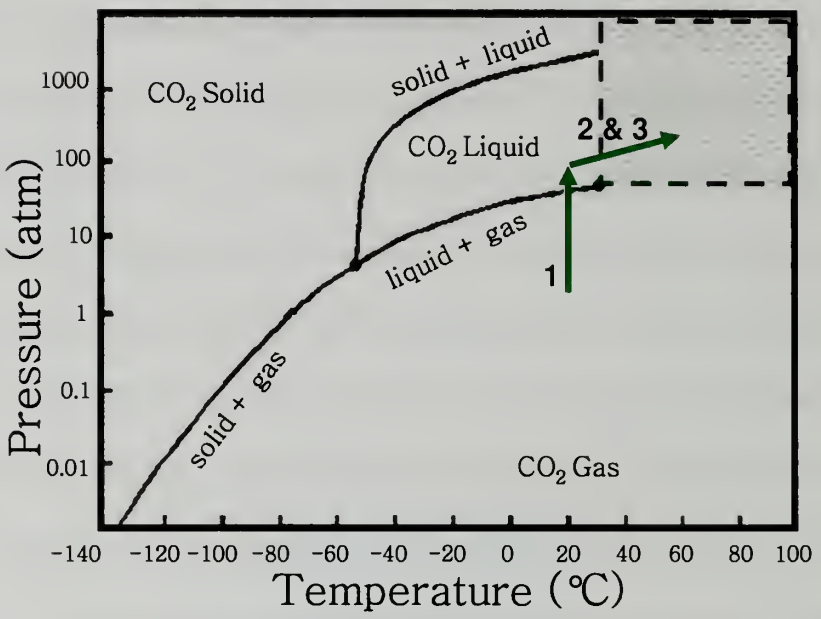

Figure 4.4: Modified Process Conditions; Steps involved in patterned silica film fabrication: **1**. UV exposure; **2**. Post exposure bake (PEB); **3**. Silica infusion; **4**. Calcination. CO_2 phase diagram adapted and modified from an electronic resource[16]

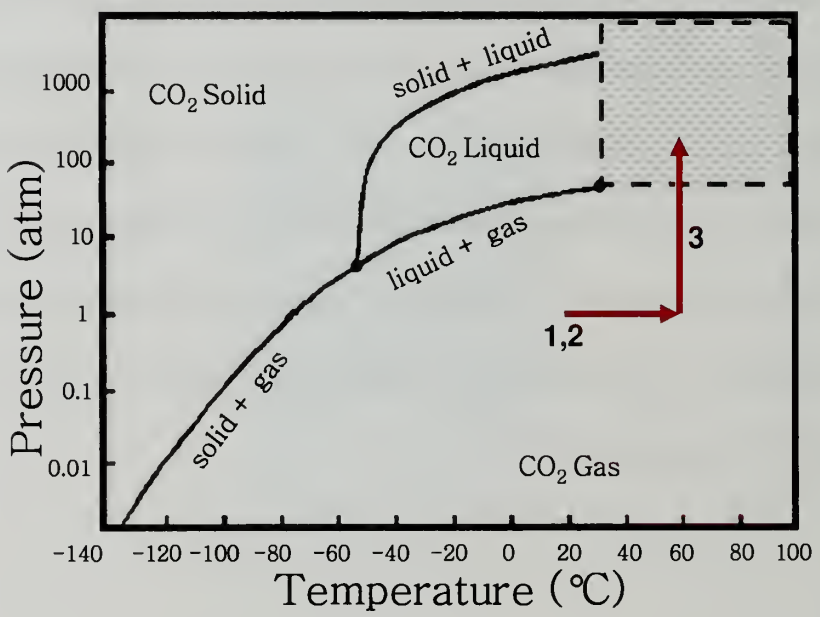

Figure 4.5: Original Process Conditions. CO_2 phase diagram adapted and modified from an electronic resource[16]

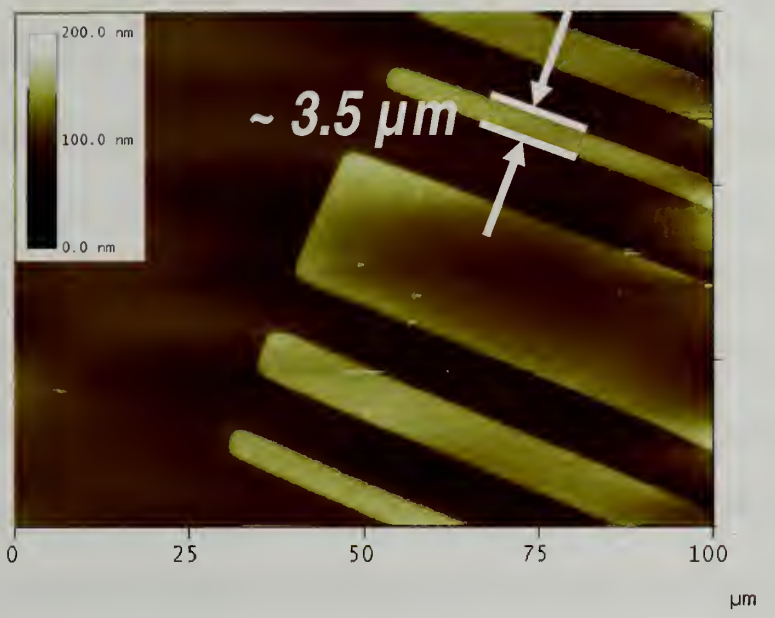

Figure 4.6: SFM image of the patterned silicate film (after calcination) templated from PtbocSt and prepared by following the modified process conditions

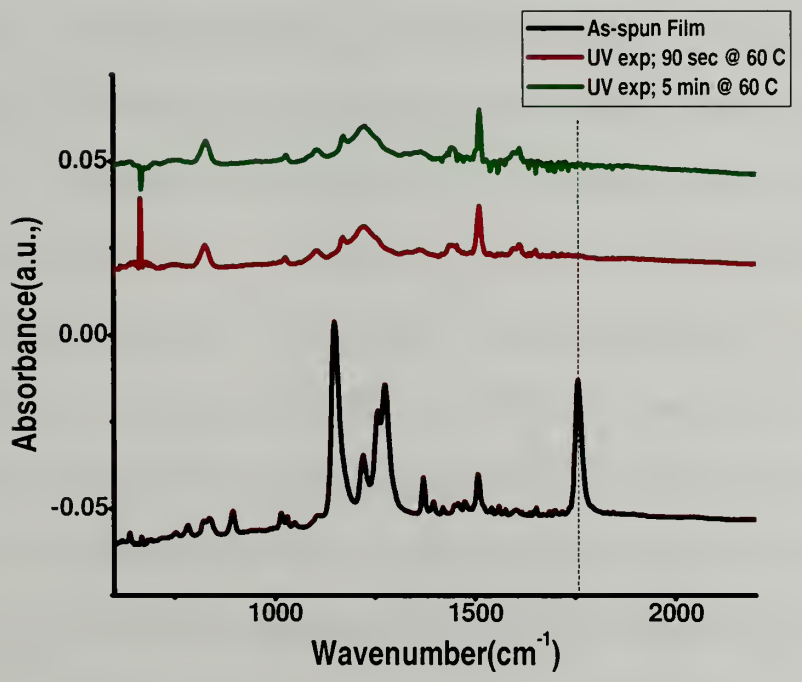

Figure 4.7: FT-IR traces showing complete deprotection of PtbocSt

4.3.2 Micro-Patterned Mesoporous Silicate Films from PS-b-PtbocSt Templates

After optimizing the process conditions for fabrication of patterned silicate films from PtbocSt films, micropatterned mesoporous silicate films with sharp domain and device level structures are fabricated using an appropriate chemically amplifiable block copolymer. Anionically synthesized PS-b-PtbocSt is used as templates as shown in Figure 4.8. After UV exposure, post exposure bake and the domain selective silica deposition are done simultaneously in the presence of TEOS dissolved in sc CO_2 at 125 bar and 60 °C. After depressurization, the film was etched in oxygen plasma to remove the organic components of the film and further calcined thermally at 400 °C to de-template and to complete the condensation of the silicate framework. SFM image of the calcined silica film in Figure 4.9, shows the micron-scale holes templated from the photomask. A section profile of the SFM image showed in Figure 4.10 reveal sharp sidewalls within the ~ 200 nm deep features, suggesting that hydrolysis and condensation of TEOS proceeded simultaneously with deprotection reactions in the exposed regions, whereas little if any condensation is noted in the unexposed regions.[17] It is worth mentioning that diffusion of generated acid catalyst from unexposed to exposed regions in chemically amplifiable polymers is highly limited compared to that in low-T_g polymers, like Pluronic F108. In the case of former polymers, the acid diffusion is coupled with deprotection reaction front at the junction of exposed and unexposed regions, whereas in the case of latter polymers, diffusion proceeds freely at the junction. Figure 4.9 and 4.10 clearly indicate that the device level structures can be replicated with high fidelity using chemically amplifiable block copolymers as templates.

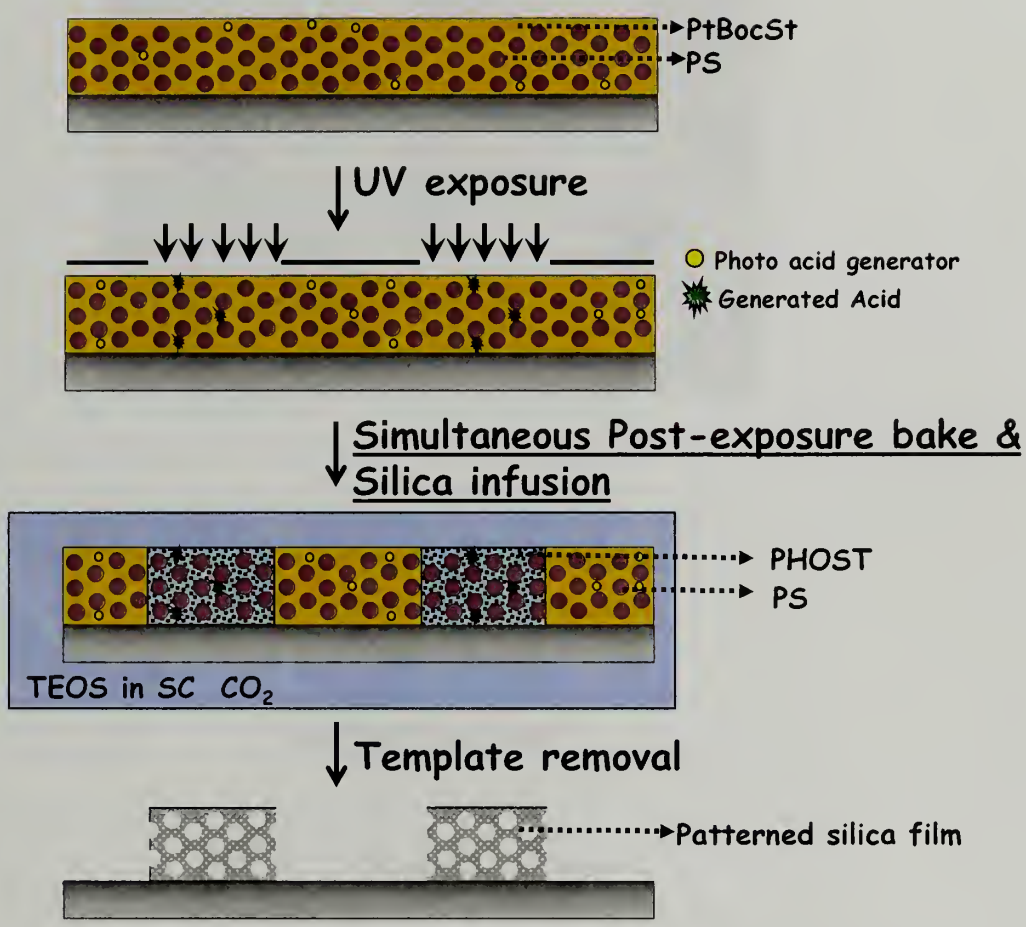

Figure 4.8: Schematic showing the steps involved in preparation of micropatterned mesoporous silicate films

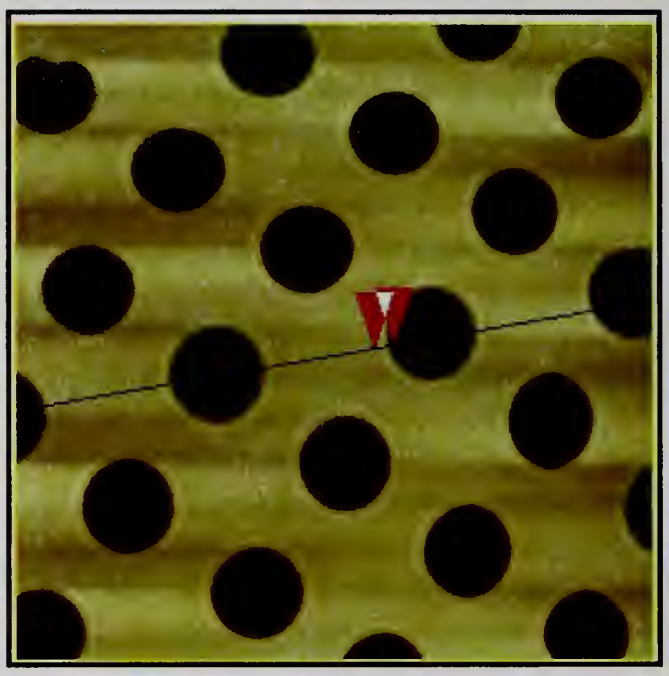

Figure 4.9: SFM image of the micropatterned mesoporous silicate films templated from PS-b-PtbocSt films

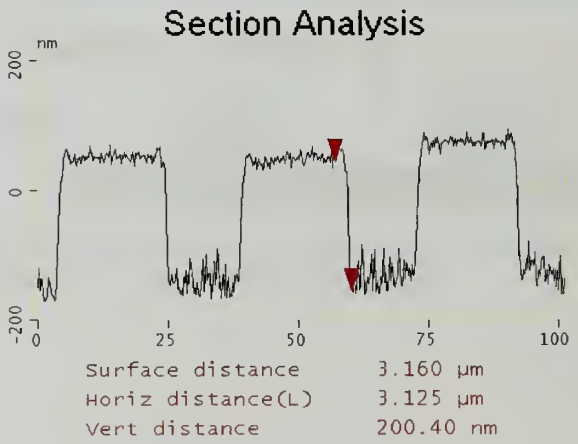

Figure 4.10: Section analysis of the SFM image shown in Figure 4.9

Figure 4.11: TEM image of the micropatterned mesoporous silicate films templated from PS-b-PtbocSt films

Domain level replication can be verified from the TEM image in Figure 4.11, which shows the mesoporous structures templated from block copolymer microphase segregation. However, the pores are not ordered. This can be attributed to the weak phase segregation inherent to the underlying block copolymer template that has been reproduced in the silica film[17].

4.4 Conclusions

In conclusion, it is found that chemically amplifiable polymers restrict acid diffusion and enabled high fidelity replication of device level structures. Although acid is regenerated after deprotection, it is unreactive as they are getting trapped. Process conditions have been modified in such a way that the acid can be used for TEOS condensation before it is deactivated. By using PS-b-PtbocSt templates, micro patterned mesoporous silicate films with domain and device level definitions are produced. It is worth mentioning that the method described, in this chapter, to pattern mesoporous silica films can be easily integrated into existing fabrication processes and reduce the number of process steps by eliminating the need for subsequent etching. Such an approach may reduce the cost, resources and waste generation, for example, in fabrication of thick lines for BEOL (Back end of the line) processes[18] and potentially lower metallization layers as well. It should be noted that the resolution of features reported in this chapter is largely driven by our choice of mask and the limits of contact exposure.

4.5 References

1. Gupta, R. R.; RamachandraRao, V. S.; Watkins, J. J., *Macromolecules* **2003,** 36, 1295.

2. Pai, R. A.; Humayun, R.; Schulberg, M. T.; Sengupta, A.; Sun, J. N.; Watkins, J. J., *Scieuce* **2004,** 303, 507.

3. Ito H, W. C. F. J., *Digest of Technical Papers of 1982 symposium on VLSI technology* **1982**, 86.

4. Ito H, W. C., *Technical Papers of SPE Regional Technical Conference on Photopolymers* **1982**, 331.

5. Ito, H., Chemical amplification resists for microlithography. In *Microlithography - Molecular Imprinting*, 2005; Vol. 172, pp 37.

6. Ito, H., *Ibm Journal of Research and Development* **1997,** 41, 69.

7. Ito, H.; Willson, C. G., *Polym. Eng. Sci.* **1983,** 23, 1012.

8. Ito, H.; Willson, C. G., *Acs Symposium Series* **1984,** 242, 11.

9. Li, M. Q.; Douki, K.; Goto, K.; Li, X. F.; Coenjarts, C.; Smilgies, D. M.; Ober, C. K., *Chem. Mater.* **2004,** 16, 3800.

10. Felix, N. M.; Tsuchiya, K.; Ober, C. K., *Adv. Mater.* **2006,** 18, 442.

11. McKean, D. R.; Schaedeli, U.; Macdonald, S. A., *Journal of Polymer Science Part A-Polymer Chemistry* **1989,** 27, 3927.

12. Houle, F. A.; Hinsberg, W. D.; Morrison, M.; Sanchez, M. I.; Wallraff, G.; Larson, C.; Hoffnagle, J., *J. Vac. Sci. Technol., B* **2000,** 18, 1874.

13. Lavery, K. A.; Vogt, B. D.; Prabhu, V. M.; Lin, E. K.; Wu, W. L.; Satija, S. K.; Choi, K. W., *J. Vac. Sci. Technol., B* **2006,** 24, 3044.

14. Lin, E. K.; Soles, C. L.; Goldfarb, D. L.; Trinque, B. C.; Burns, S. D.; Jones, R. L.; Lenhart, J. L.; Angelopoulos, M.; Willson, C. G.; Satija, S. K.; Wu, W. L., *Science* **2002,** 297, 372.

15. Wallraff, G.; Hutchinson, J.; Hinsberg, W.; Houle, F.; Seidel, P.; Johnson, R.; Oldham, W., *J. Vac. Sci. Technol., B* **1994,** 12, 3857.

16. Shakhashiri, *Carbon Dioxide*. http://scifun.chem.wisc.edu/chemweek/PDF/CarbonDioxide.pdf (May 2008),

17. Nagarajan, S.; Bosworth, J. K.; Ober, C. K.; Russell, T. P.; Watkins, J. J., *Chem. Mater.* **2008,** 20, 604.

18. Hoofman, R.; Verheijden, G.; Michelon, J.; Iacopi, F.; Travaly, Y.; Baklanov, M. R.; Tokei, Z.; Beyer, G. P., *Microelectron. Eng.* **2005,** 80, 337.

CHAPTER 5

DUAL-TONE PATTERNED MESOPOROUS SILICATE FILMS TEMPLATED FROM CHEMICALLY AMPLIFIED BLOCK COPOLYMERS

5.1 Introduction

Precisely patterned mesoporous metal oxide films exhibit great promise for many applications including microelectronics[1], micro fluidics[2], photonics[3] and sensors[4]. While the formation and characterization of mesoporous films are of scientific interest, the ability to pattern these films in an efficient manner is of technological interest. Photolithography has been used conventionally for patterning. In this case, a subtractive and less efficient strategy is adopted by coating a photosensitive layer on top of the mesoporous film, followed by developing an image in the photosensitive layer with an aid of UV exposure and transferring the developed image into the underlayer by selective etching. Finally, the top layer of photosensitive film is removed via wet cleaning or dry etching[5]. To account for unconventional patterning of mesoporous films, wide variety of promising strategies including soft lithography[3, 6-8], micropen lithography[9, 10], ink-jet printing[9, 11], dip-pen lithography[12], electron beam lithography[13], x-ray direct writing[14, 15], micro-patterned self-assembled monolayer templating[6, 16-18], photochemical variation in acid concentration and surfactant degradation.[19, 20] However, in all these strategies, mesoscopic structures are synthesized by an approach called evaporation induced self-assembly (EISA)[21]. As described in the previous chapters, the morphology of the final mesoporous silica film can not be completely controlled in EISA, as the structure evolution and precursor condensation occur simultaneously. Moreover, the use of excess alcohol to control the condensation of precursor requires long processing times.

It is desirable to adopt a synthetic route that can provide complete control over the morphology of final mesoporous film and a patterning strategy that is cost-effective and additive in nature. The method described in previous chapter to fabricate directly patterned mesoporous films via two-step approach, enables complete control over the morphology of the final mesoporous film. Moreover, direct definition followed by replication of the pattern obviates the need for additional etching-cleaning steps and offers a cost-effective, compressed process routine to patterned mesoporous films. It was found that a chemically amplifiable block copolymer, for example, poly (styrene-b-tert-butoxy carbonyloxy styrene) (PS-b-PtbocSt)[22], is one of the appropriate templates to yield mesoporous films with sharp microscopic features. Although PS-b-PtbocSt was a suitable candidate to prove the concept of restricting the acid diffusion and further yielding sharp microscopic features, it was not sufficient to provide well-ordered nanoscopic structures as well. Since PS and PtbcoSt are weakly segregating systems, PS-b-PtbocSt exhibited modest microphase separation and, hence, the nanoscopic structure in the mesoporous silica film was not well-ordered. Moreover, using this method, one can only obtain a negative tone replication of the photomask. This chapter describes a versatile approach to positive and negative tone patterned mesoporous silicate films in which various nanoscopic morphologies including long-range ordered structures can be tuned. This chapter will also discuss the possibility of replicating high resolution device level structures registered via projection lithography.

Similar to PtbocSt, Poly (tert-butyl methacrylate) (PtbMA) and Poly (tert-butyl acrylate) (PtbA) can also be chemically amplified[23-26]. Acid cleavable ester groups present in these polymers are responsible for imparting a polarity switch upon UV

exposure and post-exposure bake. In fact, tert-butyl acrylate polymers undergo chemical amplification in two stages as shown in Figure 5.1. In the first stage, ester linkage in PtbA (hydrophobic) is cleaved to form hydrophilic, poly (acrylic acid) (PAA). In the second stage, PAA is converted into crosslinked poly (acrylic anhydride) after a high temperature bake. Such two stage chemical amplification is utilized to produce dual-tone patterned mesoporous silicate films as shown in the Figure 5.2.

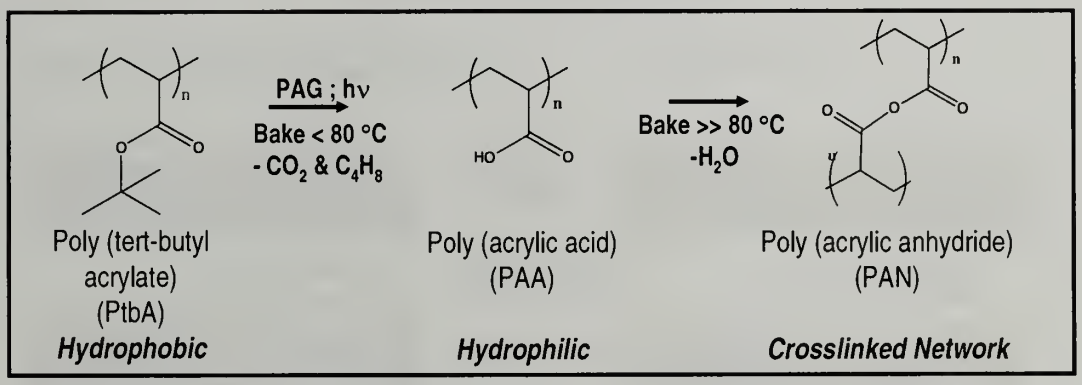

Figure 5.1: Two stage chemical amplification process: Acid catalyzed deprotection of poly (tert-butyl acrylate) (PtbA) to poly (acrylic acid) (PAA) at post-exposure bake (< 80 °C) and formation of poly(acrylic anhydride at an elevated temperature bake

An asymmetric diblock copolymer comprised of chemically amplifiable poly tert-butyl acrylate block (volume fraction > 70%) and a hydrophobic block is spin coated onto a silicon wafer from a solution containing a small amount of PAG and a crosslinker (if necessary). To generate negative tone replication of the photomask, the template is first photo-lithographically exposed to generate acid in the template. Post-exposure bake and

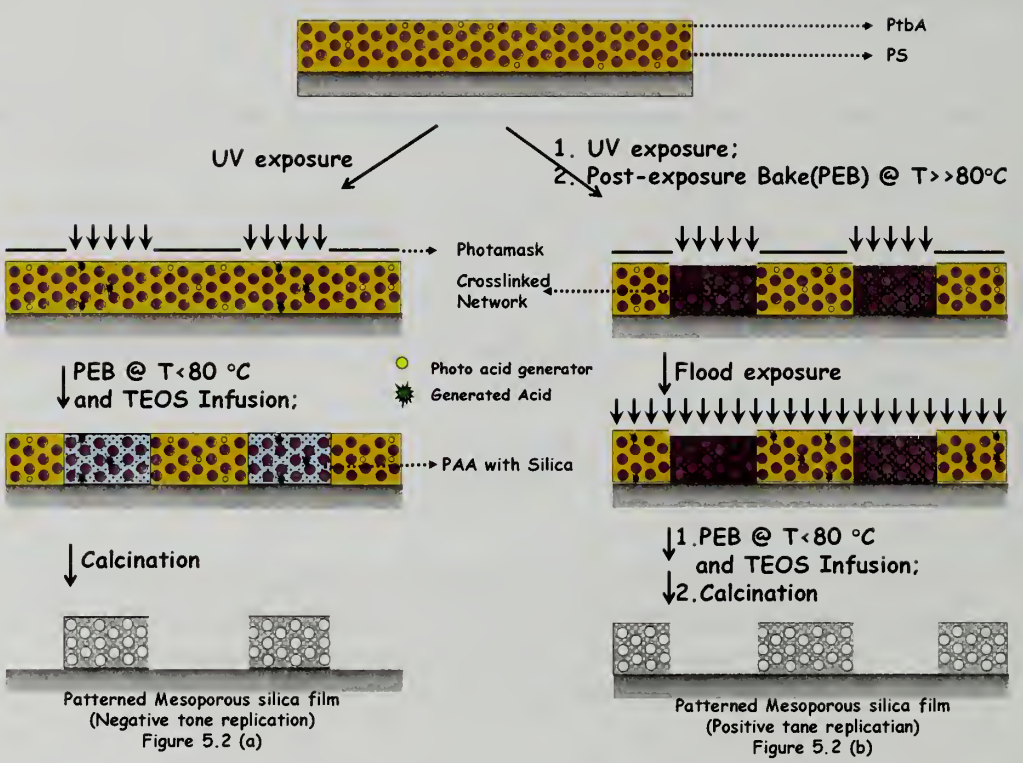

Figure 5.2: Steps involved in fabrication of Dual-tone patterned mesoporous silicate films templated from PS-b-PtbA films

TEOS infusion is performed simultaneously in the presence of sc CO_2, to ensure that the acid generated is utilized to deprotect PtbA and condense TEOS in the PAA domains. Removal of template by calcination yields negative tone patterned mesoporous silicate films. To get positive tone replication, the template is baked at a much higher temperature (>> 80 °C) after photo-lithographic UV exposure in ambient conditions. Such high temperature baking ensures deprotection and further crosslinking via anhydride formation in the UV exposed regions. Further, the template is flood exposed to UV (with no photomask) to generate acid in the initially unexposed regions. At this stage, the template is placed inside the high pressure reactor to perform simultaneous post-exposure bake and silica deposition. By optimizing the degree of crosslinking, dilation of the initially exposed regions of the template in sc CO_2 can be restricted to minimize or stop the delivery of precursor to such crosslinked regions. Absence of precursor in the crosslinked regions, the presence of precursor and, further, their condensation in uncrosslinked regions yield positive tone patterned mesoporous silicate films.

5.2 Experimental Section:

Materials: Poly (styrene-b-tert-butyl acrylate) (Polymer source Inc.,), triphenyl sulfonium triflate (Sigma-Aldrich), tetraethyl orthosilicate (Sigma-Aldrich), tetra methoxy methyl glycoluril (donated by Altec Chemicals), chloroform, ethanol and hexane (Sigma-Aldrich) were used as received.

Template Preparation: A 3 wt. % solution of PS-b-PtbA was prepared in chloroform containing 5 wt % (with respect to polymer) TPST. Approximately 250 nm thick template films were spin coated from this solution onto Si wafer at 1500 rpm for 60 seconds.

Template Annealing: Thermal annealing was performed in a vacuum oven at 120 °C for 12 hours. Solvent annealing was performed by placing the template on a Si wafer inside a glass jar. Approximately, 5ml of solvent (chloroform or ethanol-hexane mixture) in a vial, placed in the glass jar, is allowed to swell the polymer film for about 24 hours. The template was then taken out of the jar and used for further studies.

Photolithographic UV Exposure: A laboratory scale tray lamp, purchased from UV Products, was used to irradiate the templates through a photomask which was in soft contact with template during the UV exposure. The wafer piece and the photomask were sandwiched between quartz plates and this assembly is placed under the UV lamp. The UV lamp is well-sealed to avoid entry of stray light. The photomask used in this study is a quartz plate containing square packed metal dots. The diameter of each dot is ~ 13 microns. UV radiation emitted from the lamp used in our study was in the range of 220 – 300 nm with maximum at 254 nm. All of the template films were exposed in the range of 20 – 60 mJ/cm^2.

Domain Selective Silica Deposition: Silica deposition was performed by exposing the templates to silica precursor, tetraethyl orthosilicate (TEOS), dissolved in supercritical carbon dioxide (sc CO_2) at 60 °C and 125 bar in a high pressure reactor. To perform post exposure bake and silica deposition simultaneously, an irradiated film spin coated onto a ~ 1.25"×1.25" Si wafer piece was placed inside the reactor along with

TEOS (5.0 – 10.0 μL). After sealing, the reactor was filled with CO_2 upto 70 bar at room temperature (21 °C – 24 °C). Then the reactor was heated to 60 °C using external band heaters to reach the desired pressure of 125 bar. The reaction time was maintained at 2 hours and then CO_2 was slowly released at the rate of ~0.3 bar/minute. The organic template was removed by calcination at 400 °C for 6 hours at the heating rate of 1.67°C/min.

Characterization of Organic Template and Mesoporous Silicate Films: The surface morphologies (top view) of the films were imaged using a scanning force microscope (SFM, Digital Instruments Dimension 3000) and an optical microscope (Olympus BX60). To image the pore structure, transmission electron microscopy was performed on calcined films using a JEOL 1000 CX microscope operating at 100 keV. PS-b-PtbA samples, for TEM imaging, were prepared by spin coating the copolymer onto Si wafer having a thick (200 nm) sacrificial thermal oxide layer. After spinning or after annealing, the film was floated off the substrate by etching the thermal oxide in 5% HF aqueous solution. Such floated films are picked up in Cu grid and stained with ruthenium tetraoxide.

Mesoporous silica sample, for TEM imaging, were prepared by scraping the silica film off the substrate using a razor blade to make slurry of pieces of film in ethanol. A few drops of this slurry were placed on a Formvar® resin-coated copper grid (Electron Microscopy Sciences) and dried prior to examination under microscope.

5.3. Results and Discussion

5.3.1 Micro-Patterned Mesoporous Silicate Films from PS-b-PtbA Templates

5.3.1.1 Template Characterization

In this study, poly (styrene-b-tert-butyl acrylate) (PS-b-PtbA), purchased from Polymer Source Inc., is used as templates. The total molecular weight of PS-b-PtbA is 101,000 gm/mol and the volume fraction of PtbA (f_{PtbA}) is ~ 81 %. The chemical structure of PS-b-PtbA is shown in Figure 5.3. Suitable volume fraction and conveniently low T_g of PtbA, helped to obtain various morphologies (Figure 5.4-5.7) from the same block copolymer via different annealing conditions. Figure 5.4 shows the TEM image of an as-spun film. The interaction between PS and PtbA is strong enough to trigger microphase separation immediately after spin coating. PS domains are stained with ruthenium tetraoxide for imaging contrast purposes. As can be seen, the PS domains are not well-defined (worm-like) and they are randomly oriented. Figure 5.5 shows the TEM image of the film annealed at 120 °C, above the glass transition temperatures of PS (102 °C) and PtbA (42 °C). In this case, the interface between PS and PtbA domains are sharper, while the morphology is similar to that of as-spun film. However, the morphology of PS-b-PtbA films can be tuned significantly by annealing under a solvent atmosphere. Annealing under $CHCl_3$ atmosphere for about 24 hours, resulted long range ordered cylindrical morphology as shown in Figure 5.6. When the film was annealed under ethanol and hexane mixture (1:1) for about 24 hours, a well-ordered spherical morphology (Figure 5.7) is obtained. Dramatic increase in the lateral long-range order by annealing the block copolymer films under solvent vapor has been observed and

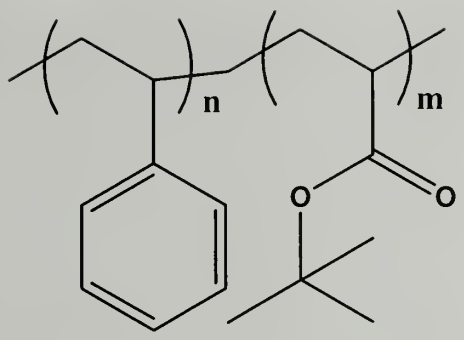

Figure 5.3: Chemical structure of poly (styrene-b-tert-butyl acrylate) (PS-b-PtbA)

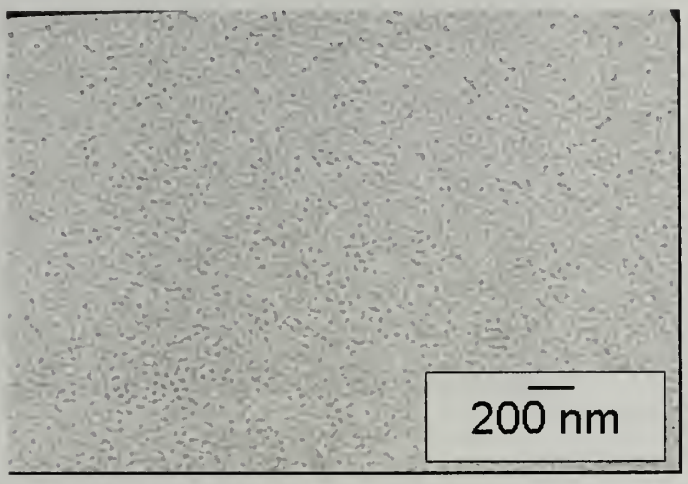

Figure 5.4: TEM image of as-spun PS-b-PtbA film. PS domains, stained with RuO_4, appear darker

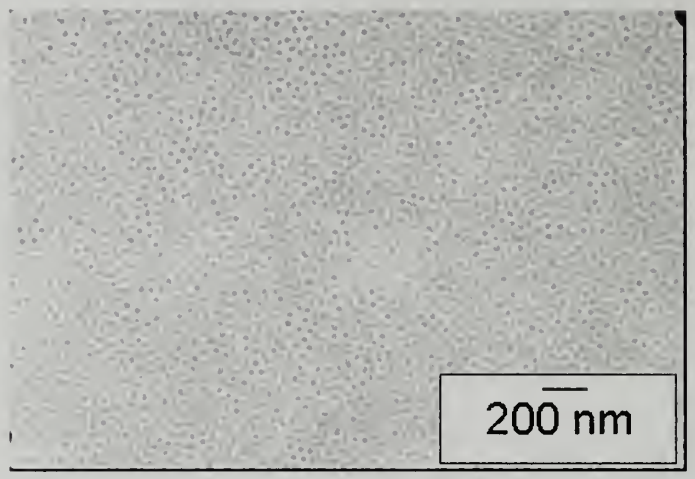

Figure 5.5: TEM image of PS-b-PtbA film annealed at 120 °C for about 12 hours

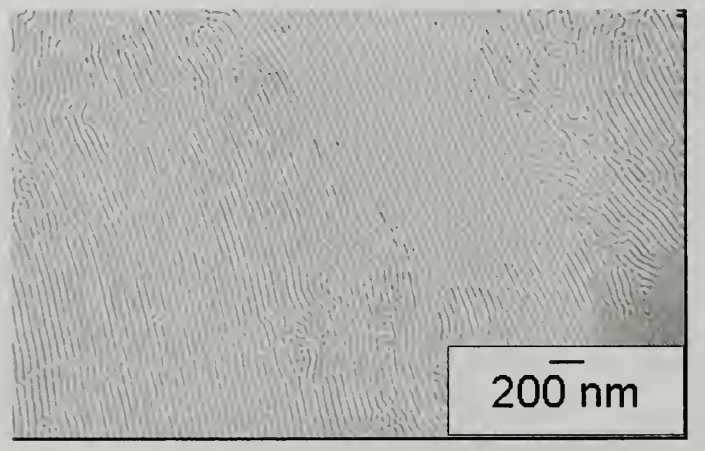

Figure 5.6: TEM image of PS-b-PtbA film, annealed under chloroform vapor for 24 hours

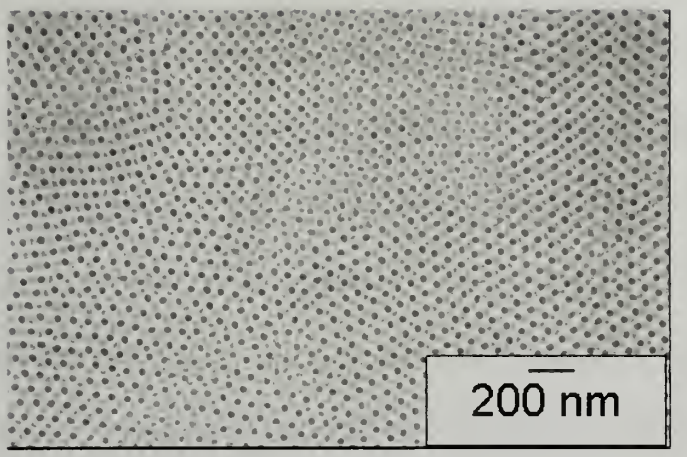

Figure 5.7: TEM image of PS-b-PtbA film, annealed under hexane:ethanol (1:1) mixture for 24 hours

well-studied previously [27-30]. It was shown that solvent annealing imparted mobility in the film, enabling rapid removal of defects and higher degree of long-range order that propagates through the entire thickness of the film. In agreement with previous reports, solvent annealing enabled long-range order in PS-b-PtbA films, as well. Annealing under $CHCl_3$, is a neutral solvent, enabled uniform swelling of both the blocks and resulted in long-range ordered cylindrical morphology. On the other hand, annealing under PtbA-selective solvent mixture, ethanol + hexane (1:1), enabled non-uniform swelling of PS and PtbA and resulted in well-ordered spherical morphology. The chosen block copolymer (f_{PtbA} ~ 81%) may be at the boundary between the cylindrical and spherical morphology. Hence, depending on the nature of the solvents used for annealing, the block copolymer may exhibit either morphology.

5.3.1.2 Negative Tone Replication

To produce negative tone patterned mesoporous silicate films, PS-b-PtbA films were photo-lithographically exposed as shown in schematic described in Figure 5.2(a) Post-exposure bake and silica deposition were performed simultaneously at 60 °C and 125 bar in the presence of TEOS dissolved in sc CO_2. After calcination, films are analyzed using SFM and TEM to characterize the patterns replicated from the photomask and block copolymer respectively. SFM image in Figure 5.8 shows a micro-well structure replicated from the photomask and the section analysis in Figure 5.9 denote precise replication with sharp sidewalls. As expected, the ability of chemically amplifiable PtbA to restrict acid diffusion helped to obtain high fidelity replication. The TEM image in Figure 5.10 shows ordered cylindrical nanopores/channels replicated from block copolymer film, annealed under $CHCl_3$.

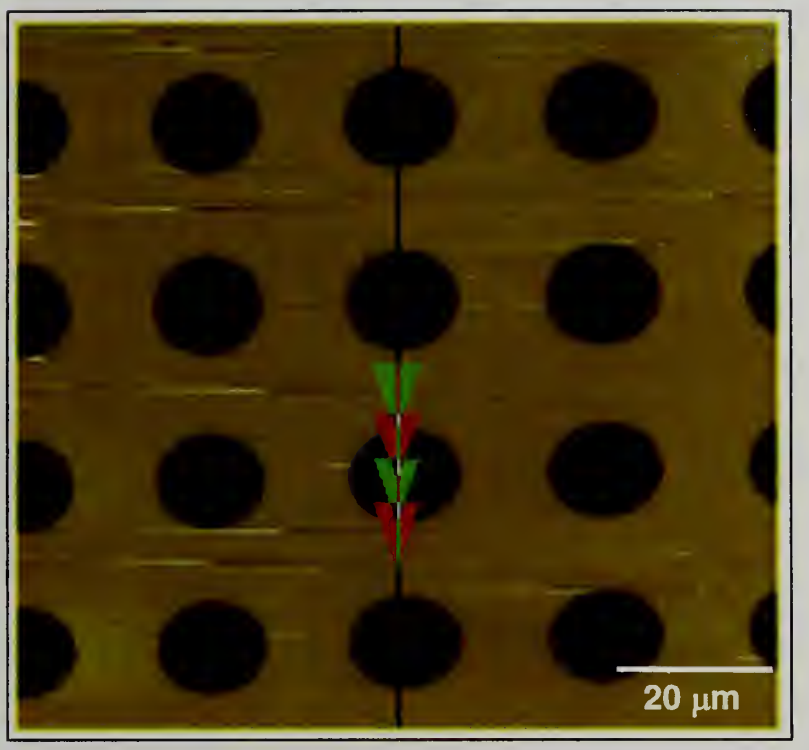

Figure 5.8: SFM image of negative tone patterned mesoporous silicate film

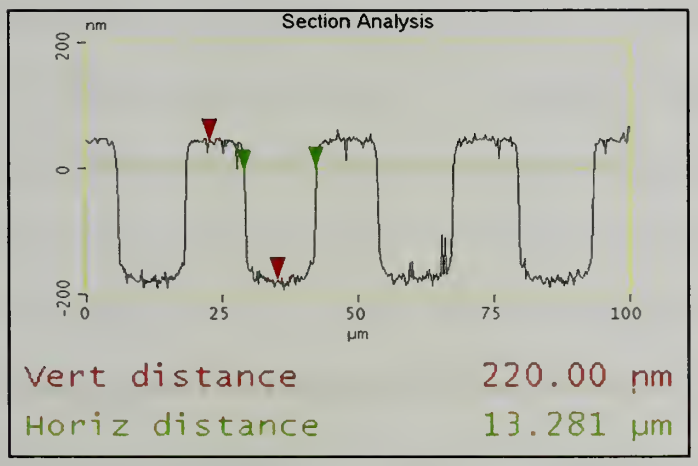

Figure 5.9: Section analysis of the SFM image shown in Figure 5.8

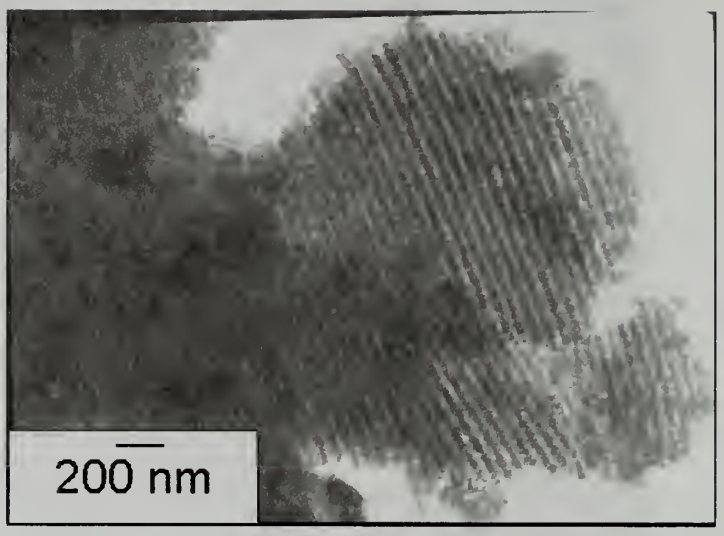

Figure 5.10: TEM image of negative tone patterned mesoporous silicate film

5.3.1.3 Positive Tone Replication

As shown in Figure 5.2(b), positive tone replication can be obtained by crosslinking the UV exposed fields via anhydride formation followed by flood exposure to activate silica deposition in the initially unexposed fields. It is essential that the UV exposed regions are crosslinked sufficiently to restrict diffusion of precursor in the CO_2-swollen domains and shut down silica deposition in such crosslinked regions. Hence external crosslinking agents are added to the template besides relying on the anhydride formation. The necessity for adding external crosslinking agents can be seen in the FT-IR results shown in figures 5.11 and 5.12. Conversion of ester (PtbA) to carboxylic acid (PAA) and then to anhydride (PAN) can be easily tracked by following the IR absorption bands, corresponding to the stretching vibrations of carbonyl groups present in the templates. Figure 5.11 & 5.12 show the FT-IR traces of PS-b-PtbA templates, exposed to

UV for 30 seconds and baked at various conditions. Baking conditions reported in these figures (5.11 & 5.12) are chosen in such a way that they span the entire range of tolerable baking conditions to retain the pattern produced after the PEB. Baking any longer than the times covered in this range or any higher than the temperatures covered in this range lead to pattern loss because of thermally activated diffusion of acid from exposed regions to unexposed regions. Such activated diffusion triggered deprotection of PtbA and smeared out the patterns.

Spectrum covering the entire IR region is shown in Figure 5.11 and only the spectral range of interest is shown in Figure 5.12, in which the FT-IR trace of as-spun template is also included. As one can notice, anhydride formation is not complete in any

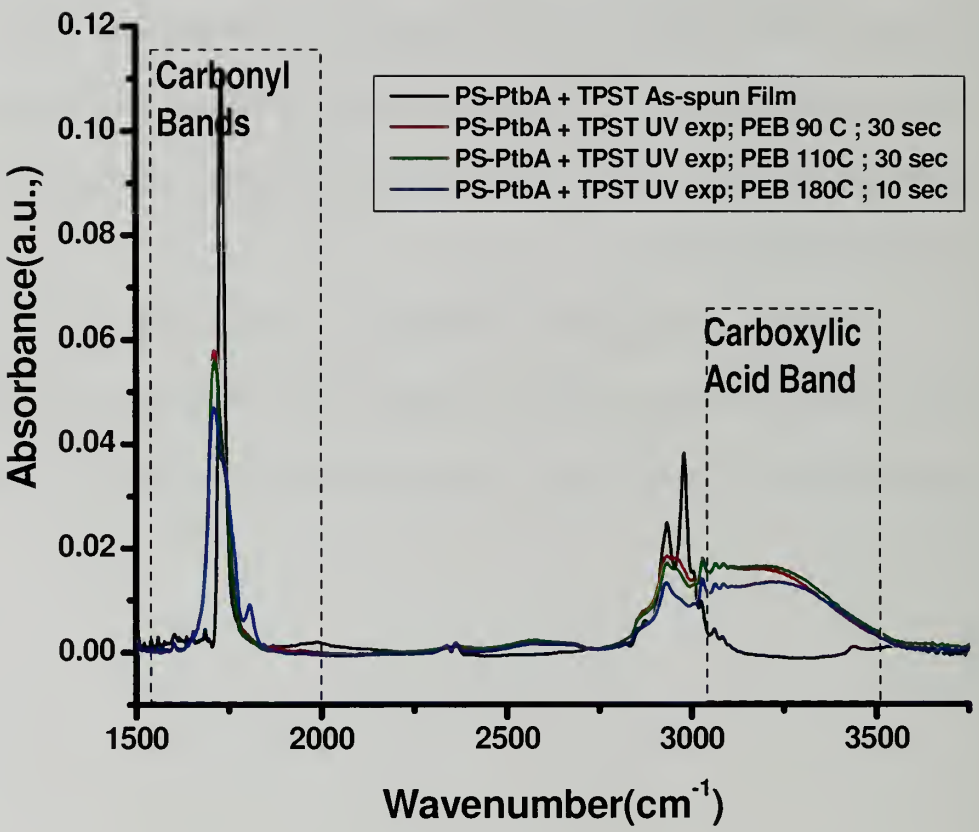

Figure 5.11: FT-IR spectra showing the extent of anhydride formation under various baking conditions

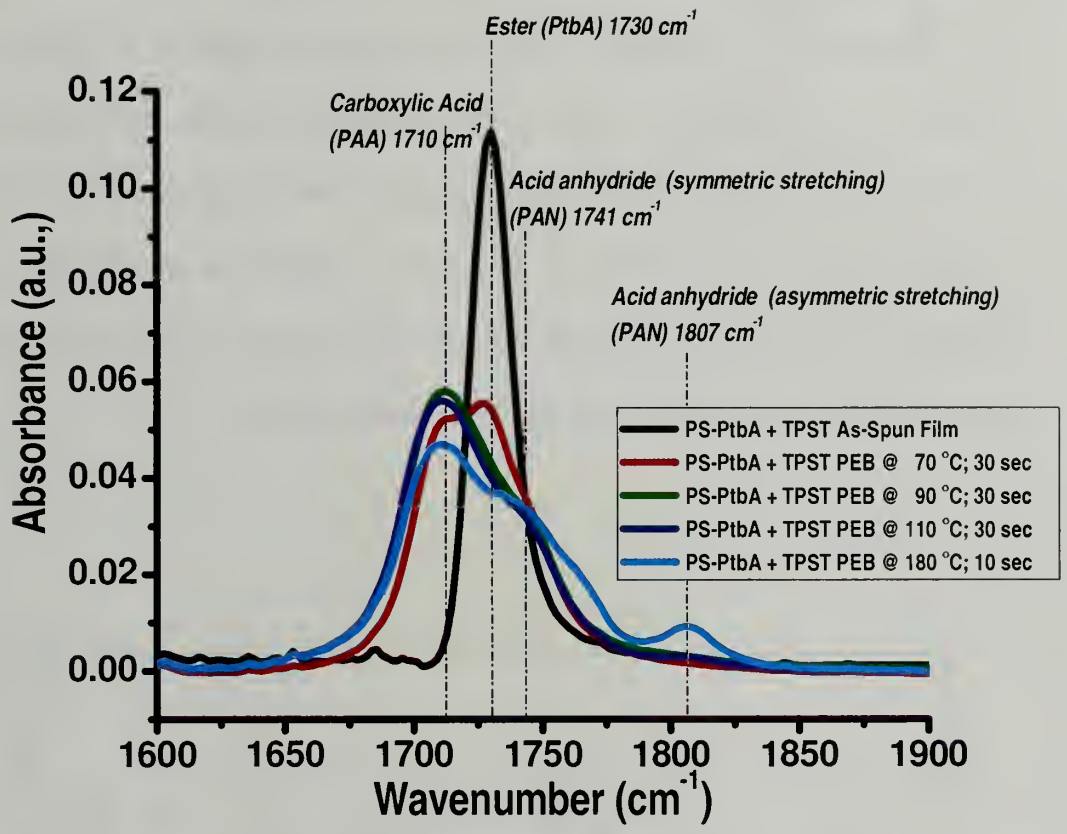

Figure 5.12: Zoomed-up FT-IR spectra showing the extent of anhydride formation under various baking conditions

of the baking chosen conditions. An absorption peak corresponding to carbonyl groups in poly acrylic acid is still dominant while there is some formation of anhydride network, suggested by peaks at 1740 and 1807 cm^{-1}. Therefore, an external crosslinker is added in the template to ensure that the UV exposed regions are sufficiently crosslinked. The crosslinker used in our study was tetra methoxy methyl glycoluril (TMMGU), which has been previously used to crosslink various polymer matrices[31] (Chapter 3). In the presence of acid and heat each TMMGU molecule generates upto four carbocations that react with

hydroxyl groups present in the polymer chain. Crosslinking reactions involving TMMGU and PAA are shown in Figure 5.13. It is found that templates containing 5 wt. % TPST and 1 wt. % TMMGU produced positive tone patterns with sharp sidewalls. Figure 5.14 shows the SFM image of the calcined mesoporous silicate films having a micro-post structure replicated from the same photo mask used previously. The fidelity of replication can be observed from the section analysis shown in Figure 5.15. The nanoporous structure present in this film is characterized using TEM and Figure 5.16 shows ordered nanochannels replicated from block copolymer.

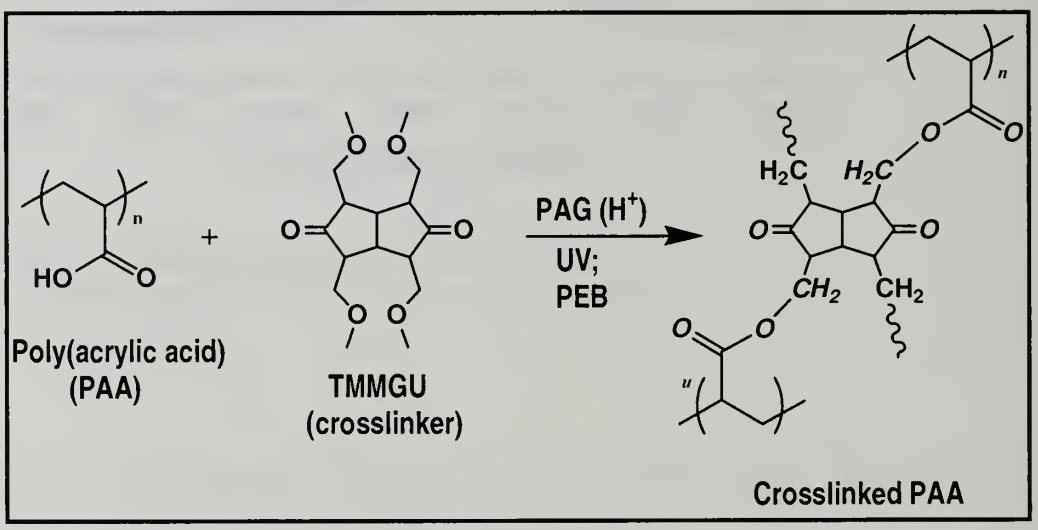

Figure 5.13: Crosslinking chemical reaction between TMMGU and PAA

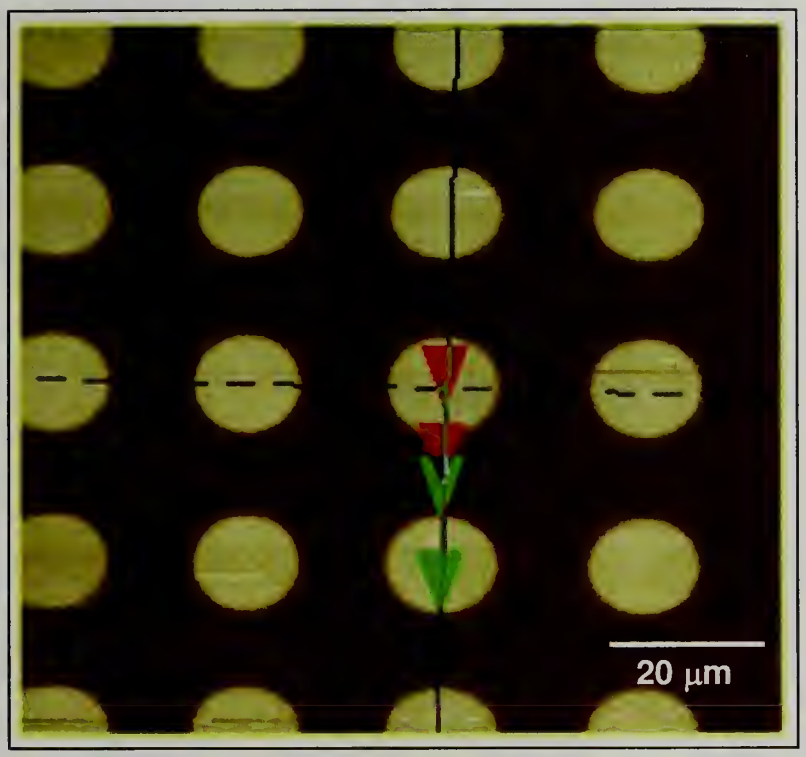

Figure 5.14: SFM image of positive tone patterned mesoporous silica film

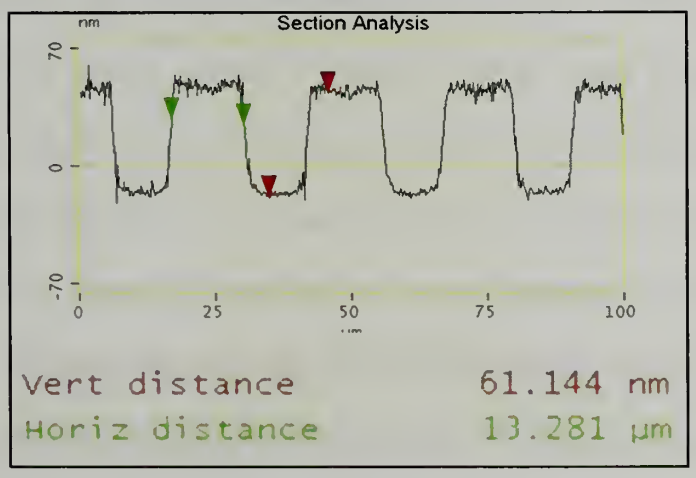

Figure 5.15: Section analysis of the SFM image shown in Figure 5.14

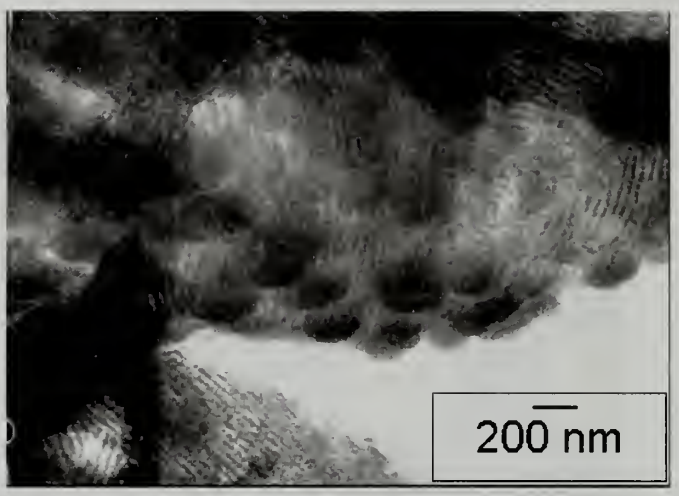

Figure 5.16: TEM image of positive tone patterned mesoporous silica film

5.3.2 Replication of High Resolution Device Level Structures

The resolution of device level features reported in this chapter and in the previous chapter is in the range of few microns, which is largely driven by the choice of photomask and the limits of contact exposure. To achieve high resolution device level definitions, pattern from the photo mask has to be transferred very effectively into the polymer template. However, contact photolithography that is being used so far in this study demands true contact between the film and the mask for an effective pattern transfer. Such true contact is difficult to realize, since non-uniformity on the film is practically unavoidable. It would be best to use projection lithography, in which case, the film is not in contact with photomask and the pattern in photomask is projected onto the film using a series of optical components.

In collaboration with an industrial partner, 193 nm photoresist films (polyacrlate based polymers) are UV-exposed, post-exposure baked and then pattern replication is attempted as shown schematically in Figure 5.17. It is to be mentioned that, these photoresist films are UV-exposed using a 193 nm optical stepper at the industrial partner's site. Silica deposition is performed at University of Massachusetts. As depicted in Figure 5.17, the objective is to infuse silica into the UV-exposed regions, as these are expected to have photo-generated acid and poly(carboxylic acid), formed after deprotection. If silica deposition is successful, then calcination would provide negative tone replication of patterns registered in the photoresist film. However, this route did not work, as there is no silica found in the exposed regions after supercritical CO_2 (sc CO_2) reaction. Various reaction parameters including time, temperature, pressure, precursor loading, moisture content in sc CO_2 and temperature-pressure sequence are changed and none of them helped to get desired results. Negative results in all these experiments suggest that the acid present in the UV exposed regions are either deactivated or not reactive enough to do silica precursor hydrolysis. Moreover, the exposed regions may also be slightly crosslinked as there is limited swellability in sc CO_2.

After learning that the UV-exposed regions do not get silica in all extreme reaction conditions, the schematic is modified to get positive tone replication, as it is shown in Figure 5.18. Patterned photoresist films are flood exposed under UV (254 nm) lamp and then taken inside the reactor, where silica deposition and post-exposure bake are performed simultaneously. In this case, silica infusion is expected to happen in the initially unexposed regions. After removing the template by calcination at 400 °C, positive tone replication of patterns in the photoresist film can be obtained. Optical and

scanning force micrographs of the calcined samples are shown in Figures 5.19 – 5.23. It can be noticed that the lines, as small as 90 nm, are replicated. It is also to be noted that after calcination, the silica structures are very thin (~ 70 % shrinkage). Increased precursor loading does not help to get thicker films; rather it leaves the wafer with silica particles. This observation suggests limited swellability of the photoresist film in sc CO_2 as well.

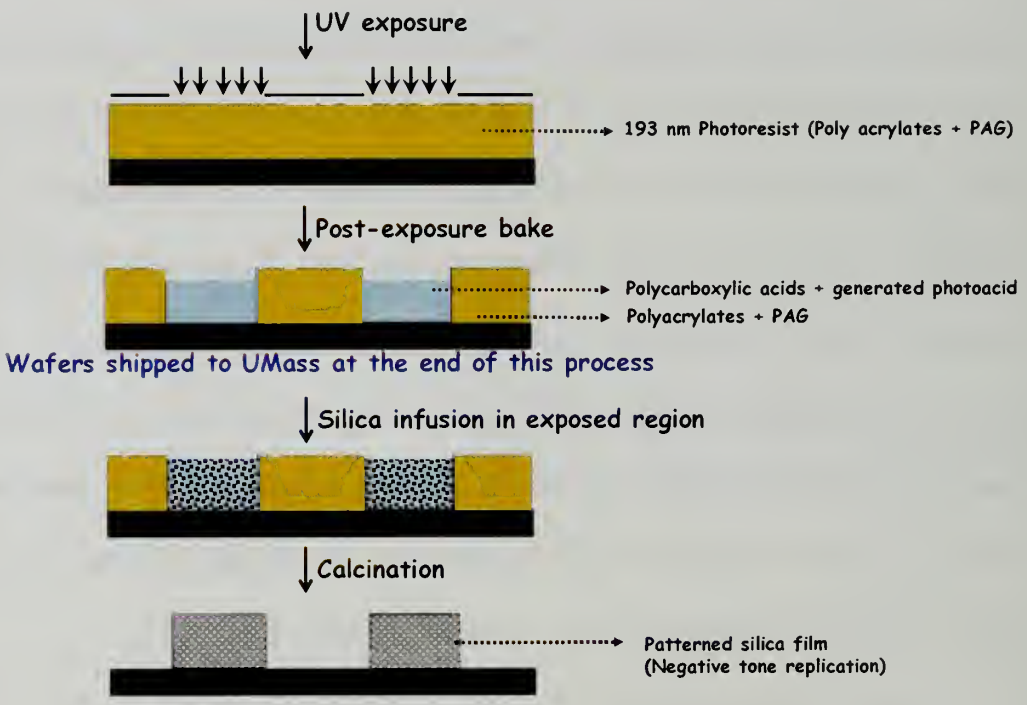

Figure 5.17: Negative tone replication of high resolution device level structures – This approach did not work

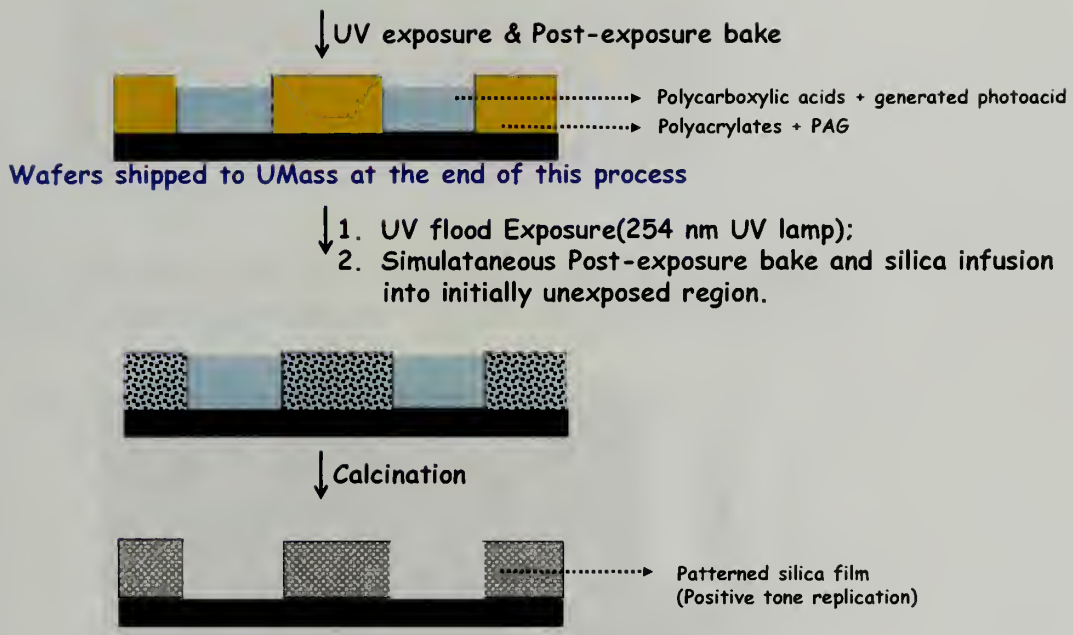

Figure 5.18: Positive tone replication of high resolution device level structures – This approach was successful

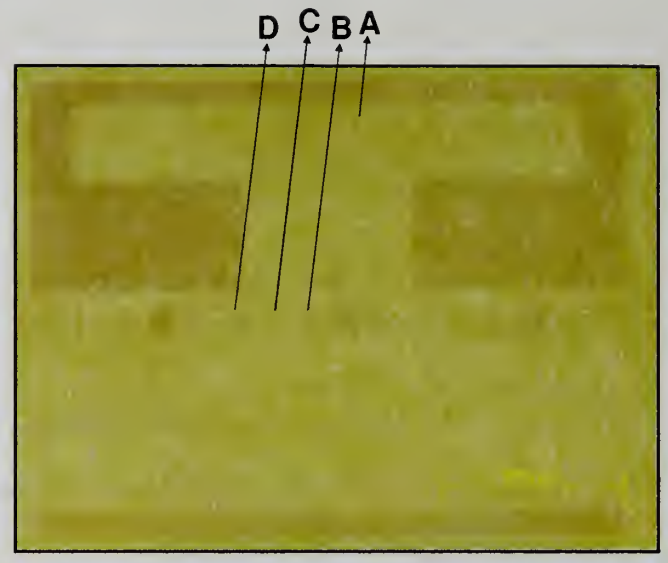

Figure 5.19: Optical Micrograph of the calcined silica film templated from the 193 photoresist film showing the locations of spots of interest

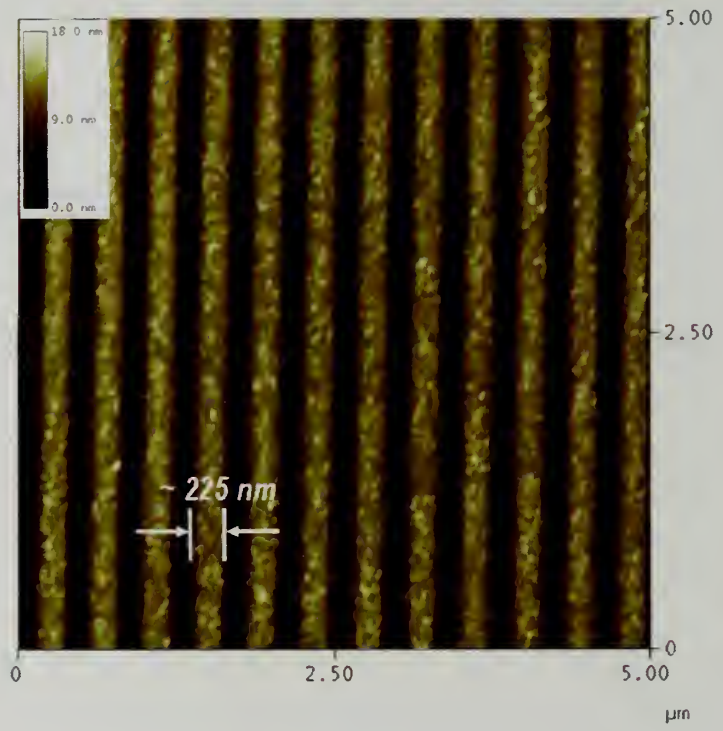

Figure 5.20: SFM image of the Spot A in the calcined silica film

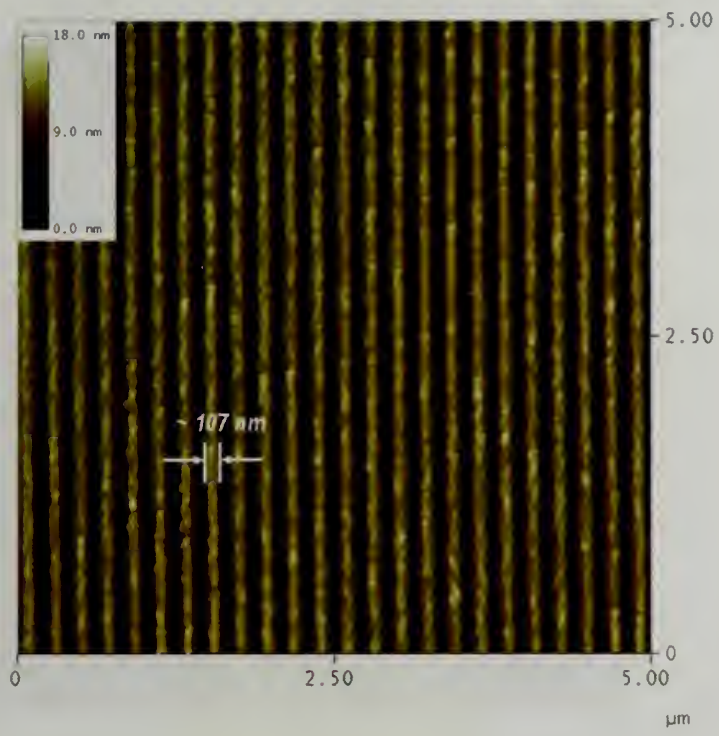

Figure5.21: SFM image of the Spot B in the calcined silica film

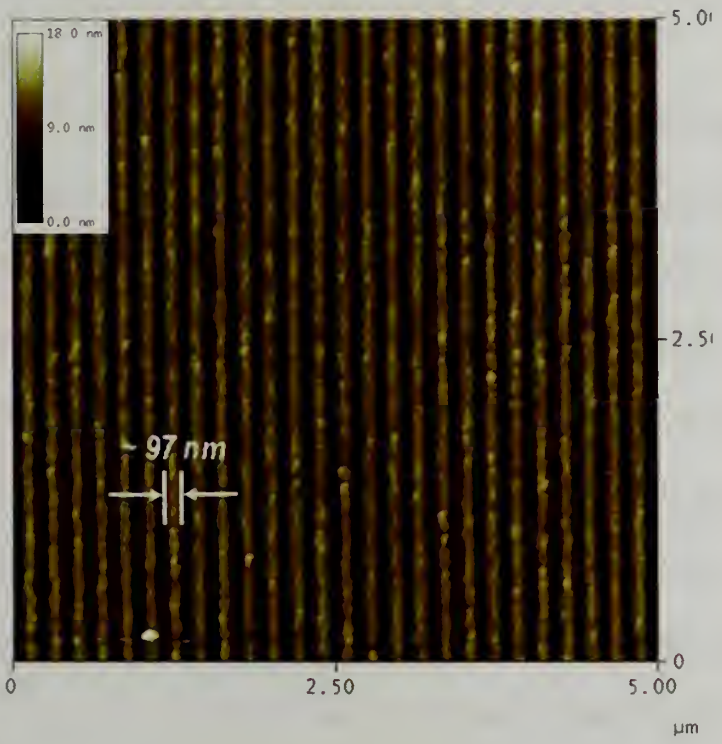

Figure 5.22: SFM image of the Spot C in the calcined silica film

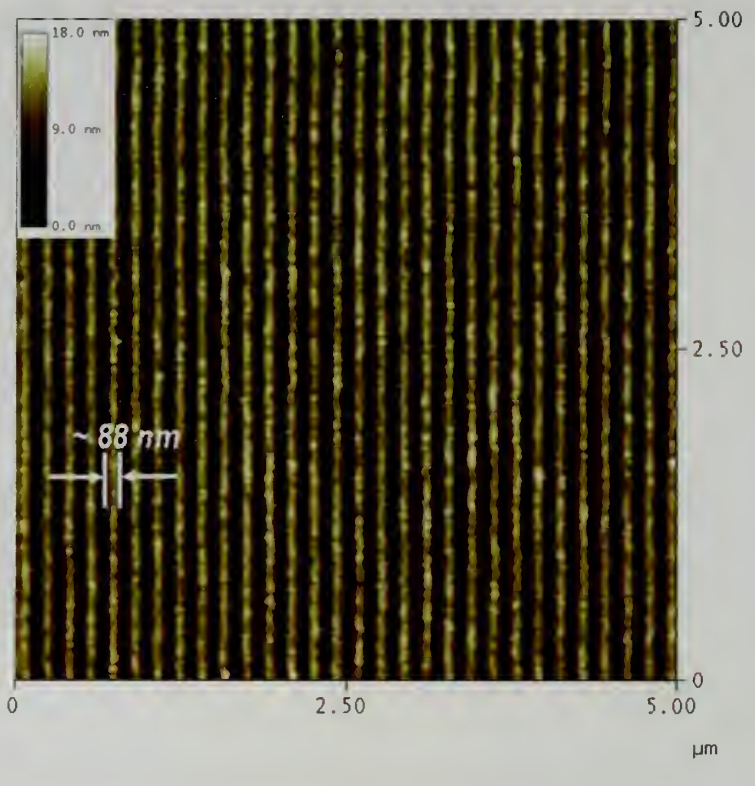

Figure 5.23: SFM image of the Spot D in the calcined silica film

5.4 Conclusions

In conclusion, this chapter described a versatile approach, offering a compressed and cost-effective process routine, to patterned mesoporous silicate films in which the porous geometry can be completely controlled over multiple length scales. From a single photomask, both positive tone (micro-posts) and negative tone (micro-wells) replications have been achieved. Such patterned mesoporous silicate films, comprised of laterally ordered cylindrical nano channels, could potentially be suitable candidate for micro fluidic applications. This chapter also reported the feasibility demonstration of producing device level structures as small as 90 nm.

5.5 References

1. Hoofman, R.; Verheijden, G.; Michelon, J.; Iacopi, F.; Travaly, Y.; Baklanov, M. R.; Tokei, Z.; Beyer, G. P., *Microelectron. Eng.* **2005,** 80, 337.

2. Schmuhl, R.; Nijdam, W.; Sekulic, J.; Chowdhury, S. R.; van Rijn, C. J. M.; van den Berg, A.; ten Elshof, J. E.; Blank, D. H. A., *Anal. Chem.* **2005,** 77, 178.

3. Yang, P. D.; Wirnsberger, G.; Huang, H. C.; Cordero, S. R.; McGehee, M. D.; Scott, B.; Deng, T.; Whitesides, G. M.; Chmelka, B. F.; Buratto, S. K.; Stucky, G. D., *Science* **2000,** 287, 465.

4. Wirnsberger, G.; Yang, P. D.; Huang, H. C.; Scott, B.; Deng, T.; Whitesides, G. M.; Chmelka, B. F.; Stucky, G. D., *J. Phys. Chem. B* **2001,** 105, 6307.

5. Yokokawa, R.; Paik, J. A.; Dunn, B.; Kitazawa, N.; Kotera, H.; Kim, C. J., *Journal of Micromechanics and Microengineering* **2004,** 14, 681.

6. Yang, H.; Coombs, N.; Ozin, G. A., *Adv. Mater.* **1997,** 9, 811.

7. Yang, P. D.; Rizvi, A. H.; Messer, B.; Chmelka, B. F.; Whitesides, G. M.; Stucky, G. D., *Adv. Mater.* **2001,** 13, 427.

8. Trau, M.; Yao, N.; Kim, E.; Xia, Y.; Whitesides, G. M.; Aksay, I. A., *Nature* **1997,** 390, 674.

9. Fan, H. Y.; Lu, Y. F.; Stump, A.; Reed, S. T.; Baer, T.; Schunk, R.; Perez-Luna, V.; Lopez, G. P.; Brinker, C. J., *Nature* **2000,** 405, 56.

10. Fan, H. Y.; Reed, S.; Baer, T.; Schunk, R.; Lopez, G. P.; Brinker, C. J., *Microporous Mesoporous Mater.* **2001,** 44, 625.

11. Mougenot, M.; Lejeune, M.; Baumard, J. F.; Boissiere, C.; Ribot, F.; Grosso, D.; Sanchez, C.; Noguera, R., *J. Am. Ceram. Soc.* **2006,** 89, 1876.

12. Su, M.; Liu, X. G.; Li, S. Y.; Dravid, V. P.; Mirkin, C. A., *J. Am. Chem. Soc.* **2002,** 124, 1560.

13. Wu, C. W.; Aoki, T.; Kuwabara, M., *Nanotechnology* **2004,** 15, 1886.

14. Malfatti, L.; Kidchob, T.; Costacurta, S.; Falcaro, P.; Schiavuta, P.; Amenitsch, H.; Innocenzi, P., *Chem. Mater.* **2006,** 18, 4553.

15. Cerrina, F., *Journal of Physics D-Applied Physics* **2000,** 33, R103.

16. Sugimura, H.; Hozumi, A.; Kameyama, T.; Takai, O., *Adv. Mater.* **2001,** 13, 667.

17. Hozumi, A.; Kojima, S.; Nagano, S.; Seki, T.; Shirahata, N.; Kameyama, T., *Langmuir* **2007,** 23, 3265.

18. Hozumi, A.; Kizuki, T.; Inagaki, M.; Shirahata, N., *J. Vac. Sci. Techno., A* **2006,** 24, 1494.

19. Doshi, D. A.; Huesing, N. K.; Lu, M. C.; Fan, H. Y.; Lu, Y. F.; Simmons-Potter, K.; Potter, B. G.; Hurd, A. J.; Brinker, C. J., *Science* **2000,** 290, 107.

20. Lu, Y. F.; Yang, Y.; Sellinger, A.; Lu, M. C.; Huang, J. M.; Fan, H. Y.; Haddad, R.; Lopez, G.; Burns, A. R.; Sasaki, D. Y.; Shelnutt, J.; Brinker, C. J., *Nature* **2001,** 410, 913.

21. Kresge, C. T.; Leonowicz, M. E.; Roth, W. J.; Vartuli, J. C.; Beck, J. S., *Nature* **1992,** 359, 710.

22. Nagarajan, S.; Bosworth, J. K.; Ober, C. K.; Russell, T. P.; Watkins, J. J., *Chem. Mater.* **2008,** 20, 604.

23. Ito, H.; Ueda, M., *Macromolecules* **1988,** 21, 1475.

24. Hinsberg, W. D.; Houle, F. A.; Sanchez, M. I.; Wallraff, G. M., *Ibm Journal of Research and Development* **2001,** 45, 667.

25. Ito, H., *Ibm Journal of Research and Development* **1997,** 41, 69.

26. Ito, H., Chemical amplification resists for microlithography. In *Microlithography - Molecular Imprinting*, 2005; Vol. 172, pp 37.

27. Kim, G.; Libera, M., *Macromolecules* **1998,** 31, 2569.

28. Kim, G.; Libera, M., *Macromolecules* **1998,** 31, 2670.

29. Kim, S. H.; Misner, M. J.; Russell, T. P., *Advanced Materials* **2004,** 16, 2119.

30. Kim, S. H.; Misner, M. J.; Xu, T.; Kimura, M.; Russell, T. P., *Advanced Materials* **2004,** 16, 226.

31. Li, M. Q.; Douki, K.; Goto, K.; Li, X. F.; Coenjarts, C.; Smilgies, D. M.; Ober, C. K., *Chem. Mater.* **2004,** 16, 3800.

CHAPTER 6

OVERALL SUMMARY AND FUTURE DIRECTIONS

6.1 Overall Summary

The objective of this dissertation was to combine the recent advances in controlling the BCP morphology in thin films with the discrete two-step replication process: (i) template formation and (ii) supercritical fluid assisted silica deposition. By doing so, novel routes to mesoporous materials that are of scientific and technological interest were developed.

Chapter 2 described an efficient route to mesoporous silicate films with perpendicular nanochannels[1]. Poly(α-methyl styrene-b-hydroxy styrene) (PMS-PHOST) copolymers were spin coated from propylene glycol monomethyl ether acetate (PGMEA) containing trace amounts of p-toluene sulfonic acid to yield a microphase segregated array of PMS cylinders in a PHOST matrix. The template array was then infused with solutions of tetraethylorthosilicate (TEOS) in sc CO_2 to selectively deposit silica within the PHOST domain. Calcination yielded the porous arrays. Atomic force microscopy, electron microscopy and grazing incidence small angle x-ray scattering studies confirm the vertical alignment of the cylindrical pores having comparable size and lateral order to those of block copolymer template.

Chapter 3, 4 & 5 described an extensive study involved in developing a simple and cost-effective route to patterned mesoporous silicate films[2]. Chapter 3 discussed the possibility of using poly (ethylene oxide) copolymers and poly (hydroxy styrene) copolymers as templates. It was found that UV exposed and uncrosslinked block copolymer films containing photo acid generators were suitable templates to produce

patterned mesoporous silicate films. Segregation of photo acid into hydrophilic domains helped to obtain excellent domain level replications. However, diffusion of photoacid from UV exposed regions to unexposed regions in CO_2 dilated polymer matrices resulted in less effective device level replications.

Chapter 4 discussed the possibilities of using chemically amplifiable copolymer films as templates to produce patterned mesoporous silicate films with sharp domain and device level replications. PS-b-PtbocSt templates restricted the diffusion of photoacid by establishing deprotection reaction gate between the UV exposed regions and unexposed regions. Such restriction enabled high fidelity replication of device level structures. However, the domain level replications were not well-ordered due to weak repulsive interactions between PS and PtbocSt.

Chapter 5 described a versatile approach to dual tone patterned mesoporous silicate films in which several nanoporous geometry can be dialed in. Two-stage chemical amplification process involved in PS-b-PtbA copolymer was utilized to produce silicate films with micro-posts (positive tone) and micro-wells (negative tone) from a single photomask. Stronger repulsive interaction between PS and PtbA and lower T_g of PtbA helped to obtain well-defined cylindrical and spherical nanostructures in the template and further in silicate network. Access to a projection lithographic tool helped to demonstrate replication of device level structures as small as 90 nm. Direct definition followed by replication of pattern obviated the need for additional etching-cleaning steps and offered a cost-effective and compressed routine, which can be easily integrated into existing processes, for example in fabrication of thick lines for BEOL (back end of the line) processes and potentially lower metallization layers as well.

6.2. Future Directions

The future directions for the work described in this dissertation can be two fold. In one category several experiments can be designed to answer certain fundamental questions relevant to this dissertation and in the other category, routes developed in this dissertation can be utilized to build future devices for specific applications.

6.2.1 In-Situ GISAXS Studies

As discussed in chapter 5, PS-b-PtbA films exhibited several morphologies depending on the annealing conditions. As-spun and thermally annealed films are comprised of randomly oriented, ill-defined cylindrical morphology. However, films annealed under chloroform vapor yielded well-defined, ordered cylindrical morphology, whereas films annealed under Hexane/Ethanol mixture yielded well-defined spherical morphology. In-situ GISAXS studies[3] on films present in appropriate solvent environment can shed light to understand the pathways to various morphologies.

6.2.2 Influence of Salts on Long Range Order in PS-b-PtbA

PS-b-PtbA films used in this study were doped with small amount of salts (triphenyl sulfonium triflate and other additives). Influence of salts[3,4] on the long range order can also be studied. Further, influence of topographically patterned substrates on enhancement of long range order can also be investigated.

6.2.3 High Pressure Spectroscopic Ellipsometric Studies

As discussed in chapter 3 and 5, crosslinked films are not suitable for silica infusion. These crosslinked films exhibit limited swellability in sc CO_2, as compared to that of uncrosslinked films. Quantitative information on extent of swelling as a function of degree of crosslinking would be helpful to dial in and further lock embedded structures in templates and in inorganic network. To obtain such quantitative information, high pressure spectroscopic ellipsometry[5] can be used to determine the CO_2 sorption in these templates.

6.2.4 Positive Tone Replications from Pluronics Blends

Although PS-b-PtbA films exhibited well-ordered morphologies when annealed under solvent atmosphere, the level of long range of order obtained from PS-b-PtbA is not as good as in Pluronics blend systems, in particular, F108 and PHOST mixtures[6]. Moreover, PS-b-PtbA is expensive and one cannot obtain microdomains as small as one would obtain from F108 blends. To fabricate micro-patterned mesoporous silicate films from F108 blended with PHOST templates, schematic shown in Figure 6.1 is currently being explored in our laboratory. Positive tone replications can be obtained by crosslinking the UV-exposed regions. Crosslinking chemistry invoked in Figure 6.1 is similar to the one in Figure 3.1 in chapter 3.

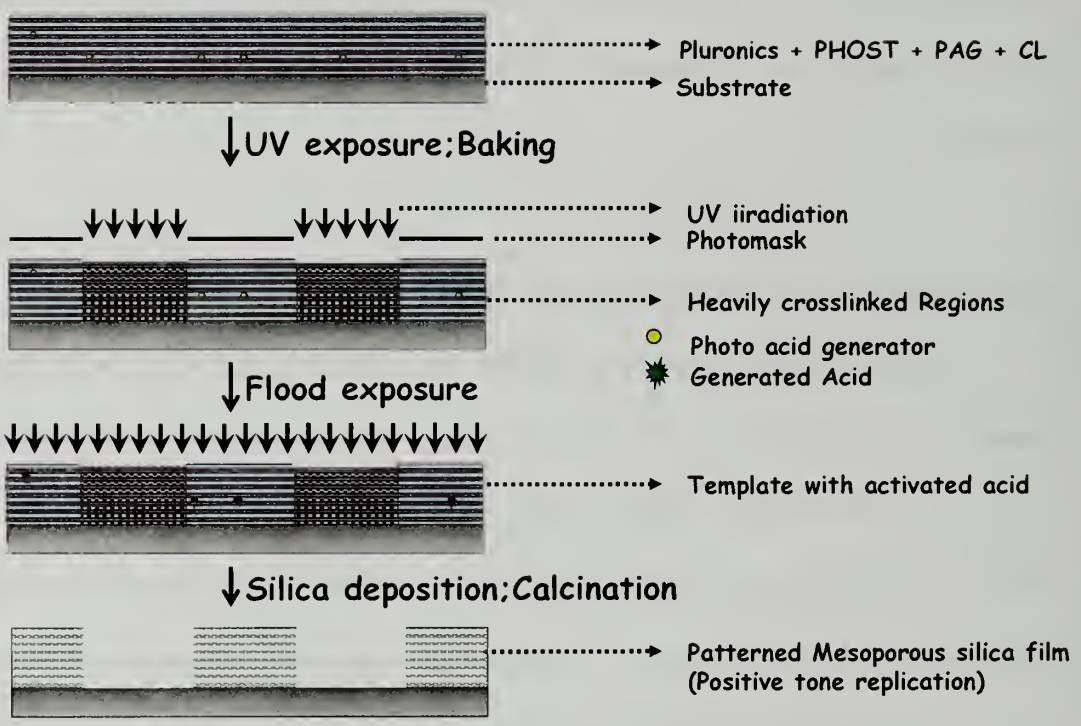

Figure 6.1: Schematic showing the steps involved in fabrication of patterned mesoporous silica films from F108 and PHOST blends

6.2.5 Fabrication of Direct Dual Damascene Structures

Based on the method developed in chapter 4 and 5, a schematic for direct definition of dual damascene structures can be proposed as shown in figure 6.2. Dual damascene process, typically followed during microelectronic chip fabrication, is used to form the interconnecting metal lines between the actual transistor in the Si substrate and the leads that connect the chip to the outside world. Briefly, dual damascene process[7] consists of

(i) etching the metal patterns (vias and trenches) into the intermetal dielectric layer (potentially, mesoporous organosilicate films)

(ii) filling the pattern with copper using any standard metallization technique and

(iii) planarizing the stack with chemical-mechanical polishing.

Typically, dual damascene processes are comprised of many sequences of photoresist coating, lithographically exposing, developing, etching and cleaning steps. Although one can foresee several materials challenges, schematic proposed in figure 6.2 can potentially be an alternative approach, as it significantly reduces the number of steps involved in dual damascene fabrication.

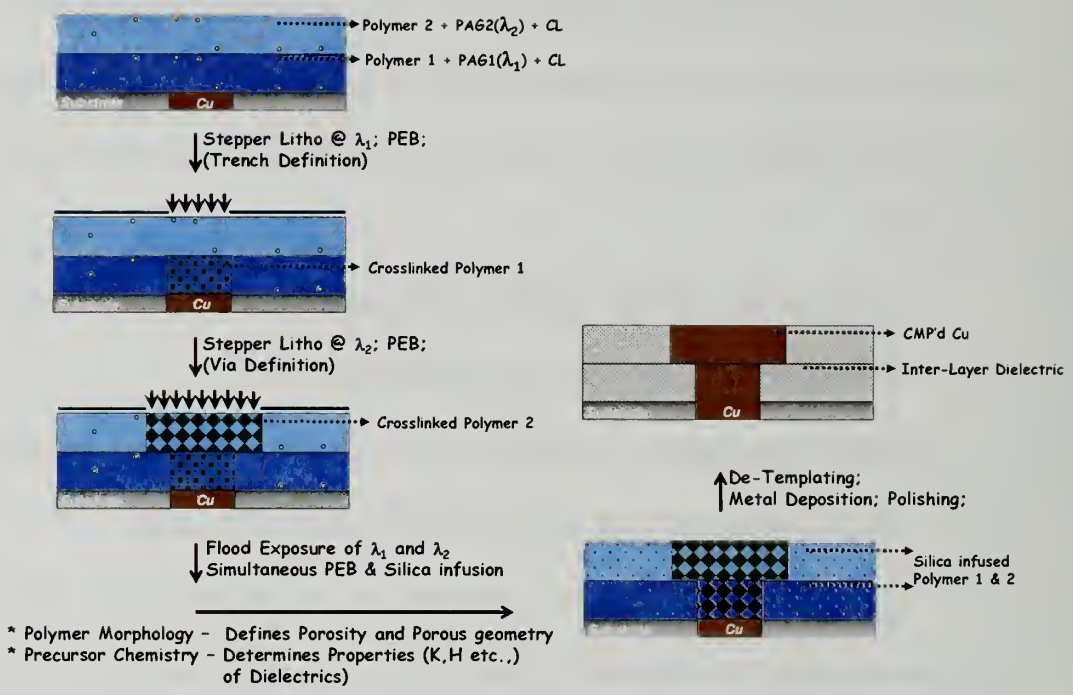

Figure 6.2: Schematic showing the steps involved in direct definition and replication of dual damascene structures using two-step replication process in sc CO_2

6.3 References

1. Nagarajan, S.; Li, M. Q.; Pai, R. A.; Bosworth, J. K.; Busch, P.; Smilgies, D. M.; Ober, C. K.; Russell, T. P.; Watkins, J. J. *Advanced Materials* 2008, *20*, 246.

2. Nagarajan, S.; Bosworth, J. K.; Ober, C. K.; Russell, T. P.; Watkins, J. J. *Chemistry of Materials* 2008, *20*, 604.

3. Kim, S. H.; Misner, M. J.; Yang, L.; Gang, O.; Ocko, B. M.; Russell, T. P. *Macromolecules* 2006, *39*, 8473.

4. Wang, J. Y.; Chen, W.; Roy, C.; Sievert, J. D.; Russell, T. P. *Macromolecules* 2008, *41*, 963.

5. Francis, T. J.; Vogt, B. D.; Wang, M. X.; Watkins, J. J. *Macromolecules* 2007, *40*, 2515.

6. Tirumala, V. R.; Pai, R. A.; Agarwal, S.; Testa, J. J.; Bhatnagar, G.; Romang, A. H.; Chandler, C.; Gorman, B. P.; Jones, R. L.; Lin, E. K.; Watkins, J. J. *Chemistry of Materials* 2007, *19*, 5868.

7. Richard C. Jaeger, *Introduction to Microelectronic Fabrication* Volume V Second Edition. Prentice Hall, New Jersey

BIBLIOGRAPHY

Aizawa, M.; Buriak, J. M., *Chem. Mater.* **2007,** 19, 5090.

Aksay, I. A.; Trau, M.; Manne, S.; Honma, I.; Yao, N.; Zhou, L.; Fenter, P.; Eisenberger, P. M.; Gruner, S. M., *Science* **1996,** 273, 892.

Albalak, R. J.; Thomas, E. L.; Capel, M. S., *Polymer* **1997,** 38, 3819.

Antonietti, M.; Wenz, E.; Bronstein, L.; Seregina, M., *Adv. Mater.* **1995,** 7, 1000.

Arbiol, J.; Cabot, A.; Morante, J. R.; Chen, F. L.; Liu, M. L., *Appl. Phys. Lett.* **2002,** 81, 3449.

Asakawa, K.; Hiraoka, T.; Hieda, H.; Sakurai, M.; Kamata, Y., *J. Photopolym. Sci. Technol.* **2002,** 15, 465.

Bates, F. S.; Fredrickson, G. H., *Annu. Rev. Phys. Chem.* **1990,** 41, 525.

Bates, F. S.; Fredrickson, G. H., *Physics Today* **1999,** 52, 32.

Beck, J. S.; Vartuli, J. C.; Roth, W. J.; Leonowicz, M. E.; Kresge, C. T.; Schmitt, K. D.; Chu, C. T. W.; Olson, D. H.; Sheppard, E. W.; McCullen, S. B.; Higgins, J. B.; Schlenker, J. L., *J. Am. Chem. Soc.* **1992,** 114, 10834.

Black, C. T.; Guarini, K. W.; Milkove, K. R.; Baker, S. M.; Russell, T. P.; Tuominen, M. T., *Appl. Phys. Lett.* **2001,** 79, 409.

Black, C. T.; Bezencenet, O., *Ieee Transactions on Nanotechnology* **2004,** 3, 412.

Black, C. T.; Ruiz, R.; Breyta, G.; Cheng, J. Y.; Colburn, M. E.; Guarini, K. W.; Kim, H. C.; Zhang, Y., *Ibm Journal of Research and Development* **2007,** 51, 605.

Blackburn, J. M.; Long, D. P.; Watkins, J. J., *Chem. Mater.* **2000,** 12, 2625.

Blackburn, J. M.; Long, D. P.; Cabanas, A.; Watkins, J. J., *Science* **2001,** 294, 141.

Bockstaller, M.; Kolb, R.; Thomas, E. L., *Adv. Mater.* **2001,** 13, 1783.

Bodycomb, J.; Funaki, Y.; Kimishima, K.; Hashimoto, T., *Macromolecules* **1999,** 32, 2075.

Boker, A.; Knoll, A.; Elbs, H.; Abetz, V.; Muller, A. H. E.; Krausch, G., *Macromolecules* **2002,** 35, 1319.

Brinker, C. J.; Lu, Y. F.; Sellinger, A.; Fan, H. Y., *Adv. Mater.* **1999,** 11, 579.

Cabanas, A.; Long, D. P.; Watkins, J. J., *Chem. Mater.* **2004,** 16, 2028.

Campbell, D.; Pethrick, R. A.; White, J. R., *Polymer Characterization*. second ed.; Stanley Thornes Ltd: Glos, 2000; p 481.

Cason, J. P.; Khambaswadkar, K.; Roberts, C. B., *Ind. Eng. Chem. Res.* **2000,** 39, 4749.

Cerrina, F., *Journal of Physics D-Applied Physics* **2000,** 33, R103.

Chan, Y. N. C.; Craig, G. S. W.; Schrock, R. R.; Cohen, R. E., *Chem. Mater.* **1992,** 4, 885.

Chen, Z. R.; Kornfield, J. A.; Smith, S. D.; Grothaus, J. T.; Satkowski, M. M., *Science* **1997,** 277, 1248.

Chen, B. C.; Lin, H. P.; Chao, M. C.; Mou, C. Y.; Tang, C. Y., *Adv. Mater.* **2004,** 16, 1657.

Chen, C. C.; Liu, Y. C.; Wu, C. H.; Yeh, C. C.; Su, M. T.; Wu, Y. C., *Adv. Mater.* **2005,** 17, 404.

Cheng, J. Y.; Ross, C. A.; Chan, V. Z. H.; Thomas, E. L.; Lammertink, R. G. H.; Vancso, G. J., *Adv. Mater.* **2001,** 13, 1174.

Cheng, J. Y.; Ross, C. A.; Thomas, E. L.; Smith, H. I.; Vancso, G. J., *Appl. Phys. Lett.* **2002,** 81, 3657.

Cheng, K. W.; Chan, W. K., *Langmuir* **2005,** 21, 5247.

Clark, T.; Ruiz, J. D.; Fan, H. Y.; Brinker, C. J.; Swanson, B. I.; Parikh, A. N., *Chem. Mater.* **2000,** 12, 3879.

Cohen, R. E., *Current Opinion in Solid State & Materials Science* **1999,** 4, 587.

Condo, P. D.; Sumpter, S. R.; Lee, M. L.; Johnston, K. P., *Ind. Eng. Chem. Res.* **1996,** 35, 1115.

Corma, A., *Chemical Reviews* **1997,** 97, 2373.

Cornelissen, J.; van Heerbeek, R.; Kamer, P. C. J.; Reek, J. N. H.; Sommerdijk,

N.; Nolte, R. J. M., *Adv. Mater.* **2002,** 14, 489.

Cummins, C. C.; Schrock, R. R.; Cohen, R. E., *Chem. Mater.* **1992,** 4, 27.

Darling, S. B.; Yufa, N. A.; Cisse, A. L.; Bader, S. D.; Sibener, S. J., *Adv. Mater.* **2005,** 17, 2446.

Dattelbaum, A. M.; Amweg, M. L.; Ecke, L. E.; Yee, C. K.; Shreve, A. P.; Parikh, A. N., *Nano Lett.* **2003,** 3, 719.

Davidson, F. M.; Schricker, A. D.; Wiacek, R. J.; Korgel, B. A., *Adv. Mater.* **2004,** 16, 646.

Davis, M. E., *Nature* **2002,** 417, 813.

De Rosa, C.; Park, C.; Thomas, E. L.; Lotz, B., *Nature* **2000,** 405, 433.

Dektar, J. L.; Hacker, N. P., *J. Am. Chem. Soc.* **1990,** 112, 6004.

DeRouchey, J.; Thurn-Albrecht, T.; Russell, T. P.; Kolb, R., *Macromolecules* **2004,** 37, 2538.

Discher, B. M.; Won, Y. Y.; Ege, D. S.; Lee, J. C. M.; Bates, F. S.; Discher, D. E.;

Hammer, D. A., *Science* **1999,** 284, 1143.

Doherty, W. J.; Armstrong, N. R.; Saavedra, S. S., *Chem. Mater.* **2005,** 17, 3652.

Doshi, D. A.; Huesing, N. K.; Lu, M. C.; Fan, H. Y.; Lu, Y. F.; Simmons-Potter, K.; Potter, B. G.; Hurd, A. J.; Brinker, C. J., *Science* **2000,** 290, 107.

Doytcheva, M.; Dotcheva, D.; Stamenova, R.; Tsvetanov, C., *Macromol. Mater. Eng.* **2001,** 286, 30.

Du, P.; Li, M. Q.; Douki, K.; Li, X. F.; Garcia, C. R. W.; Jain, A.; Smilgies, D. M.; Fetters, L. J.; Gruner, S. M.; Wiesner, U.; Ober, C. K., *Adv. Mater.* **2004,** 16, 953.

Duesberg, G. S.; Graham, A. P.; Liebau, M.; Seidel, R.; Unger, E.; Kreupl, F.; Hoenlein, W., *Nano Lett.* **2003,** 3, 257.

Edrington, A. C.; Urbas, A. M.; DeRege, P.; Chen, C. X.; Swager, T. M.; Hadjichristidis, N.; Xenidou, M.; Fetters, L. J.; Joannopoulos, J. D.; Fink, Y.; Thomas, E. L., *Adv. Mater.* **2001,** 13, 421.

Elhadj, S.; Woody, J. W.; Niu, V. S.; Saraf, R. F., *Appl. Phys. Lett.* **2003,** 82, 871.
Erts, D.; Polyakov, B.; Saks, E.; Olin, H.; Ryen, L.; Ziegler, K.; Holmes, J. D., Semiconducting nanowires: Properties and architectures. In *Functional Nanomaterials for Optoelectronics and Other Applications*, 2003; Vol. 99-100, pp 109.

Factor, B. J.; Russell, T. P.; Toney, M. F., *Phys. Rev. Lett.* **1991,** 66, 1181.

Fan, H. Y.; Lu, Y. F.; Stump, A.; Reed, S. T.; Baer, T.; Schunk, R.; Perez-Luna, V.; Lopez, G. P.; Brinker, C. J., *Nature* **2000,** 405, 56.

Fan, H. Y.; Reed, S.; Baer, T.; Schunk, R.; Lopez, G. P.; Brinker, C. J., *Microporous Mesoporous Mater.* **2001,** 44, 625.

Fasolka, M. J.; Harris, D. J.; Mayes, A. M.; Yoon, M.; Mochrie, S. G. J., *Phys. Rev. Lett.* **1997,** 79, 3018.

Fasolka, M. J.; Banerjee, P.; Mayes, A. M.; Pickett, G.; Balazs, A. C., *Macromolecules* **2000,** 33, 5702.

Fasolka, M. J.; Mayes, A. M., *Annu. Rev. Mater. Res.* **2001,** 31, 323.

Felix, N. M.; Tsuchiya, K.; Ober, C. K., *Adv. Mater.* **2006,** 18, 442.

Fink, Y.; Urbas, A. M.; Bawendi, M. G.; Joannopoulos, J. D.; Thomas, E. L., *J. Lightwave Technol.* **1999,** 17, 1963.

Forster, S.; Antonietti, M., *Adv. Mater.* **1998,** 10, 195.

Francis, T. J.; Vogt, B. D.; Wang, M. X.; Watkins, J. J., *Macromolecules* **2007,** 40, 2515.

Frechet, J. M. J., *Pure Appl. Chem.* **1992,** 64, 1239.

Garcia, R.; San Paulo, A., *Physical Review B* **1999,** 60, 4961.

Gibaud, A.; Grosso, D.; Smarsly, B.; Baptiste, A.; Bardeau, J. F.; Babonneau, F.; Doshi, D. A.; Chen, Z.; Brinker, C. J.; Sanchez, C., *J. Phys. Chem. B* **2003,** 107, 6114.

Glazer, M.; Fidanza, J.; McGall, G.; Frank, C., *Chem. Mater.* **2001,** 13, 4773.

Goldfarb, D. L.; de Pablo, J. J.; Nealey, P. F.; Simons, J. P.; Moreau, W. M.; Angelopoulos, M., *Journal of Vacuum Science & Technology B* **2000,** 18, 3313.

Guarini, K. W.; Black, C. T.; Zhang, Y.; Kim, H.; Sikorski, E. M.; Babich, I. V., *Journal of Vacuum Science & Technology B* **2002,** 20, 2788.

Guinier, A.; Fournet, G., *Small Angle Scattering of X-Rays.* Wiley: New York, 1955; p 264.

Gupta, R. R.; Lavery, K. A.; Francis, T. J.; Webster, J. R. P.; Smith, G. S.; Russell, T. P.; Watkins, J. J., *Macromolecules* **2003,** 36, 346.

Gupta, R. R.; RamachandraRao, V. S.; Watkins, J. J., *Macromolecules* **2003,** 36, 1295.

Hamley, I. W., *Nanotechnology* **2003,** 14, R39.

Harrison, C.; Park, M.; Chaikin, P. M.; Register, R. A.; Adamson, D. H., *Journal of Vacuum Science & Technology B* **1998,** 16, 544.

Hashimoto, T.; Shibayama, M.; Kawai, H., *Macromolecules* **1980,** 13, 1237.

Haupt, M.; Miller, S.; Glass, R.; Arnold, M.; Sauer, R.; Thonke, K.; Moller, M.; Spatz, J. P., *Adv. Mater.* **2003,** 15, 829.

Hawker, C. J.; Russell, T. P., *Mrs Bulletin* **2005,** 30, 952.

Hayward, R. C.; Alberius, P. C. A.; Kramer, E. J.; Chmelka, B. F., *Langmuir* **2004,** 20, 5998.

Hess, D. M.; Watkins, J. J., *Manuscript in preparation.*

Hieda, H.; Yanagita, Y.; Kikitsu, A.; Maeda, T.; Naito, K., *J. Photopolym. Sci. Technol.* **2006,** 19, 425.

Hinsberg, W. D.; Houle, F. A.; Sanchez, M. I.; Wallraff, G. M., *Ibm Journal of Research and Development* **2001,** 45, 667.

Hoofman, R.; Verheijden, G.; Michelon, J.; Iacopi, F.: Travaly, Y.; Baklanov, M. R.; Tokei, Z.; Beyer, G. P., *Microelectron. Eng.* **2005,** 80, 337.

Horiuchi, S.; Fujita, T.; Hayakawa, T.; Nakao, Y., *Langmuir* **2003,** 19, 2963.

Houle, F. A.; Hinsberg, W. D.; Morrison, M.; Sanchez, M. I.; Wallraff, G.; Larson, C.;

Hoffnagle, J., *Journal of Vacuum Science & Technology B* **2000,** 18, 1874.

Hozumi, A.; Kizuki, T.; Inagaki, M.; Shirahata, N., *Journal of Vacuum Science & Technology A* **2006,** 24, 1494.

Hozumi, A.; Kojima, S.; Nagano, S.; Seki, T.; Shirahata, N.; Kameyama, T., *Langmuir* **2007,** 23, 3265.

Hua, X. F.; Kuo, M. S.; Oehrlein, G. S.; Lazzeri, P.; Iacob, E.; Anderle, M.; Inoki, C. K.; Kuan, T. S.; Jiang, P.; Wu, W. L., *Journal of Vacuum Science & Technology B* **2006,** 24, 1238.

Huang, E.; Rockford, L.; Russell, T. P.; Hawker, C. J., *Nature* **1998,** 395, 757.

Huang, L.; Wind, S. J.; O'Brien, S. P., *Nano Lett.* **2003,** 3, 299.

Hwang, W.; Ham, M. H.; Sohn, B. H.; Huh, J.; Kang, Y. S.; Jeong, W.; Myoung, J. M.; Park, C., *Nanotechnology* **2005,** 16, 2897.

Imperor-Clerc, M.; Davidson, P.; Davidson, A., *J. Am. Chem. Soc.* **2000,** 122, 11925.

Innocenzi, P.; Kidchob, T.; Falcaro, P.; Takahashi, M., *Chem. Mater.* **2008,** 20, 607.

Ito, H.; Willson, C. G., *Polym. Eng. Sci.* **1983,** 23, 1012.

Ito, H.; Willson, C. G., *ACS Symp. Ser.* **1984,** 242, 11.

Ito, H.; Ueda, M., *Macromolecules* **1988,** 21, 1475.

Ito, H.; Ueda, M.; Ebina, M., *ACS Symp. Ser.* **1989,** 412, 57.

Ito, H., *Ibm Journal of Research and Development* **1997,** 41, 69.

Ito, H., Chemical amplification resists for microlithography. In *Microlithography - Molecular Imprinting*, 2005; Vol. 172, pp 37.

Jeong, H. K.; Chandrasekharan, R.; Chu, K. L.; Shannon, M. A.; Masel, R. I., *Ind. Eng. Chem. Res.* **2005,** 44, 8933.

Jeoung, E.; Galow, T. H.; Schotter, J.; Bal, M.; Ursache, A.; Tuominen, M. T.; Stafford, C. M.; Russell, T. P.; Rotello, V. M., *Langmuir* **2001,** 17, 6396.

Jones, C. A.; Zweber, A.; DeYoung, J. P.; McClain, J. B.; Carbonell, R.; DeSimone, J. M., *Crit. Rev. Solid State Mater. Sci.* **2004,** 29, 97.

Jung, Y. W.; Park, S. S.; Kim, Y.; Ha, C. S., *Composite Interfaces* **2007,** 14, 545.

Kane, R. S.; Cohen, R. E.; Silbey, R., *Chem. Mater.* **1996,** 8, 1919.

Kim, G.; Libera, M., *Macromolecules* **1998,** 31, 2569.

Kim, G.; Libera, M., *Macromolecules* **1998,** 31, 2670.

Kim, H. C.; Jia, X. Q.; Stafford, C. M.; Kim, D. H.; McCarthy, T. J.; Tuominen, M.; Hawker, C. J.; Russell, T. P., *Adv. Mater.* **2001,** 13, 795.

Kim, D. H.; Lin, Z. Q.; Kim, H. C.; Jeong, U.; Russell, T. P., *Adv. Mater.* **2003,** 15, 811.

Kim, S. O.; Solak, H. H.; Stoykovich, M. P.; Ferrier, N. J.; de Pablo, J. J.; Nealey, P. F., *Nature* **2003,** 424, 411.

Kim, H. C.; Kreller, C. R.; Tran, K. A.; Sisodiya, V.; Angelos, S.; Wallraff, G.; Swanson, S.; Miller, R. D., *Chem. Mater.* **2004,** 16, 4267.

Kim, S. H.; Misner, M. J.; Russell, T. P., *Adv. Mater.* **2004,** 16, 2119.

Kim, S. H.; Misner, M. J.; Xu, T.; Kimura, M.; Russell, T. P., *Adv. Mater.* **2004,** 16, 226.

Kim, D. H.; Lau, K. H. A.; Robertson, J. W. F.; Lee, O. J.; Jeong, U.; Lee, J. I.; Hawker, C. J.; Russell, T. P.; Kim, J. K.; Knoll, W., *Adv. Mater.* **2005,** 17, 2442.

Kim, S. H.; Misner, M. J.; Yang, L.; Gang, O.; Ocko, B. M.; Russell, T. P., *Macromolecules* **2006,** 39, 8473.

Kimura, M.; Misner, M. J.; Xu, T.; Kim, S. H.; Russell, T. P., *Langmuir* **2003,** 19, 9910.
Kitchens, C. L.; Roberts, C. B., *Ind. Eng. Chem. Res.* **2004,** 43, 6070.

Kresge, C. T.; Leonowicz, M. E.; Roth, W. J.; Vartuli, J. C.; Beck, J. S., *Nature* **1992,** 359, 710.

Kropewnicki, T.; Doan, K.; Tang, B.; Bjorkman, C., *Journal of Vacuum Science & Technology a-Vacuum Surfaces and Films* **2001,** 19, 1384.

Kumar, N.; Parajuli, O.; Hahm, J. I., *J. Phys. Chem. B* **2007,** 111, 4581.

Lapshin, R. V., *Nanotechnology* **2004,** 15, 1135.

Lavery, K. A.; Vogt, B. D.; Prabhu, V. M.; Lin, E. K.; Wu, W. L.; Satija, S. K.; Choi, K. W., *Journal of Vacuum Science & Technology B* **2006,** 24, 3044.

Lazzari, R., *J. Appl. Crystallogr.* **2002,** 35, 406.

Leibler, L., *Macromolecules* **1980,** 13, 1602.

Levine, J. R.; Cohen, L. B.; Chung, Y. W.; Georgopoulos, P., *J. Appl. Crystallogr.* **1989,** 22, 528.

Li, R. R.; Dapkus, P. D.; Thompson, M. E.; Jeong, W. G.; Harrison, C.; Chaikin, P. M.; Register, R. A.; Adamson, D. H., *Appl. Phys. Lett.* **2000,** 76, 1689.

Li, M. Q.; Douki, K.; Goto, K.; Li, X. F.; Coenjarts, C.; Smilgies, D. M.; Ober, C. K., *Chem. Mater.* **2004,** 16, 3800.

Li, M. Q.; Ober, C. K., *Materials Today* **2006,** 9, 30.

Lin, E. K.; Soles, C. L.; Goldfarb, D. L.; Trinque, B. C.; Burns, S. D.; Jones, R. L.; Lenhart, J. L.; Angelopoulos, M.; Willson, C. G.; Satija, S. K.; Wu, W. L., *Science* **2002,** 297, 372.

Lin, Z. Q.; Kim, D. H.; Wu, X. D.; Boosahda, L.; Stone, D.; LaRose, L.; Russell, T. P., *Adv. Mater.* **2002,** 14, 1373.

Lin, Y.; Boker, A.; He, J. B.; Sill, K.; Xiang, H. Q.; Abetz, C.; Li, X. F.; Wang, J.; Emrick, T.; Long, S.; Wang, Q.; Balazs, A.; Russell, T. P., *Nature* **2005,** 434, 55.
Linstrom, P. J.; Mallard, M. G. NIST Standard Reference Database Number 69. http://webbook.nist.gov (June 2005),

Lopes, W. A.; Jaeger, H. M., *Nature* **2001,** 414, 735.
Lu, Y. F.; Yang, Y.; Sellinger, A.; Lu, M. C.; Huang, J. M.; Fan, H. Y.; Haddad, R.; Lopez, G.; Burns, A. R.; Sasaki, D. Y.; Shelnutt, J.; Brinker, C. J., *Nature* **2001,** 410, 913.

Lu, Q. Y.; Gao, F.; Komarneni, S.; Mallouk, T. E., *J. Am. Chem. Soc.* **2004,** 126, 8650.
Ludwigs, S.; Boker, A.; Voronov, A.; Rehse, N.; Magerle, R.; Krausch, G., *Nat. Mater.* **2003,** 2, 744.

Macdonald, S. A.; Schlosser, H.; Ito, H.; Clecak, N. J.; Willson, C. G., *Chem. Mater.* **1991,** 3, 435.

Mal, N. K.; Fujiwara, M.; Tanaka, Y., *Nature* **2003,** 421, 350.

Malfatti, L.; Kidchob, T.; Costacurta, S.; Falcaro, P.; Schiavuta, P.; Amenitsch, H.; Innocenzi, P., *Chem. Mater.* **2006,** 18, 4553.

Mansky, P.; Liu, Y.; Huang, E.; Russell, T. P.; Hawker, C., *Science* **1997,** 275, 1458.

Mansky, P.; DeRouchey, J.; Russell, T. P.; Mays, J.; Pitsikalis, M.; Morkved, T.; Jaeger, H., *Macromolecules* **1998,** 31, 4399.

McKean, D. R.; Schaedeli, U.; Macdonald, S. A., *Journal of Polymer Science Part a-Polymer Chemistry* **1989,** 27, 3927.

Minelli, C.; Geissbuehler, I.; Hinderling, C.; Heinzelmann, H.; Vogel, H.; Pugin, R.; Liley, M., *J. Nanosci. Nanotechnol.* **2006,** 6, 1611.

Misner, M. J.; Skaff, H.; Emrick, T.; Russell, T. P., *Adv. Mater.* **2003,** 15, 221.

Morkved, T. L.; Lu, M.; Urbas, A. M.; Ehrichs, E. E.; Jaeger, H. M.; Mansky, P.; Russell, T. P., *Science* **1996,** 273, 931.

Mou, C. Y.; Lin, H. P., *Pure Appl. Chem.* **2000,** 72, 137.

Mougenot, M.; Lejeune, M.; Baumard, J. F.; Boissiere, C.; Ribot, F.; Grosso, D.; Sanchez, C.; Noguera, R., *J. Am. Ceram. Soc.* **2006,** 89, 1876.

Murakami, Y.; Yamakita, S.; Okubo, T.; Maruyama, S., *Chem. Phys. Lett.* **2003,** 375, 393.

Nagarajan, S.; Bosworth, J. K.; Ober, C. K.; Russell, T. P.; Watkins, J. J., *Chem. Mater.* **2008,** 20, 604.

Nagarajan, S.; Li, M. Q.; Pai, R. A.; Bosworth, J. K.; Busch, P.; Smilgies, D. M.; Ober, C. K.; Russell, T. P.; Watkins, J. J., *Adv. Mater.* **2008,** 20, 246.

Naito, K.; Hieda, H.; Sakurai, M.; Kamata, Y.; Asakawa, K., *IEEE Trans. Magn.* **2002,** 38, 1949.

Namatsu, H., *J. Photopolym. Sci. Technol.* **2002,** 15, 381.

Nardin, C.; Widmer, J.; Winterhalter, M.; Meier, W., *European Physical Journal E* **2001,** 4, 403.

Neagu, C.; Puskas, J. E.; Singh, M. A.; Natansohn, A., *Macromolecules* **2000,** 33, 5976.

Nguyen, T. Q.; Wu, J. J.; Doan, V.; Schwartz, B. J.; Tolbert, S. H., *Science* **2000,** 288, 652.

Ober, C. K.; Gabor, A. H.; GallagherWetmore, P.; Allen, R. D., *Adv. Mater.* **1997,** 9, 1039.

Okabe, A.; Fukushima, T.; Ariga, K.; Aida, T., *Angewandte Chemie-International Edition* **2002,** 41, 3414.

Olayo-Valles, R.; Lund, M. S.; Leighton, C.; Hillmyer, M. A., *J. Mater. Chem.* **2004,** 14, 2729.

Olayo-Valles, R.; Guo, S. W.; Lund, M. S.; Leighton, C.; Hillmyer, M. A., *Macromolecules* **2005,** 38, 10101.

O'Neil, A.; Watkins, J. J., *Mrs Bulletin* **2005,** 30, 967.

Pai, R. A.; Humayun, R.; Schulberg, M. T.; Sengupta, A.; Sun, J. N.; Watkins, J. J., *Science* **2004,** 303, 507.

Pai, R. A.; Watkins, J. J., *Adv. Mater.* **2006,** 18, 241.

Paik, J. A.; Fan, S. K.; Kim, C. J.; Wu, M. C.; Dunn, B., *J. Mater. Res.* **2002,** 17, 2121.

Park, M.; Harrison, C.; Chaikin, P. M.; Register, R. A.; Adamson, D. H., *Science* **1997,** 276, 1401.

Park, C.; De Rosa, C.; Thomas, E. L., *Macromolecules* **2001,** 34, 2602.

Park, C.; Yoon, J.; Thomas, E. L., *Polymer* **2003,** 44, 6725.

Park, S.; Wang, J. Y.; Kim, B.; Chen, W.; Russell, T. P., *Macromolecules* **2007,** 40, 9059.

Park, S. M.; Craig, G. S. W.; La, Y. H.; Solak, H. H.; Nealey, P. F., *Macromolecules* **2007,** 40, 5084.

Park, S.; Kim, B.; Wang, J. Y.; Russell, T. P., *Adv. Mater.* **2008,** 20, 681.

Ratner, D. B.; Tsukruk, V. V., *Scanning Probe Microscopy of Polymers*. American Chemical Society: Washington, DC, 1996; p 367.

Register, R. A.; Angelescu, D. E.; Pelletier, V.; Asakawa, K.; Wu, M. W.; Adamson, D. H.; Chaikin, P. M., *J. Photopolym. Sci. Technol.* **2007,** 20, 493.

Reiter, G.; Castelein, G.; Hoerner, P.; Riess, G.; Blumen, A.; Sommer, J. U., *Phys. Rev. Lett.* **1999,** 83, 3844.

Richards, R. W.; Peace, S. K., *Polymer Surfaces and Interfaces III*. John Wiley & Sons: West Sussex, 1999; p 304.

Rockford, L.; Liu, Y.; Mansky, P.; Russell, T. P.; Yoon, M.; Mochrie, S. G. J., *Phys. Rev. Lett.* **1999,** 82, 2602.

Rockford, L.; Mochrie, S. G. J.; Russell, T. P., *Macromolecules* **2001,** 34, 1487.

Russell, T. P.; Coulon, G.; Deline, V. R.; Miller, D. C., *Macromolecules* **1989,** 22, 4600. Sankaran, V.; Yue, J.; Cohen, R. E.; Schrock, R. R.; Silbey, R. J., *Chem. Mater.* **1993,** 5, 1133.

Sayari, A., *Chem. Mater.* **1996,** 8, 1840.

Schaffer, E.; Thurn-Albrecht, T.; Russell, T. P.; Steiner, U., *Nature* **2000,** 403, 874.

Schmuhl, R.; Nijdam, W.; Sekulic, J.; Chowdhury, S. R.; van Rijn, C. J. M.; van den Berg, A.; ten Elshof, J. E.; Blank, D. H. A., *Anal. Chem.* **2005,** 77, 178.

Schuth, F.; Schmidt, W., *Adv. Mater.* **2002,** 14, 629.

Scott, B. J.; Wirnsberger, G.; Stucky, G. D., *Chem. Mater.* **2001,** 13, 3140.

Segalman, R. A.; Yokoyama, H.; Kramer, E. J., *Adv. Mater.* **2001,** 13, 1152.

Shakhashiri Carbon Dioxide.
http://scifun.chem.wisc.edu/chemweek/PDF/CarbonDioxide.pdf (May 2008),

Shin, K.; Leach, K. A.; Goldbach, J. T.; Kim, D. H.; Jho, J. Y.; Tuominen, M.; Hawker, C. J.; Russell, T. P., *Nano Lett.* **2002,** 2, 933.

Sirard, S. M.; Ziegler, K. J.; Sanchez, I. C.; Green, P. F.; Johnston, K. P., *Macromolecules* **2002,** 35, 1928.

Socrates, G., *Infrared Characteristic Group Frequencies.* Second ed.; John Wiley & Sons: West Sussex, 1994; p 249.

Spatz, J. P.; Herzog, T.; Mossmer, S.; Ziemann, P.; Moller, M., *Adv. Mater.* **1999,** 11, 149.

Spatz, J. P.; Mossmer, S.; Hartmann, C.; Moller, M.; Herzog, T.; Krieger, M.; Boyen, H. G.; Ziemann, P.; Kabius, B., *Langmuir* **2000,** 16, 407.

Spatz, J. P.; Chan, V. Z. H.; Mossmer, S.; Kamm, F. M.; Plettl, A.; Ziemann, P.; Moller, M., *Adv. Mater.* **2002,** 14, 1827.

Stein, A.; Melde, B. J.; Schroden, R. C., *Adv. Mater.* **2000,** 12, 1403.

Su, M.; Liu, X. G.; Li, S. Y.; Dravid, V. P.; Mirkin, C. A., *J. Am. Chem. Soc.* **2002,** 124, 1560.

Sugimura, H.; Hozumi, A.; Kameyama, T.; Takai, O., *Adv. Mater.* **2001,** 13, 667.

Sun, Z. C.; Gutmann, J. S., *Physica a-Statistical Mechanics and Its Applications* **2004,** 339, 80.

Tadd, E. H.; Bradley, J.; Tannenbaum, R., *Langmuir* **2002,** 18, 2378.

Temple, K.; Kulbaba, K.; Power-Billard, K. N.; Manners, I.; Leach, K. A.; Xu, T.; Russell, T. P.; Hawker, C. J., *Adv. Mater.* **2003,** 15, 297.

Thurecht, K. J.; Hill, D. J. T.; Whittaker, A. K., *Macromolecules* **2005,** 38, 3731.
Thurn-Albrecht, T.; Schotter, J.; Kastle, C. A.; Emley, N.; Shibauchi, T.; Krusin-Elbaum, L.; Guarini, K.; Black, C. T.; Tuominen, M. T.; Russell, T. P., *Science* **2000,** 290, 2126.

Thurn-Albrecht, T.; Steiner, R.; DeRouchey, J.; Stafford, C. M.; Huang, E.; Bal, M.; Tuominen, M.; Hawker, C. J.; Russell, T. P., *Adv. Mater.* **2000,** 12, 1138.

Tirumala, V. R.; Pai, R. A.; Agarwal, S.; Testa, J. J.; Bhatnagar, G.; Romang, A. H.; Chandler, C.; Gorman, B. P.; Jones, R. L.; Lin, E. K.; Watkins, J. J., *Chem. Mater.* **2007,** 19, 5868.

Tolbert, S. H.; Firouzi, A.; Stucky, G. D.; Chmelka, B. F., *Science* **1997,** 278, 264.
Tompkins, H. G.; McGahan, W. A., *Spectroscopic Ellipsometry and Reflectometry*. Second ed.; John Wiley & Sons: West Sussex, 1999; p 353.
Trau, M.; Yao, N.; Kim, E.; Xia, Y.; Whitesides, G. M.; Aksay, I. A., *Nature* **1997,** 390, 674.

Tseng, W. H.; Hsieh, P. Y.; Ho, R. M.; Huang, B. H.; Lin, C. C.; Lotz, B., *Macromolecules* **2006,** 39, 7071.

Urbas, A.; Sharp, R.; Fink, Y.; Thomas, E. L.; Xenidou, M.; Fetters, L. J., *Adv. Mater.* **2000,** 12, 812.

Vavasour, J. D.; Whitmore, M. D., *Macromolecules* **1992,** 25, 5477.

Villar, M. A.; Rueda, D. R.; Ania, F.; Thomas, E. L., *Polymer* **2002,** 43, 5139.

Vogt, B. D.; Pai, R. A.; Lee, H. J.; Hedden, R. C.; Soles, C. L.; Wu, W. L.; Lin, E. K.;

Bauer, B. J.; Watkins, J. J., *Chem. Mater.* **2005,** 17, 1398.

Wallraff, G.; Hutchinson, J.; Hinsberg, W.; Houle, F.; Seidel, P.; Johnson, R.; Oldham, W., *Journal of Vacuum Science & Technology B* **1994,** 12, 3857.

Wang, J. Y.; Chen, W.; Roy, C.; Sievert, J. D.; Russell, T. P., *Macromolecules* **2008,** 41, 963.

Watkins, J. J.; McCarthy, T. J., *Macromolecules* **1994,** 27, 4845.

Watkins, J. J.; McCarthy, T. J., *Chem. Mater.* **1995,** 7, 1991.

Watkins, J. J.; McCarthy, T. J., *Macromolecules* **1995,** 28, 4067.

Whitesides, G. M.; Mathias, J. P.; Seto, C. T., *Science* **1991,** 254, 1312.

Wirnsberger, G.; Scott, B. J.; Stucky, G. D., *Chemical Communications* **2001**, 119.

Wirnsberger, G.; Yang, P. D.; Huang, H. C.; Scott, B.; Deng, T.; Whitesides, G. M.; Chmelka, B. F.; Stucky, G. D., *J. Phys. Chem. B* **2001,** 105, 6307.

Wissinger, R. G.; Paulaitis, M. E., *Journal of Polymer Science Part B-Polymer Physics* **1987,** 25, 2497.

Wu, C. W.; Aoki, T.; Kuwabara, M., *Nanotechnology* **2004,** 15, 1886.

Wu, Y. Y.; Cheng, G. S.; Katsov, K.; Sides, S. W.; Wang, J. F.; Tang, J.; Fredrickson, G. H.; Moskovits, M.; Stucky, G. D., *Nat. Mater.* **2004,** 3, 816.

Xie, B.; Muscat, A. J., *Microelectron. Eng.* **2004,** 76, 52.

Xu, T.; Goldbach, J. T.; Russell, T. P., *Macromolecules* **2003,** 36, 7296.

Yamaguchi, A.; Uejo, F.; Yoda, T.; Uchida, T.; Tanamura, Y.; Yamashita, T.; Teramae, N., *Nat. Mater.* **2004,** 3, 337.

Yang, H.; Coombs, N.; Ozin, G. A., *Adv. Mater.* **1997,** 9, 811.

Yang, P. D.; Deng, T.; Zhao, D. Y.; Feng, P. Y.; Pine, D.; Chmelka, B. F.; Whitesides, G. M.; Stucky, G. D., *Science* **1998,** 282, 2244.

Yang, P. D.; Zhao, D. Y.; Margolese, D. I.; Chmelka, B. F.; Stucky, G. D., *Nature* **1998,** 396, 152.

Yang, P. D.; Wirnsberger, G.; Huang, H. C.; Cordero, S. R.; McGehee, M. D.; Scott, B.; Deng, T.; Whitesides, G. M.; Chmelka, B. F.; Buratto, S. K.; Stucky, G. D., *Science* **2000,** 287, 465.

Yang, P. D.; Rizvi, A. H.; Messer, B.; Chmelka, B. F.; Whitesides, G. M.; Stucky, G. D., *Adv. Mater.* **2001,** 13, 427.

Yin, D.; Horiuchi, S.; Masuoka, T., *Chem. Mater.* **2005,** 17, 463.

Yokokawa, R.; Paik, J. A.; Dunn, B.; Kitazawa, N.; Kotera, H.; Kim, C. J., *Journal of Micromechanics and Microengineering* **2004,** 14, 681.

Young, R. J.; Lovell, P. A., *Introduction to Polymers*. second ed.; Chapman & Hall: New York, 1991; p 443.

Zhang, Z. T.; Dai, S.; Blom, D. A.; Shen, J., *Chem. Mater.* **2002,** 14, 965.

Zhao, D. Y.; Feng, J. L.; Huo, Q. S.; Melosh, N.; Fredrickson, G. H.; Chmelka, B. F.; Stucky, G. D., *Science* **1998,** 279, 548.